UNIVERSITÉ DE MONTRÉAL

STUDY OF THE FILM BLOWING PROCESS AND ON-LINE MEASUREMENTS OF BIREFRINGENCE

AKBAR GHANEH-FARD

DÉPARTEMENT DE GÉNIE CHIMIQUE

ÉCOLE POLYTECHNIQUE DE MONTRÉAL

THÈSE PRÉSENTÉE EN VUE DE L'OBTENTION

DU DIPLÔME DE PHILOSOPHIAE DOCTOR (Ph.D.)

(GÉNIE CHIMIQUE)

NOVEMBRE 1996

UNIVERSITÉ DE MONTRÉAL

ÉCOLE POLYTECHNIQUE DE MONTRÉAL

Cette thèse intitulée:

STUDY OF THE FILM BLOWING PROCESS AND ON-LINE MEASUREMENTS OF BIREFRINGENCE

présentée par: GHANEH-FARD Akbar

en vue de l'obtention du diplôme de: Philosophiae Doctor

a été dûment acceptée par le jury d'examen constitué de:

M. LEGROS Robert, Ph.D., président

M. CARREAU Pierre, Ph.D., membre et directeur de recherche

M. LAFLEUR Pierre, Ph.D., membre et co-directeur de recherche

M. AJJI Abdellah, Ph.D., membre

M. CAMPBELL Gregory A., Ph.D., membre

To my very best friends,

my parents

for their incredible support, encouragement, and dedication

and my wife

Faranak

for her wonderful love, care, and patience

ACKNOWLEDGEMENTS

First of all, I would like to thank God for the health, talent and all countless blessings He has given me throughout the years.

I am deeply indebted to my adviser Professor Pierre Carreau for suggesting the problem, his encouragement, guidance, financial support, and insistence on maintaining a high quality scientific work. This thesis would not have been at its present state without his numerous constructive comments. I would also like to express my thanks to my co-adviser Professor Pierre Lafleur for his kindness, counsel, and contribution to the work.

I would also like to thank all my fellow graduate students and staff of the "Département de génie chimique" for their help and friendship. My special gratitude goes to all people who helped me in solving technical problems during the course of this work, in particular, L. Parent and R. Delisle both of the "Département de génie chimique" and P.A. Dion of the "Département de génie physique". I also thank F. Mighri, a Ph.D. candidate, for his great help in translating the "résumé" and "condensé en français" as well as Dr. M. Aressy for providing me with some rheological data.

I would like to extend my appreciation to Professor G.G. Fuller from Stanford University, Professor W.R. Burghardt and Mr. K. Hongladarom from Northwestern

University and Dr. A. Ajji from National Research Council of Canada for providing me with helpful information on the analysis of the transmission of light beam.

I wish to acknowledge financial support received from the FCAR programme of the Province of Quebec and from NSERC. A scholarship from the Government of I. R. Iran is also gratefully acknowledged. I am also thankful to Union Carbide, Petromont, and Novacor for supplying the polymers used in this study.

I would like to express my sincerest gratitude to my parents, parents-in-law, brothers, and friends for their support and encouragement. My parents have provided me with the best possible education both at home and at school. I can never adequately express my thanks to them. Finally, with special fondness, I wish to express my very deep thanks to my darling wife, Faranak, for her love, care, passion, understanding, and patience. I will eternally be grateful to her.

RÉSUMÉ

Ce travail présente une étude approfondie de l'instabilité, de la cinématique ainsi que de la dynamique dans le soufflage des gaines en résines polyoléfines. Dans l'étude des instabilités des bulles, quatre différents types de polyoléfines ont été utilisés, soit un polyéthylène haute densité (PEHD), un polyéthylène basse densité (PEBD), un polyéthylène linéaire basse densité (PELBD) et un polypropylène (PP). Une attention particulière a été donnée à l'effet de la hauteur de la ligne de figeage ("FLH") sur l'instabilité de la bulle. Cet effet a été généralement ignoré dans la littérature. Les quatre résines étudiées ont montré différents comportements de stabilité. Le PEBD est le plus stable alors que le PP est le plus instable. Aucune corrélation n'a été observée entre la stabilité de la bulle et les propriétés rhéologiques en cisaillement dynamique des différentes résines. L'instabilité augmente avec l'augmentation du ratio d'étirage ("TUR"), celui du gonflement ("BUR") ainsi que la diminution du FLH. De plus, dans le cas du PEBD, quelques points d'opération ne sont pas possibles, débouchant sur plus d'un régime permanent. Nos résultats ne concordent pas bien avec les prédictions de Cain et Denn (1988).

L'utilisation de la technique de biréfringence nous a permis d'obtenir le niveau des contraintes dans la zone fondue ainsi que l'orientation totale dans la zone solidifiée. La transmission de la lumière selon un angle oblique à travers le film a été analysée dans le but de calculer la biréfringence dans le procédé. Il a été démontré que la technique de

biréfringence permet de déterminer le tenseur des contraintes dans la zone fondue en utilisant différents chemins de passage de la lumière. Dans le cas du PELBD, la valeur de la biréfringence est très faible dans la zone fondue et augmente rapidement pendant la cristallisation. La biréfringence du film solidifié est largement dominée par la phase cristalline. L'augmentation de la biréfringence a été observée même après la fin de la cristallisation apparente. Ce comportement est peut-être dû à la continuation de l'élongation et/ou à celle de la cristallisation de la zone solidifiée.

Dans l'étude de l'histoire thermo-mécanique du film à l'état fondu, trois différentes résines, soit un PEHD, un PEBD et un PELBD, ont été utilisées. L'analyse de Cogswell des écoulements convergents a été utilisée pour caractériser le comportement élongationnel de ces différents polymères. Les effets des paramètres de mise en forme incluant TUR, BUR, FLH, la température d'extrusion ainsi que le débit d'écoulement sur les taux de déformation, la température et la biréfringence et la pression à l'intérieur de la bulle (P_i) ont été étudiés. Les résultats expérimentaux révèlent que les trois différents polymères possèdent des comportement différents. Les bulles correspondant à chacun de ces polymères présentent des formes différentes ainsi que des profils de vitesses axiales non identiques ce qui mène à des profils de taux de déformation différents. Le taux de déformation maximal dans la direction d'étirage du PEHD est plus élevé que celui du PELBD. Dans le cas du PEBD, ce taux de déformation maximal est atteint à des hauteurs très basses. Le PELBD exige une P_i la plus élevée alors que le PEBD exige une P_i la plus faible. Le PELBD présente alors la

biréfringence la moins élevée alors que le PEBD présente celle la plus élevée. Des interactions entre différents paramètres de procédé affectant le P_i ont été observées. L'instabilité de la bulle a été corrélée avec la viscosité uniaxiale apparente et la pression interne P_i. Le polymère le plus stable, soit PEBD, possède la viscosité élongationelle la plus élevée et possède une pression interne P_i la plus faible. Les contraintes dans le film à l'état fondu ont été calculées en utilisant les données de la biréfringence, de la pression interne P_i, du diamètre de la bulle ainsi que celles de la vitesse axiale du film. Les contraintes ainsi que les taux de déformation ne peuvent pas être corrélés par une simple équation constitutive. Cependant, ils ont été utilisés pour calculer une viscosité élongationelle apparente biaxiale des polymères. À la fin de la zone fondue, le PEBD montre la viscosité élongationelle la plus élevée ainsi que le taux de déformation le plus faible.

ABSTRACT

This work presents an extensive study of instability, kinematics, and dynamics of film blowing of different polyolefin resins. In the study of bubble instabilities, four different polyolefins, namely a high density polyethylene (HDPE), a low density polyethylene (LDPE), a linear low density polyethylene (LLDPE), and a polypropylene (PP), were used. Special attention was given to the effect of the frost line height (FLH) on the bubble stability, effect mostly ignored in the literature. The four resins show different stability behaviors. The LDPE has the most stable operating space and the PP is the most unstable one. No correlation was observed between bubble stability and oscillatory shear rheological properties of the resins. Instability is enhanced by increasing take-up-ratio (TUR), increasing blow-up-ratio (BUR), and decreasing FLH. Furthermore, for the LDPE, some operating points were not attainable and multiple steady states were observed. Our results are in a poor agreement with the predictions of Cain and Denn's analysis (1988).

The flow birefringence technique was employed to assess the stress level in the melt zone and total orientation in the solid zone. The transmission of light through the blown film at oblique angle was analyzed in order to be able to calculate birefringence in this process. It is demonstrated that the birefringence technique is able to fully determine the stress tensor in the molten film by using different light paths. An optical train with a polarization modulation scheme based on a rotating half wave plate was used to carry out on-line birefringence

measurements. For LLDPE, the birefringence value is shown to be very small in the molten zone and increases rapidly as crystallization proceeds. The birefringence of the solidified film is strongly dominated by the crystalline phase contribution. The increase in the birefringence is observed even after the completion of the apparent crystallization. This behavior may be an indication of continued stretching and/or further crystallization in the solid zone.

In the study of thermo-mechanical history of melt in film blowing, three various polyethylene resins, a HDPE, a LDPE, and a LLDPE, were investigated. The convergent flow analysis of Cogswell was used to characterize the elongational flow behavior of the polymers. The effects of key processing parameters including TUR, BUR, FLH, extrusion temperature, and polymer flow rate on the strain rate, temperature, and birefringence profiles along the length of the bubble as well as the pressure inside the bubble (P_i) were extensively investigated. The experimental results reveal that the three polymers display different behaviors. They show different bubble shapes and axial film velocity profiles which lead to quite different strain rate profiles. The peak machine direction strain rate of the HDPE is higher than that of the LLDPE. For the LDPE, it occurs at very low axial positions. The LLDPE requires the highest P_i and the LDPE, the lowest. Consistent with this, the LLDPE shows the lowest in-plane birefringence and the LDPE, the highest. Interactions between various process parameters affecting the P_i value are observed. Bubble instability is correlated to apparent uniaxial viscosity and P_i. The most stable polymer (LDPE) has the highest elongational viscosity and requires the lowest P_i. Stresses in the molten blown film were

calculated using the birefringence, pressure, bubble diameter, and film velocity data. The stresses and strain rates cannot be correlated through any simple constitutive equation. The stress and strain rate data were used to calculate an apparent non-uniform biaxial elongational viscosity of the melts. At the end of the melt zone, the LDPE exhibited the highest elongational viscosity and the lowest rate of deformation.

CONDENSÉ EN FRANÇAIS

Le soufflage des gaines a été utilisé durant plusieurs années comme l'un des principales techniques de production de films biaxialement orientés. Dans ce procédé, une extrudeuse force la résine de polymère fondu à passer avec un débit constant à travers une filière annulaire. Le tube fondu de polymère sortant de la filière est tiré verticalement vers le haut à l'aide de deux rouleaux. Simultanément, de l'air est introduit à travers une ouverture située au centre de la filière afin de gonfler le tube fondu pour ainsi former une bulle dont le diamètre peut atteindre plusieurs fois le diamètre de la filière. L'orientation biaxiale dans le film rend la technique de soufflage des gaines avantageuse car on peut contrôler les propriétés du film avec précision. La bulle gonflée est refroidie de l'extérieur par de l'air, et le polymère est ainsi solidifié à une certaine distance au dessus de la sortie de la filière. Cette distance est appelée la ligne de figeage ("FLH"). La bulle solidifiée est applatie à l'aide de deux rouleaux pour former une feuille à deux couches. Les trois paramètres principaux dans le soufflage des gaines sont:

- le rapport de gonflement ("BUR"),
- le rapport d'étirage ("TUR"),
- la ligne de figeage ("FLH").

Le rapport de gonflement est défini comme étant le rapport entre le diamètre final de la bulle et celui de la filière. Le rapport d'étirage est défini comme étant le rapport entre la vitesse d'étirage et celle de l'extrudat à la sortie de la filière.

Le procédé de soufflage des gaines est un procédé complexe dans lequel il y a interactions entre la rhéologie des polymères fondus, le transfert de chaleur, l'aérodynamique et la cinématique de la surface libre. Le polymère fondu est soumis à différents états de contraintes développées durant les différents stages du procédé. L'objectif de l'étude de ce procédé est d'obtenir un taux maximal de production de film avec des propriétés physiques et mécaniques optimales. Les propriétés finales du film sont contrôlées par l'orientation moléculaire ainsi que par l'état de cristallisation induite par les contraintes. Plusieurs paramètres influencent d'une manière complexe le développement de la morphologie dans le film gonflé. Ces paramètres sont:

1. Les caractéristiques du polymère: le poids moléculaire, la distribution du poids moléculaire, les ramifications des chaînes, etc...
2. Les caractéristiques des équipements: dimensions de la filière, l'entrefer ainsi que le système de refroidissement.
3. Les variables du procédé: le débit du polymère fondu, la température d'extrusion, le BUR et le TUR.

L'influence de chacun de ces paramètres sur les propriétés finales du film est étroitement liée à celle des autres paramètres. La rhéologie élongationelle du polymère fondu joue aussi un rôle important sur les propriétés finales du film.

L'objectif principal de cette thèse est d'approfondir notre connaissance sur les effets de la rhéologie des polymères fondus dans le soufflage des gaines. Pour atteindre cet objectif,

les instabilités des bulles, la cinématique ainsi que la dynamique du procédé sont à examiner. Une nouvelle technique expérimentale utilisant la biréfringence a été mise en place pour déterminer les niveaux des contraintes dans le film fondu. Cette technique est avantageuse parce qu'elle ne nécessite aucun contact avec le film; ceci est dans le but d'éviter les perturbations dans le procédé. Les viscosités élongationelles biaxiales ont été déterminées à partir des mesures des contraintes et des vitesses de déformation. De plus, les comportements de différentes résines polyoléfines lors du procédé ont été corrélés avec leurs propriétés rhéologiques.

Dans l'étude des instabilités des bulles, quatre différents types de polyoléfines ont été utilisés, soit un polyéthylène haute densité (PEHD), un polyéthylène basse densité (PEBD), un polyéthylène linéaire basse densité (PELBD) et un polypropylène (PP). Les propriétés viscoélastiques de ces polymères ont été mesurées avec un rhéomètre de type CSM de Bohlin, en utilisant deux disques parallèles concentriques. En général, trois types d'instabilités ont été observés:

a - Variation axisymétrique du diamètre de la bulle.

b - Mouvement hélicoïdal de la bulle.

c - Variation de la ligne de solidification.

Ces instabilités sont nommées respectivement instabilité de bulle, instabilité hélicoïdale et instabilité de la ligne de figeage. Pour les quatre polymères étudiés, l'ordre de stabilité est présenté comme suit:

PEBD > PEHD > PELBD > PP.

Les instabilités des bulles ne peuvent pas être corrélées avec les propriétés rhéologiques en cisaillement. Nous rappelons qu'il est impossible de prédire les propriétés élongationelles à partir des données obtenues en cisaillement simple. Dans le cas du PEBD, quelques points opérationnels ne sont pas possibles, débouchant sur plus d'un régime permanent. Les instabilités de bulle à des faibles BUR ont été observées pour les résines PELBD et le PP. Les effets de sortie de filière tels que le gonflement de l'extrudat ainsi que propriétés élongationelles peuvent jouer un rôle important sur la stabilité de la bulle. Nos résultats montrent que l'instabilité de la ligne de figeage augmente avec l'augmentation du TUR et du BUR ainsi que la diminution du FLH. Il est intéressant de signaler que le taux d'étirage dans le procédé de soufflage des gaines augmente lui aussi avec l'augmentation du TUR et du BUR ainsi que la diminution du FLH. Nous pouvons spéculer que lorsque le taux d'étirage (donc la contrainte de traction) augmente et atteint une valeur critique, les phénomènes d'instabilités commencent à apparaître. Les instabilités hélicoïdales ont été observées avec tous les polymères et les forces de traînée de l'air jouent un rôle important dans ce type l'instabilité. Finalement, nos résultats expérimentaux sont en faible accord (ou simplement en désaccord) avec les prédictions des modèles existants dans la littérature.

Dans l'étude de l'histoire thermo-mécanique du film à l'état fondu, trois différentes résines, soit un PEHD, un PEBD et un PELBD, ont été utilisées. L'analyse de Cogswell des écoulements convergents a été utilisée pour caractériser le comportement élongationel de ces

différents polymères. Les déplacements, utilisés pour déterminer les vitesses axiales ainsi que les taux de déformation, ont été mesurés à l'aide de la technique standard de traceur. Le profil de l'épaisseur du film fondu a été calculé à partir de l'équation de conservation de masse en utilisant les profils des vitesses et des diamètres. La mesure de la température le long de la bulle a été effectuée à l'aide d'un pyromètre infrarouge (IRCON 3400). Les mesures de biréfringence ont été obtenues en utilisant un système optique avec un système de polarisation modulaire. La pression à l'intérieur de la bulle a été obtenue à l'aide d'un capteur de pression. Les effets des paramètres de mise en forme incluant TUR, BUR, FLH, la température d'extrusion ainsi que le débit d'écoulement sur les taux de déformation, la température et la biréfringence et la pression à l'intérieur de la bulle ont été étudiés

L'analyse de la transmission de la lumière à travers le film gonflé selon un angle oblique montre que les contraintes normales selon les deux directions MD (direction machine) et TD (direction transversale) peuvent être déterminées par la mesure de la biréfringence. Dans le cas du PELBD, la valeur de la biréfringence est très faible dans la zone fondue et augmente rapidement pendant la cristallisation. La biréfringence du film solidifié est largement dominée par la phase cristalline. L'augmentation de la biréfringence a été observée même après la fin de la cristallisation apparente. Ce comportement est peut-être dû à la continuation de l'élongation et/ou à celle de la cristallisation de la zone solidifiée. Les mesures de la biréfringence dans la zone fondu montrent aussi que le PEBD possède la biréfringence la plus élevée et le PELBD possède la biréfringence la moins élevée.

Les trois résines de polyéthylène utilisées donnent des diamètres de bulle ainsi que des vitesses axiales différents, ce qui mène à des profils des taux de déformation différents. Le taux de déformation maximal dans la direction d'étirage du PEHD est plus élevé que celui du PELBD. Dans le cas du PEBD, ce taux de déformation maximal est atteint à des hauteurs très basses. Il a été observé que les taux de déformation dans les directions MD et TD augmentent considérablement avec l'augmentation du TUR ainsi que celle du débit du polymère. Le taux de déformation dans la direction TD augmente lui aussi avec l'augmentation du BUR. L'augmentation du FLH affecte en grande partie le taux de déformation dans la direction MD pour le PEHD et le PELBD. La température d'extrusion montre un effet marginal sur les taux de déformation pour le PEHD et le PELBD. Cependant, elle montre quelques effets sur le taux de déformation dans la direction MD dans le cas du PEBD. Les résultats démontrent que le TUR n'est pas suffisant pour définir le procédé de soufflage des gaines; on doit aussi spécifier le débit du polymère.

Il a été observé que les variables du procédé ont un effet marginal sur la température au plateau dans la zone de cristallisation. Cependant, la longueur du plateau change avec la variation du FLH. Ceci indique que les cinétiques de cristallisation dépendent du taux de refroidissement de la bulle. De plus, la longueur du plateau du profil de la température est approximativement identique pour les résines PEBD et PELBD. Le PEHD montre un plateau plus large. La température de la bulle dans la zone fondue diminue avec la diminution du FLH, du BUR ainsi qu'avec la température d'extrusion.

Le PELBD exige une pression à l'intérieur de la bulle (P_i) la plus élevée alors que le PEBD exige une P_i la plus faible. L'ordre décroissant de pression exigée à l'intérieur de la bulle pour les différents polymères est présenté comme suit:

PELBD > PEHD > PEBD.

Ceci est en accord avec les résultats de biréfringence obtenus dans notre travail. Plus la pression à l'intérieur de la bulle est élevée, plus le polymère est orienté dans la direction TD, donc une biréfringence moins élevée. La pression à l'intérieur de la bulle augmente avec l'augmentation du BUR et du débit du polymère ainsi que la diminution de la température d'extrusion. Les effets du TUR et du FLH dépendent des polymères utilisées ainsi que des conditions opératoires. Il y a des interactions entre les différents paramètres du procédé qui affectent la valeur de la pression. Le PELBD est le plus sensible aux variations des variables du procédé, alors que le PEHD est le moins sensible. Nos résultats expérimentaux démontrent que la pression à l'intérieur de la bulle est une variable dépendante. Elle dépend de plusieurs variables tels que la rhéologie du polymère fondu, l'épaisseur du film, la température de la bulle, la vitesse axiale, le rayon de la bulle et le débit du polymère.

En comparant les résultats de pression et de biréfringence avec les viscosités élongationelles uniaxiales des différentes résines, nous notons que la pression à l'intérieur de la bulle diminue et la biréfringence augmente avec augmentation de la viscosité élongationelle. Nous notons aussi que les données de la pression et de la biréfringence peuvent être corrélées avec les instabilités de la bulle. Le polymère le plus instable, qui est le PELBD, exige la

pression à l'intérieur de la bulle la plus élevée ainsi que la biréfringence la plus faible.

Les contraintes dans le film fondu ont été calculées en utilisant les données de la biréfringence, de la pression, du diamètre de la bulle, ainsi que la vitesse du film. Les contraintes normales dans les directions MD et TD augmentent considérablement avec la diminution du FLH, l'augmentation du TUR et du débit du polymère. Elles augmentent légèrement avec la diminution de la température d'extrusion. En augmentant le BUR, des contraintes normales dans la direction TD plus élevées ont été obtenues. Avec les mêmes conditions opératoires, le PELBD montre un rapport de contraintes (entre celles dans la direction MD et celles dans la direction TD) le moins élevé. Un film plus isotrope est ainsi obtenu avec le PELBD. Ceci peut être attribué à l'absence de longues chaînes ramifiées dans le PELBD. On ne peut pas obtenir une corrélation simple entre les contraintes et les taux de déformation dans le soufflage des gaines; les équations rhéologiques connues ne peuvent probablement pas décrire les résultats expérimentaux. Les résultats des taux de déformation ne sont pas suffisants pour représenter les effets de la rhéologie à l'état fondu et pour distinguer les comportements des différentes résines utilisées dans le soufflage des gaines. Pour avoir une corrélation entre les propriétés finales du film et les conditions opératoires ainsi que les caractéristiques des résines utilisées, on doit utiliser les données des contraintes ainsi que celles des taux de déformation.

Les viscosités élongationelles biaxiales non-uniformes le long de la bulle ont été

calculées en utilisant les résultats des contraintes ainsi que ceux des taux de déformation. À la fin de la zone fondue, le PEBD montre la viscosité élongationelle la plus élevée ainsi que le taux de déformation le plus faible.

Comme résultats de notre étude expérimentale extensive, plusieurs questions demeurent sans réponse et pourront être étudiées dans le futur. Certaines recommandations sont présentées ci-dessous.

1. Pour mieux connaître le procédé de soufflage de gaines il est indispensable de mesurer la viscosité élongationelle des matériaux utilisés, particulièrement les viscosités élongationelles biaxiale et planaire. Ainsi, on pourra être en mesure de relier les différents comportements (stabilité, cinématique, dynamique, etc, ...) aux paramètres rhéologiques.

2. Nous supposons que la biréfringence du film dans les zones fondu ou solide pourra être une variable appropriée pour corréler les propriétés du film aux propriétés rhéologiques ainsi que les paramètres du procédé. Il serait très intéressant d'examiner cette possibilité. La mesure de la biréfringence sur la ligne de production pourra servir comme une technique avantageuse de contrôle de la qualité du film.

3. Étant donné (selon la littérature) que le modèle de Carreau ainsi que celui de K-BKZ peuvent prédire la majorité des comportements viscoélastiques des polymères, il est

recommandé d'examiner et de comparer les prédictions de ces modèles dans le soufflage des gaines. Comme certaines de nos observations expérimentales ne peuvent pas être décrites par des modèles rhéologiques connus, il est nécessaire de développer de nouveaux modèles afin de décrire les nouvelles situations observées. Dans le but de tester les modèles dans le soufflage des gaines, il est recommandé d'utiliser la pression à l'intérieur de la bulle ainsi que la biréfringence parce qu'elles apparaissent comme étant les paramètres les plus critiques.

4. Il est recommandé de mesurer la viscosité élongationelle biaxiale des différents polymères à l'aide de la technique de soufflage des gaines sous des conditions isothermes, et de comparer ces résultats avec les viscosités élongationelles biaxiales et planaires obtenues en régime permanent. Cette étude pourra clarifier l'utilisation de la technique de soufflage de gaines comme une technique rhéométrique.

TABLE OF CONTENTS

LIST OF TABLES

Paper #1

Paper #3

Paper #4

LIST OF FIGURES

Paper #1

Paper #2

Paper #3

Paper #4

NOMENCLATURE

A	Jones Vector
C	Stress-optical coefficient
C_p	Specific heat
d	Film Thickness (Paper #2)
D	Bubble diameter
D_i	Inner die diameter
D_o	Outer die diameter
D_r	Diameter range
F_z	Bubble drawing force at the frost line height
g	Acceleration due to gravity
G'	Storage modulus
G''	Loss modulus
h	Film Thickness (Papers #3 and #4)
h_c	Heat transfer coefficient
h_f	Final film thickness
Δh_f	Heat of crystallization
I	Light intensity
I_0	Incident light intensity
J	Jones matrix
k	Boltzmann constant (1.381×10^{-23} J/K)
M	Mueller matrix
M_n	Number-average molecular weight
M_w	Weight-average molecular weight
M_z	z-average molecular weight
n	Refractive index tensor
n	Average refractive index

Δn	Birefringence
P_i	Pressure inside the bubble
P_l	Position of the left bubble edge
P_r	Position of the right bubble edge
ΔP	Pressure difference across the bubble
Q	Volumetric polymer flow rate
r	Bubble radius
R_1	Radius of curvature in the machine direction
R_3	Radius of curvature in the transverse direction
R_f	Final bubble diameter
S	Stokes vector
t	Time
t_p	Fresnel transmission coefficient for parallel polarization
t_s	Fresnel transmission coefficient for perpendicular polarization
T	Temperature
T_c	Cooling air temperature
T_s	Temperature of the surroundings
v_z	Axial film velocity
V	Nip rolls speed
w	Mass flow rate of molten polymer at die exit
X	Fraction of crystallinity
z	Axial distance

Greek letters

α	Orientation angle
α_1, α_2	Polarizabilities
$\dot{\gamma}$	Strain rate tensor

$\dot{\bar{\gamma}}$	Rate of deformation
δ	Retardation
$\Delta_1, \Delta_2, \Delta_3$	Normal optical differences
ϵ	Emissivity
$\dot{\epsilon}$	Uniaxial elongational strain rate
η	Shear viscosity
η_0	Zero shear viscosity
η_{be}	Biaxial elongational viscosity
η_E	Uniaxial elongational viscosity
η^*	Complex viscosity
θ, θ_i	Bubble inflation angle
θ_r	θ-component of refraction angle
λ	Relaxation time (Paper #1)
λ	Wave length (Papers #2 and #3)
ρ	Density
σ	Stress tensor
ϕ_i	Off-center angle of incidence
ϕ_r	ϕ-component of refraction angle
ω	Frequency

Abbreviation

BI	Bubble instability
BUR	Bow-up-ratio
DHI	Degree of helical instability
FI	FLH instability
FLH	Frost line height
HDPE	High density polyethylene

LDPE	Low density polyethylene
LLDPE	Linear low density polyethylene
MD	Machine direction
MI	Melt index
PE	Polyethylene
PH	Partially helical
PP	Polypropylene
PS	Polystyrene
SAXS	Small angle X-ray scattering
SEM	Scanning electron microscopy
TD	Transverse direction
TEM	Transmission electron microscopy
TUR	Take-up-ratio
WAXS	Wide angle X-ray scattering

Subscripts

(CP)	Circular polarizer
(f)	Final
(PSG)	Polarization state generator
(S)	Sample
(0)	Incident
(1)	Exiting

Superscripts

(')	Air-film interface
(")	Film-air interface

CHAPTER 1

INTRODUCTION

1.1. The Process Description

The technology of the film blowing process has a long history. It was first applied to cellulosic derivatives by solution processing at least as far back as 1915 (Kang et al., 1990). The first production unit of the blown film extrusion of polyethylene resins was probably built in the USA in 1939 (Wagner, 1978). The film blowing process has been extensively used over the years for the production of biaxially oriented, thin polymeric films. The process is a very important one commercially, since a substantial fraction of polyolefin production is being converted thereby into wrapping film (Pearson, 1985). In this process, an extruder melts the resin and forces it through an annular die at constant flow rate. The molten tube leaving the die is drawn upwards by the nip rolls. Simultaneously, air is introduced through an opening in the center of the die inflating the tube and forming a film bubble up to several times the diameter of the die. This two-directional orientation is one of the primary attractions of film blowing, since it allows for precise control of the film properties. The molten film bubble is cooled by means of an air ring, located just above the die, that directs air on the outer surface of the bubble. In some cases additional cooling is provided by internal cooling device. The polymer solidifies some distance above the die exit; this height, which is called frost line height (FLH), may vary slightly around the circumference of the bubble because of non-

uniform air flow patterns. The solidified bubble is flattened into a double-layered sheet by nip rolls. It is then pulled, folded, and wound on cylindrical cores. Blown film installations are operated in most cases in the vertical position, the film being extruded upward, rarely in the downward direction.

Due to the axial tension of the nip rolls the velocity of the molten polymer in the neck zone will gradually increase upon leaving the annular die, and therefore the thickness of the molten polymer tube will decrease progressively as the polymer is drawn away from the die. At some distance from the die a point will be reached whereby the pressure inside the bubble will exceed the melt strength of the thin walled tube and this will cause the tube to expand radially. The amount by which it expands relative to the die diameter is called the blow-up-ratio (BUR) and is controlled by the amount of the air inside the bubble. This radial expansion will enhance transverse-direction (TD) molecular orientation, superimposed on the molecular orientation in machine direction (MD) due to take-up tension. In this bubble expanding zone, the film will thin further and experience a greater cooling rate due to the increased surface area, hence the polymer will be solidified very rapidly. The solidification process will enhance the mechanical strength of the film, whereby it will be able to support that particular pressure inside the bubble. No further expansion will occur at this point and the bubble diameter will remain constant. FLH and BUR as well as take-up ratio (TUR), defined as the ratio of the take-up velocity to the extrudate velocity at the die exit, are important parameters characterizing the film blowing process.

The film blowing process is a complex manufacturing process involving interactions between melt rheology, heat transfer, aerodynamics, and free surface kinematics. In this process the molten polymer is subjected to different stress fields that develop at various stages of the process. First, as the melt flows through the annular die, it is subjected to shearing stresses, resulting in a partial molecular orientation in the machine direction (MD). Upon leaving the die, where the melt is suddenly free of the constraints imposed by contact with the die wall, this orientation may be partially relaxed but further orientation of the macromolecules will occur as a result of biaxial stretching. The level of extensional stresses will then increase with increasing viscosity due to cooling. Depending on the cooling rate of the melt a second relaxation process may also take place, causing reorientation of macromolecules (Maddams and Preedy, 1978a). In the vicinity of the frost line height the melt under stress starts to crystallize.

The goal of studying the film blowing process, as in most polymer processing operations, is to obtain a maximum production rate with optimal physical and mechanical properties. Ultimate film properties are controlled by molecular orientation and stress-induced crystallization. Many parameters influence the morphology development of blown films in a very complex way. These parameters include the polymer characteristics (such as molecular weight, molecular weight distribution, and branching) and the equipment characteristics (such as die size, die gap, and cooling system) as well as processing variables (such as polymer flow rate, extrusion temperature, FLH, BUR, and TUR). The influence of each of these parameters

on film properties is found to be highly interactive with the others. Melt elongational rheology should also play an important role on the final film properties. The studies in the literature are reviewed below. The readers are also referred to the literature reviews that are included in the four articles presented in this dissertation.

1.2. The Review of Literature

Despite numerous experimental and theoretical studies towards film blowing, there still remain many aspects of the process which are not still well understood. This is mainly because of the complexity of the process, experimental difficulties in measurements of relevant variables, and lack of relevant elongational rheological data.

It was first Pearson and Petrie (1970a, 1970b) who attempted to theoretically analyze the isothermal film blowing process of a Newtonian fluid. They used the thin shell approximation which enabled them to use local rectangular Cartesian coordinates. They also derived force balance equations in film blowing. Since their attempts, several publications dealing with the studies of both isothermal and non-isothermal film blowing are reported. In these studies, attention has been paid to using various rheological constitutive equations as a pivotal element in modeling the process.

Agassant et al. (1991) have presented a different Newtonian analysis of film blowing

in which the pulling force at the die exit is first calculated and then the entire stress history in the film is predicted, independently of any hypothesis on the material behaviour. Kanai and White (1985) and Kanai (1987) have also used the Newtonian model in the non-isothermal simulation of film blowing. Furthermore, they have incorporated a crystallisation term in the heat transfer equation. The power law model has been employed by Han and Park (1975b) and Yamane and White (1987). Later investigators have also considered the crystallization effect. In summary, predicted results by these models show that crystallization does not significantly affect bubble shape but retards the continued growth of velocity profile and thinning of the film. The crystallization model of Yamane and White (1987) predicts that activation energy has a much greater effect on bubble shape than variations in non-Newtonian characteristics. Decreasing activation energy and power law exponent both produce long narrow necked bubble.

However, since the flow in film blowing is eventually extensional, the viscoelastic nature of molten polymer cannot be neglected. Hence, the viscous models should not be expected to fit experimental data quantitatively and one has to use a suitable viscoelastic model to simulate the process. Also, the linear viscoelasticity may not be valid since neither the strain rate nor the total strain is sufficiently small (Dealy and Wissbrun, 1990). The efforts to incorporate viscoelastic rheological models in modeling of film blowing are reviewed below.

Petrie (1973) used a simple Maxwell model. Based on a limited amount of computation, he predicted that increasing elasticity of material decreases the bubble radius and the film thickness. In a later paper (1975), Petrie compared experimental data of film blowing with predictions of elastic and viscous models and showed that experimental data were lying between these models.

Gupta et al. (1982) described the viscoelastic nature of the melt using the White-Metzner equation modified to take into account the non-isothermal effects. They measured stress, strain rate, and temperature profiles in film blowing of a polystyrene (PS) and used these data to calculate equivalent first normal stress differences. These were then compared with the first normal stress differences measured in shear to test the validity of the model, based on the assumption that material parameters, i.e., relaxation time and viscosity, do not depend on the flow field. They showed good agreement for isothermal conditions and non-isothermal conditions with BUR<1. However, for non-isothermal conditions with BUR>1 there were some discrepancies between predicted and experimentally measured values. Concerned with the TD stress, it was seen that the predicted results did not fit experimental data at all.

Luo and Tanner (1985) have considered the upper convected Maxwell and Leonov models in isothermal and non-isothermal film blowing. They showed that the Leonov model gave unrealistic results for film thickness because it did not predict enough stiffening with

increasing elongational rate. They also noted that with the Leonov model the numerical system was highly unstable. They compared the predictions for the non-isothermal upper convected Maxwell model with the Gupta's data on PS (1980). Owing to numerical instability, they did not get any convergent results for cases in which BUR<1 but for all runs with BUR>1, a convergent numerical result was obtained. The model predicted the experimental bubble shapes, temperature profiles, strain rates and stresses fairly well. It is worth mentioning that Luo and Tanner had to modify the relaxation time and process parameters, i.e., pressure difference across the bubble and bubble drawing force, to fit their model to experimental data. Moreover, they pointed out that the temperature dependency of rheological properties should be incorporated in the film blowing modeling.

Cain and Denn (1988) have used the Marrucci model, in addition to the Newtonian and Maxwell models and predicted that multiple solutions exist; simply defining pressure difference and take-up force does not uniquely determine the bubble profile. Furthermore, it was predicted that for some operating conditions, there were no steady-state solutions.

Alaie and Papanastasiou (1993) have recently analyzed melt film blowing by means of the Wagner like PSM (Papanastasiou, Scriven, and Macosko) model which is a nonlinear integral constitutive equation. The effects of shear history in the die were taken into account. Their model also incorporates spectrum of relaxation times, shear thinning and extension thinning or thickening. The model predicts that with increasing elasticity, the bubble radius

and film thickness both decrease but the velocity of film increases. Furthermore, predicted thickness, radius, temperature, and MD stress profiles show a good agreement with experimental data of PS (Gupta, 1980), but TD stresses are slightly overestimated near the die exit and underestimated at the freezing end. It is worth noting that due to an error in unit conversions they have mistakenly reported that the TD stress is being greater than the MD stress for a Gupta's experiment.

All the models presented in the previous paragraphs are valid up to the freeze line. Cao and Campbell (1990) have proposed a viscoplastic-elastic model to simulate the process from the die exit to the nip rolls. They have replaced the conventional kinematic boundary conditions by a rheological boundary condition, the plastic-elastic transition (PET). Below the PET a modified Maxwell model and above the PET a modified Hookean model was used. In contrast to the liquidlike models, their model does not predict the bubble radius to collapse to zero above the PET. It appears that the model shows a good agreement with some Gupta's data (1980) on the bubble radius and film velocity. This was, however, achieved by altering some material parameters. In another study, Ashok and Campbell (1992) have described a two phase simulation of film blowing of crystalline polymers, considering the film as a crystallized and an amorphous layers. An upper convected Maxwell equation was applied to the amorphous phase while a plastic-elastic model was used to describe the deformations of the crystallized phase. Although there are some limitations such as neglecting radial temperature gradient and avoiding extrudate swell problem, the model predictions of the

bubble radius and axial velocity are apparently in qualitative agreement with experimental data of Kanai and White on a HDPE (1984). Ashok and Campbell did not discussed how incorporating crystallization effects improved the film blowing simulation.

The extrudate swelling effect on film blowing has been analyzed by Seo and Wissler (1989), using viscous models. A comparison of numerical results and experimental data has revealed that extrudate swelling effect is important when the take-up ratio is low, but its influence is negligible when take-up ratio is high. A bicomponent two-layer blown film coextrusion has been theoretically studied by Yoon and Park (1992) in which a Newtonian fluid and an upper convected Maxwell fluid constitute the two layers. It is shown that when the relaxation time is small the bubble dynamics is not much different from that of a Newtonian single- layer flow. With increasing relaxation time, however, the viscoelasticity effect becomes so strong that it eventually dominates the bubble dynamics. Then, the two-layer bubble basically takes on the shape predicted for a single-layer Maxwell fluid.

More recently, Tas (1994) has attempted to assess the Wagner, Leonov, Giesekus, and PTT models for predicting stresses in film blowing of LDPE resins. He has compared model predictions with experimentally measured stress profiles for only two of his experiments. For one of the experiments, the PTT and Leonov models appear to predict the MD stress better than the other models. For the other experiment, the MD stress is overpredicted by the PTT and Giesekus models but underpredicted by the Leonov and

Wagner models. The TD stress is predicted fairly well by the Wagner model but overpredicted by the others in both experiments. Therefore, it is difficult to say which model does the best job in predicting stresses. Nevertheless, Tas has shown that the PTT model is the most successful in predicting the MD stress at the freeze line. He has also concluded that the shear prehistory in the die should be incorporated in the film blowing modeling.

In summary, we note that there are several efforts in the literature to simulate film blowing by using both purely viscous and viscoelastic models. However, it is safe to say that only limited success has been so far achieved. In most of the simulation studies it is clearly stated that material parameters and/or processing parameters are altered in order to fit experimental data. The abilities of film blowing models have been examined with the limited published data, mostly those of Gupta (1980) on PS. It is not demonstrated whether the models are able to predict the behavior of at least two rheologically different melts in film blowing. It is obvious that one major problem in validating the film blowing models is the lack of sufficient and reliable kinematic and dynamic data due to experimental difficulties. The stresses in the molten bubble are considered to be the most critical parameters to assess rheological equations. Only very few stress data in the literature have been so far determined via force balances by measuring the bubble drawing force at the nip rolls, using mechanical transducers. However, the reliability of these data is questionable due to the fact that the bubble force measurement is influenced by different frictional forces during flattening of the bubble, pinching-off and taking-up. To overcome this problem, we have used the flow

birefringence technique which provides a non-contacting indirect measurement of the stresses occurring in the bubble. The question regarding the rheological constitutive equation that does the best job in predicting the geometry, kinematics, and dynamics of the bubble still remains unanswered. It is evident that film blowing will continue to pose challenges to rheologists in order to analyze melt behavior in this very complex process.

The most extensive experimental studies on the kinematics and dynamics of film blowing are those of Han and Park (1975a) on HDPE, LDPE and PP, Gupta (1980) on PS, Kwack (1984) on LDPE , LLDPE and PET, Kanai and White (1984) on LDPE, LLDPE, HDPE, Winter (1983) on LDPE and HDPE, and Tas (1994) on LDPE. Bubble instabilities in film blowing have been well documented (Kanai and White, 1984; Ast, 1974; Han and Park, 1975c; Han and Shetty, 1977; Minoshima and White, 1986; White and Yamane, 1987). The production rate of film blowing and attainable range of film physical properties can be seriously limited by bubble instabilities. It has been observed that the long-chain branched polyethylenes are the most stable, followed by the broad-distribution linear polyethylenes. The narrower molecular weight distribution polyethylenes are the most unstable (Minoshima and White, 1986). Sweeney and Campbell (1993) have observed that the effects of processing parameters on bubble stability are highly interactive.

The work of Kanai and White (1984) represents a fairly complete body of study of the kinematics and dynamics of film blowing. They observed slightly different bubble shapes for

HDPE, LDPE and LLDPE ; HDPE being more notably thin-necked and inflating in a shorter distance. They also measured strain rates, bubble temperature, pressure inside the bubble, and bubble drawing force in their comparative study of various polyethylene resins. In general, they observed that the strain rates increased with increasing TUR, decreasing FLH, and increasing BUR. The bubble temperature was found to decay almost linearly and reach a plateau. The plateau was much broader for HDPE. The length of plateau decreased as the FLH decreased. The MD stress at the FLH was found to increase with the TUR for all the melts, being most rapid in the rate of increase for LDPE. The MD stress at the FLH for LLDPE was the lowest and most independent on FLH. It is worth mentioning that the bubble drawing force was measured with a commercial tensiometer in their experiments which may result in considerable error due to the fact that the bubble tension is quite low. Kanai and White also found that LDPE generally required much higher inflation pressure than the other melts. The pressure inside the bubble was found to increase with increasing TUR and decreasing BUR. This is apparently in contradiction with the findings of Wagner (1978) who observed for a LDPE that the pressure decreased with increasing TUR and remained almost constant with increasing BUR for a LDPE. Wagner also observed that the lower melt flow index polymers required higher inflation pressures.

Han and Kwack (1983) and Kwack and Han (1983) observed that the resin having a narrow molecular weight distribution (MWD) and low degree of long chain branching (LCB) tended to give a greater thickness reduction than the resin having a broad MWD and high

degree of LCB due to its extensional-thinning behavior. Moreover, they observed that a more uniform tensile strength in the MD and TD was achievable with a LLDPE resin than with a LDPE resin. This may be attributable to the absence of long side chain branching in the LLDPE resin.

Huang and Campbell (1985, 1986) have measured the strain rates and bubble temperature in film blowing of a LDPE and a LLDPE and observed that the peak strain rates occur closer to the die exit and are higher in magnitude for the LDPE than the LLDPE. It was shown that for LLDPE, addition of a small quantity of the LDPE caused a significant increase in the strain rates at lower axial positions.

Babel and Campbell (1993, 1995) and Tas (1994) have attempted to correlate mechanical properties of blown films with the kinematics and dynamics of the process. Babel and Campbell (1993) suggested that the plastic strain, defined as the strain put in the film after the onset of crystallization, could be a correlating variable. However, the experimental data appear to be too scattered to claim any clear correlation. This idea was initially proposed by Farber and Dealy (1974) who postulated that the orientation in the film results from the plastic strain in the immediate neighbourhood of the FLH. In another article, Babel and Campbell (1995) have related film properties to both plastic strain and strain rates. However, such correlations based on a limited set of experimental data are easily questionable as the quantitative determination of the plastic strain and strain rates is a very difficult task. Tas

(1994) has recently examined mechanical properties of blown films in terms of the MD stress at the freeze line, calculated from the PTT model using the experimentally determined kinematics and temperatures. In his work, the freeze line height was defined as the position where the film became opaque. He has shown that some mechanical properties can be correlated to the MD stresses and concluded that equal MD stresses at the freeze line result in equal properties, regardless of the type of LDPE and equipment as well as processing conditions. He was not successful in correlating film properties to the TD stresses or the stress ratio, that is: the ratio of the MD stress to the TD stress. This was probably due to the fact that the PTT model did not predict the TD stresses at all well. However, the influence of the TD stresses on final film properties may not be neglected.

Summarizing the literature review on the experimental observations on film blowing, we notice that many aspects have not received any treatment and some of the experimental observations appear to lead to contradictory conclusions. Bubble instabilities are not well understood. They obviously involve different rheological factors and the role of aerodynamic forces and cooling effects are not understood. The effects of some processing parameters on strain rates have not been yet investigated. No comprehensive study of the pressure inside the bubble is available in the literature, although it is an important parameter; one can only find some scattered data. The most difficult parameter to measure in film blowing is bubble drawing force and this information can be only rarely found in the literature. It is widely believed that final film properties can be predicted from stresses, deformations, and thermal

history encountered by the melt during biaxial deformation. However, the relationships between these quantities are still poorly understood, mostly because of lack of sufficient and reliable data. Therefore, this experimental study was carried out to provide a better understanding of the process and to shed light on the different behaviors of various polyolefins.

1.3. Objectives of the Dissertation

The main objective of this thesis is to advance our understanding of the effects of the rheology of molten polymers on film blowing. To achieve this goal, bubble instabilities and the kinematics as well as dynamics of the process are to be extensively examined. The stable operating space for various polyolefins are to be determined and the effects of processing conditions on different forms of instabilities are to be illustrated. It is to implement the flow birefringence technique for on-line determination of stresses in the molten film as a novel non-contacting technique in film blowing. It is also to provide a complete set of data, that is: bubble diameter, axial film velocity, bubble temperature, strain rate, and stress profiles along the length of the bubble as well as the pressure inside the bubble, on a series of polyethylene resins in a wide range of operating conditions to alleviate ambiguities and contradictions found in the literature. Biaxial elongational viscosities are to be determined from stress and strain rate measurements. Finally, The different behaviors of various polyolefins are to be correlated to their rheological parameters.

1.4. Organization of the Articles

This thesis is presented as four articles. The first article entitled "Study of Instabilities in Film Blowing" aims at determining the stable operating space for different polyolefins. We study the stability behavior of three different polyethylene resins as well as of a polypropylene (PP) resin using a quantitative criterion. We characterize different forms of instability and discuss the effects of film blowing parameters. We give special attention to the effect of the frost line height, as it is a response to cooling conditions and, therefore, significantly influences ultimate film properties. It is demonstrated that bubble instabilities cannot be correlated with the shear viscosity data. Furthermore, it is observed that for LDPE, some operating points are not attainable and multiple steady states exist. Finally, we find that our experimental results are in little agreement with the theoretical predictions of Cain and Denn (1988).

The second article entitled "Application of Birefringence to Film Blowing" is devoted to analyze the transmission of light through the blown film at oblique angle which enables one to calculate birefringence in this process. We discuss the problems facing the birefringence measurement in film blowing. We also discuss the rheological application of the birefringence technique and its limitations. It is shown that the technique is able to fully determine the stress tensor in the molten film by using different light paths.

In the third and the fourth articles, an extensive study of the effects of material characteristics and processing parameters on the thermo-mechanical history experienced by molten polymer in bubble forming zone is presented. We report experimental results of the on-line birefringence as well as strain rate and bubble temperature measurements in film blowing. In the third article entitled "On-line Birefringence Measurement in Film Blowing of a linear Low Density Polyethylene", we examine the effects of key processing parameters on the strain rate, bubble temperature, and birefringence profiles for a LLDPE. We describe the birefringence profiles along the length of the bubble in the melt, crystallization, and solidified zones. We also interpret the bubble temperature profile in the light of the energy balance equation. We make use of the stress-optical law and also the force balance equation perpendicular to the film to calculate stresses in the molten blown film. We finally compare our stress data with predictions of a simple Newtonian fluid and find that the trends of our data, regarding the effects of the processing conditions, are qualitatively well predicted.

In the last article entitled "Study of Kinematics and Dynamics of Film Blowing of Different Polyethylenes", we compare the behaviors of three PE resins, a HDPE, a LDPE, and a LLDPE. Based on the results of bubble instabilities, PP is excluded in this study as its stable operating space is too small. In this article, special attention is also given to the measurements of the pressure inside the bubble over a wide range of film blowing conditions. We find that the pressure inside the bubble is clearly a dependent variable and also a rather complex response to several variables. We use the convergent flow analysis of Cogswell to

characterize the elongational flow behavior of the polymers, in attempt to establish correlations between rheology and processing in film blowing. It is observed that there is a correlation between the pressure inside the bubble, apparent uniaxial elongational viscosity, and bubble instability. We also calculate an apparent non-uniform biaxial elongational viscosity along the length of the bubble using the stress and strain rate data. Finally, we note that relationships between stresses and strain rates in film blowing in some cases may not be described by any simple rheological equation such as the Newtonian model. Therefore, the findings in the third article should not mislead one to conclude that the Newtonian model might be a suitable model to qualitatively describe the film blowing process.

In brief, this work aims at gaining a better understanding of the rheology of molten polymers on film blowing. Some important facts which mostly ignored in the literature are revealed in this study. A very interesting feature of this work is to employ the flow birefringence technique as an alternative method to measure stresses occurring in the bubble forming zone. Although the technique has its limitations, it appears to be a promising tool to determine stresses. It is hoped that our experimental results in this study will stimulate more work to develop more realistic mathematical models and to explore better correlations between final film properties and processing conditions as well as polymer characteristics.

CHAPTER 2

FIRST ARTICLE:

STUDY OF INSTABILITIES IN FILM BLOWING

A. Ghaneh-Fard, P.J. Carreau, and P.G. Lafleur

Centre de recherche appliquée sur les polymères

(CRASP)

Department of Chemical Engineering

Ecole Polytechnique

PO Box 6079, Stn "Centre-Ville", Montreal, QC, H3C 3A7 CANADA

AIChE J., May 1996, **42**, 1388

Correspondence concerning this article should be addressed to P.J. Carreau.

2.1. Abstract

This paper reports results on bubble instabilities observed in film blowing using four different polyolefins, namely a high density polyethylene (HDPE), a low density polyethylene (LDPE), a linear low density polyethylene (LLDPE) and a polypropylene (PP). Special attention is given to the effect of the frost line height on the bubble stability, effect mostly ignored in the literature. A video-camera system was used to record the bubble shape and oscillations. In general, three forms of instabilities and combinations were observed: (a) axisymmetric periodic variations in the bubble diameter, (b) helical motions of the bubble, and (c) variations in the position of the solidification line. The four resins show different stability behaviors. The LDPE has the most stable operating space and the PP is the most unstable one. No correlation was observed between bubble stability and oscillatory shear rheological properties of the resins. Instability is enhanced by increasing take-up-ratio, increasing blow-up-ratio, and decreasing frost line height. Furthermore, for the LDPE, some operating points were not attainable and multiple steady states were observed. Our results are in a poor agreement with the predictions of Cain and Denn (1988)'s analysis.

Key-words: Film Blowing, Bubble Instability, Polyolefins.

2.2. Introduction

Blown film extrusion, sketched in Figure 1, is an important polymer processing operation and is used to produce most of the plastic films. The molten polymer is extruded at a constant flow rate through an annular die. The film is deformed axially by the tension of the take-up device and circumferentially by the introduction of air inside the polymer tube.

A stable bubble is a requirement not only for the continuous operation of the process but also for the production of an acceptable film (Fleissner, 1988). The restriction of stable operating conditions also limits the rate of production and due to process/physical property interactions, limits the attainable range of physical properties (Sweeney et al., 1992).

Instability in film blowing was first reported by Ast (1974) and Han and Park (1975). Han and co-workers (Han and Park, 1975; Han and Shetty, 1977) observed that lowering the extrusion temperature stabilized the blown bubble for HDPE and LDPE. The work of White and co-workers (Kanai and White, 1984; Minoshima and White, 1986; White and Yamane, 1987) is the most extensive. Comparing bubble stability of different polyethylene (PE) resins, Minoshima and White (1986) have concluded that the long chain branched PEs are the most stable followed by the broad distribution linear PEs. The narrower molecular weight distribution PEs are the most unstable. In other words, LDPE has the widest stable operating region and it has been attributed to the strain hardening behavior of LDPE in elongational

flow. Minoshima and White (1986) have also examined the influence of molecular structure of PE on draw resonance in melt spinning, which is kinematically similar to film blowing. LDPE was again the most stable but broadening molecular weight distribution in linear PEs was destabilizing for melt spinning. Ghijsels et al. (1990) have suggested that, in film blowing, a small axial take-up force is needed to stretch the low melt strength film in absence of strain hardening as for LLDPE. In this situation a low-tension bubble becomes sensitive to surrounding air flows and gravity forces, leading to bubble instabilities. Improving stability behavior of LLDPE by using a dual-iris cooling system or by blending with LDPE has been shown by Obijeski and Pruitt (1992). Sweeney et al. (1992) have demonstrated that the video analysis system is an effective, non-contact, real time device for quantifying instabilities during film blowing. In another study, Sweeney and Campbell (1993) have recently observed that there is a strong level of interactions between various process parameters affecting the bubble stability.

We are aware of only two theoretical studies on bubble stability, those of Yeow (1976) and Cain and Denn (1988). They both used an isothermal Newtonian model and a linear stability analysis with different numerical techniques. Cain and Denn have also carried out a mathematical analysis of stability assuming that the melt is a upper convected Maxwell fluid. However, because of these simplifying assumptions these models do not show a good agreement with experimental observations. This will be discussed later.

The main objective of this study is to determine the stable operating space for different polyolefins. The stability behavior of three different polyethylene resins as well as of a polypropylene resin was studied using a quantitative criterion. Different forms of instability are defined and the effect of film blowing parameters are illustrated. These parameters are: the frost line height (*FLH*), shown in Figure 1, the blow-up-ratio (*BUR*), defined as the ratio of the final bubble diameter to the die diameter, and the take-up-ratio (*TUR*), which is the ratio of the take-up velocity to the extrudate velocity at the die exit. *BUR* and *TUR* are obviously two key parameters of the film blowing process. Increasing the values of these parameters is explicitly desirable in a commercial film production. On the other hand, even though *FLH* does not control the film geometry, its effect on final film properties cannot be denied as it is a response to cooling conditions. That is why we have examined the influence of *FLH* on bubble stabilities. This article is a part of an extensive study of film blowing being carried out in our laboratory. Future work will focus on the elongational properties of polymers determined *in-situ* during film blowing using a rheo-optical technique.

2.3. Experimental

2.3.1. Materials

Four different film-grade polyolefins were used in this study: a high density polyethylene (HDPE), a low density polyethylene (LDPE), a linear low density polyethylene

(LLDPE), and a polypropylene (PP). The HDPE and the LLDPE were supplied by Du Pont, the LDPE by Novacor and the PP by Himont. Densities, melt indices (*MI*) and the available molecular characteristics of the four polymers are summarized in Table 1.

2.3.2. Rheological Measurements

The dynamic rheological properties, storage and loss moduli, G' and G'', complex viscosity, η^*, were measured using a CSM Bohlin rheometer in a concentric disk configuration under a dry nitrogen atmosphere. The frequency used ranged from 0.001 Hz to 30 Hz and the applied stress was adjusted to maintain the experiments in the linear domain. Measurements were carried out at temperature of 180°C for the HDPE, the LDPE and the LLDPE and 240°C for the PP. Concentric disks of diameter equal to 25 mm with a gap between 1 and 1.2 mm were used for all measurements.

2.3.3. Blown film extrusion

A 45 mm Killion single screw extruder with a helical blown film die (outer diameter = 50.82 mm and die gap at exit = 680 μm) was used in this study. The extrusion was carried out at a temperature of 180°C for the polyethylenes and 240°C for the PP. It was found that for our blown film system the PP was not processable at 230°C and was very unstable at 250°C. The polymer flow rate was maintained at about 6.8 kg/h for all experiments.

The film blowing process was initiated by grabbing the tube of molten polymer, leaving the die, and making it pass over the nip rolls. Inflation of the polymer bubble was accomplished by opening the air valve. The action of the nip rolls not only provided the axial tension but also formed an air tight seal so that a constant pressure could be maintained in the bubble. The nip rolls speed and amount of air inside the bubble were then simultaneously adjusted to achieve the desired *BUR* and *TUR* values. Cooling of the bubble was done by using a single lip air ring which was located just above the die, directing air at room temperature on the surface of the bubble. The *FLH* was set up at the desired value by adjusting the cooling air flow rate. However, it was observed that the *FLH* was also influenced by other variables such as polymer mass flow rate, melt temperature, *BUR*, and *TUR*.

The densities of the molten polymers were measured using an Instron capillary rheometer, replacing the capillary by a plug. The description of the method can be found elsewhere (Terry and Yang, 1964). The polymer mass flow rate (w*)* was measured by weighing the amount of extrudate collected in a known interval of time. This information together with the density of the molten polymer at the die exit (ρ) and the nip rolls speed (*V*) were used to calculate the *TUR* as:

$$TUR = \frac{V}{w}\rho\left(\frac{\pi}{4}\left(D_o^2 - D_i^2\right)\right) \qquad \textbf{(1)}$$

where D_o and D_i are the outer and inner die diameters respectively.

A video-camera system was used to record the bubble shape and oscillations. The recorded tapes were analyzed by an image analyzer to obtain the bubble diameter and degree of helical instability using the distances of the bubble edges from a reference line at a height well above FLH over a period of time (Figure 2). The concept of the diameter range (D_r), first introduced by Sweeney et. al. (1992), was used as a criterion for degree of the helical instability. The average diameter (D_{mean}) and degree of the helical instability (DHI) are then obtained from the following equations:

$$D_{mean} = P_{l,mean} - P_{r,mean} \tag{2}$$

$$D_{max} = P_{l,max} - P_{r,min} \tag{3}$$

$$D_{min} = P_{l,min} - P_{r,max} \tag{4}$$

$$D_r = D_{max} - D_{min} \tag{5}$$

$$DHI = \frac{D_r}{D_{mean}} \times 100 \tag{6}$$

where P_r is the position of the right bubble edge and P_l the position of the left bubble edge. The maximum, minimum and mean values were obtained from five measurements. We define a bubble as stable if the degree of instability is less than 20%, partially helical if the degree of instability is between 20-40%, and helically unstable if the degree of instability is greater than 40% .

Film blowing experiments were carried out at three different values of *TUR* and at different frost line heights. Due to the limited width of the nip rolls the maximum attainable *BUR* with our apparatus was about 5. The operating conditions used for all experiments were within the range of typical industrial conditions.

2.4. Results

2.4.1. Rheological Measurements

The complex viscosities, η^*, for the four polymers used in this study at their extrusion temperature are shown in Figure 3. At low frequencies, the HDPE has the highest viscosity and the PP, the lowest. The HDPE is more shear-thinning and does not depict a plateau in the low frequency region. At high angular frequencies, the viscosities of the HDPE and the LLDPE are about the same and those of the LDPE and the PP are identical. The zero shear viscosities (η_0) were determined using the Carreau-Yasuda model (Bird et al., 1987) and are reported in Table 1.

Figure 4 reports data of the storage modulus, G', for the four melts. The most elastic melt is the HDPE followed by the LLDPE, the LDPE and the PP. Using these linear viscoelastic data, we can obtain a characteristic relaxation time for the melts, defined by:

$$\lambda\ (\omega) = \frac{G'}{G''\ \omega} \tag{7}$$

and the values are reported in Figure 5. The behavior described by the relaxation times of these melts is quite similar to that of the complex viscosities. At high frequencies the relaxation times of the melts are close to each other. However, at low frequencies, they are quite different; the HDPE has the highest relaxation time and the PP, the lowest, in the same order as the viscosity and the storage modulus. Note that no plateau for λ is observed indicating that the terminal zone for these polymers has not been reached at the lowest frequencies.

2.4.2. Bubble Instabilities

In general, three forms of instabilities and combinations were observed as follows : (a) axisymmetric periodic variations of the bubble diameter, (b) helical motions of the bubble, and (c) variations in the position of the solidification line. We call the first two forms of these instabilities, after previous authors (Han and Park, 1975; Han and Shetty, 1977; Kanai and White, 1984; Minoshima and White, 1986; White and Yamane, 1987), bubble instability and helical instability respectively. However, we label the third form *FLH* instability. The term "meta-stable state" used by the previous authors for such time-dependent oscillations in *FLH* is misleading.

When the bubble was inflated by a small amount of air, i.e. at low *BUR*, a bubble instability , schematically shown in Figure 6, was observed. This did not appear with the LDPE and the HDPE. No distinct *FLH* was recognizable and the pressure inside the bubble also fluctuated. The magnitude of the diameter fluctuations increased with time and eventually lead to bubble breakage, as already reported by Minoshima and White (1986).

A *FLH* instability was observed for different operating conditions with the HDPE, the LLDPE, and the PP. Due to the frost line height fluctuations, the pressure inside the bubble oscillated and the bubble diameter changed slightly following the frost line height fluctuations. For similar conditions Minoshima and White (1986) observed fluctuations in the bubble tension and Fleissner (1988) noticed significant thickness variations of the film.

Helical instability taking place at high *BUR* was observed with all the polymers. A helical motion develops between the die exit and the nip rolls, as schematically depicted in Figure 2. In this case, the pressure inside the bubble remained nearly constant.

FLH instability usually grew with time and then combined with helical instability and eventually caused the collapse of the bubble. Helical motion of the bubble normally developed when the frost line height moved from the upper limit to the lower one. In the case of the LLDPE and the PP, other types of instabilities were observed leading to the collapse of the bubble.

2.4.2.1. Stability Behavior of LDPE

The instability behavior of the LDPE, the HDPE, the LLDPE, and the PP resins is discussed with the help of diagrams of the *FLH* versus the *BUR* for the three *TUR* values studied. Figure 7 shows the bubble stability behavior for the LDPE. The symbols on the graphs represent operating conditions. In all cases the bubble is very stable (○ symbols), except for a small unstable space (▽ symbols) at low *TUR* and intermediate *BUR* when the *FLH* is between 150 and 250 mm. As the *TUR* increases, this unstable space, corresponding to partially helical instability, disappears. Furthermore, at high *BUR* there is a minimum *FLH* for which the bubble is stable. Below this *FLH* value, the bubble is very close to the air ring and helical motions develop for all of the polymers investigated. In the case of the LDPE this minimum *FLH* is about 150 mm at a *BUR* value of 4. This instability may probably be caused by high axial force exerted on the bubble due to the cooling air flow at low *FLH*. Campbell et al. (1992) have measured the axial force acting on a non-deformable model bubble. They have shown that the air jet produces a significant axial force on the model bubble when the forming region is very close to the air ring.

As the *TUR* value increased to 10.8 and 15.5, an interesting phenomenon was observed. As seen in Figure 7 we could not obtain operating points in the hatched area. This area starts from a *BUR* value of about 3 for *TUR* = 10.8 and from a *BUR* value of about 2 for *TUR* = 15.5 and gets wider when increasing *TUR* and/or *BUR* values. In this region, it was

observed that a very small change in the cooling air flow rate drastically changed the *FLH* value and no stable bubble with a *FLH* value of 200 mm could be obtained. Figure 8 shows the diagram of the FLH versus the cooling air flow rate at a BUR value of 4.0 and a *TUR* value of 10.8. The amount of air inside was adjusted to maintain a constant *BUR*. From this figure we see that as the cooling air flow rate is increased, the *FLH* value decreases along the upper line (path (1)) until a flow rate of 0.160 m^3/s is reached corresponding to a *FLH* value of 290 mm. At that point any small increase in the air flow rate will bring down the *FLH* to 150 mm. Then, as the cooling air flow rate is decreased, the *FLH* slowly increases along the lower line (path (2)) until a flow rate of 0.146 m^3/s is reached. Any slight decrease of the air flow rate below this point will bring back the *FLH* to 400 mm.

Any point inside the space bound by these two steady-state limits represents unstable *FLH*. For example, if one tries to operate at a *FLH* equal to 250 mm, as shown in Figure 8 by the cross point, the conditions will be unstable: a pulse increase in the cooling suddenly makes the *FLH* fall until the *FLH* reaches 150 mm; on the other hand, a sudden pulse decrease in cooling makes the *FLH* increase until it reaches 330 mm. These unstable operating points should not be confused with unstable bubble shapes as mentioned before. Furthermore, it is obvious from the figure that at the same cooling air flow rate, two possible *FLH* values exist. In other words, there are multiple stable steady-state conditions at which film blowing may operate. Multiple steady-state solutions were predicted by Pearson and Petrie (1970) for the isothermal film blowing of a Newtonian liquid. They obtained two *BUR*

values for specified bubble pressure, *FLH*, and *TUR*. Cain and Denn (1988) have more recently predicted multiple and non-existing solutions for the film blowing of Newtonian, upper convected Maxwell as well as Marrucci fluids. However, their results were obtained assuming specified values for the take-up force and the bubble pressure (the take-up velocity and the amount of inflating air were controlled in our experiments as in industrial film blowing conditions). The results of Cain and Denn (1988) could not show multiple and non-existing solutions for these conditions.

Similar results are reported in Figures 9 and 10 for different *TUR* and *BUR* values. In these cases the amount of air inside the bubble was kept unchanged and consequently there were slight *BUR* changes corresponding to changes in the *FLH*. At high *BUR*, the bubble was unstable for very low *FLH* values, and a stable bubble was obtained at high *FLH* (see Figure 10).

2.4.2.2. Stability Behavior of HDPE

The stability behavior of the HDPE is shown in Figure 11. One can see that at low *TUR* value of 4.5 interrelation between *BUR* and *FLH* plays an important role in the stability of the bubble. At *FLH* = 200 mm, the bubble is stable up to a *BUR* value of about 2.5 (○ symbols), afterwards helical instability (▽ and □ symbols) appears. The behavior at *FLH* = 290 mm is quite different; up to a *BUR* value of about 2.7 the bubble is stable, then it

becomes unstable up to a *BUR* value of about 3.5 and after that, it becomes stable again. At a *FLH* value of about 350 mm the bubble is stable up to a *BUR* value of about 4.2 and then helical instability appears. For frost line heights greater than 400 mm, the bubble is stable for the entire experimental range of the *BUR*.

Figure 11 also shows a region of *FLH* and helical instabilities at low *FLH*. As the *BUR* increases this unstable space extends to the higher frost line heights. The two regions of helical instability, observed at *TUR* = 4.5, are totally suppressed at *TUR* = 16.7. However, the region of *FLH* and helical instabilities extends to the higher frost line heights. No distinct and precise boundaries between stable and unstable regions can be drawn for the *TUR* values of 11.7 and 16.7. Some stable points overlap or even coincide with unstable points, that is a switch from stable to unstable state with a slight change in the process conditions. In fact, this phenomenon was observed in a few cases in our experiments; a stable bubble became unstable by disturbing the cooling conditions or the amount of air inside the bubble and the *FLH* fluctuations increased. However, after a while the fluctuations started to decay and finally a stable bubble was restored. This uncertainty in the boundary between the stable and unstable states was more pronounced at *TUR* = 16.7, so that a transient space between the two regions is assumed.

2.4.2.3. Stability Behavior of LLDPE

As illustrated in Figure 12, all the three forms of instability were observed in film

blowing of the LLDPE resin. This polymer is relatively stable at low *TUR* for a *BUR* value varying from 1 to 4.5. Below *BUR* of unity bubble instability (*BI*) is observed, as described in Figure 6, and above a *BUR* value of 4.5 the *FLH* instability appears. Furthermore, a helically unstable space similar to that observed for the LDPE, but larger, is observed at intermediate *BUR* values.

The stable operating space is strongly deteriorated by increasing *TUR*. Although the helically unstable space disappears, the bubble stability is extremely limited by the other types of instabilities. These instabilities are extended to lower *BUR* so that the maximum attainable *BUR* at *TUR* = 15.5 is about 2.6. It also appears that the range of the *FLH* for which the bubble is stable decreases with increasing *TUR*. As shown in Figure 12, a region of bubble and *FLH* instabilities was detected at low *FLH*. Only a few stable data points were obtained at *TUR* = 15.5, because of the highly unstable behavior of the LLDPE and the limitations of the cooling system. Decreasing the air flow rate from the maximum amount normally lead to highly unstable bubbles. However, bubble instability at low *BUR* is suppressed with increasing *TUR* and the minimum attainable *BUR* of about 1 at *TUR* = 4.1 is lowered to about 0.6 at *TUR* = 15.5. To illustrate the stabilizing effect of increasing *TUR*, the fluctuations of the pressure inside the bubble were measured and reported in Figure 13. The *TUR* value was first set at 4.5 (point A) and the bubble was inflated by a small amount of air. Bubble instability was then observed, with periodic fluctuations in the inflation pressure. In a second step at time B, the *TUR* value was increased to 12.0 and the fluctuations in the pressure

reading disappeared, leading to a stable bubble with *BUR* = 1.1 and *FLH* = 300 mm. Lastly at time C, the *TUR* value was changed back to 4.5 causing fluctuations in the inflation pressure to appear slowly and then degenerating in an highly unstable bubble.

2.4.2.4. Stability Behavior of PP

Figure 14 shows that the PP has the smallest film blowing operating space among the four polymers investigated. At low *TUR* values, a stable operating condition requires very low *FLH*. The bubble is stable in this space for $3.3 \leq BUR \leq 4.2$. It is expected that the bubble be stable down to a *BUR* value of 2 even though no data were obtained below *BUR*=3.4 because of the limitations of the cooling system. It appears that below a *BUR* value of 2 the bubble is unstable for the entire range of the *FLH*. Increasing *FLH* will eventually cause the bubble to become helically unstable, and then show bubble instability.

As *TUR* is increased, the stable operating space at low *FLH* disappears. Instead, bubble and *FLH* instabilities appear as in the case of the LLDPE and the HDPE. This unstable space extends to the higher *FLH* values as the *TUR* value is increased. However, a small stable operating space appears at higher *FLH*. This space is restricted to *BUR* between 1 and 2 at *TUR*=10.8 and a maximum *BUR* value of 2.2 is obtained for *TUR*=15.5. Increasing *TUR* has a stabilizing effect on the bubble at low *BUR*, as observed for the LLDPE.

2.5. Discussions and Conclusions

The LDPE was found to have the largest operating space whereas the PP had the smallest one. For the four polymers studied the relative order of stability is as follows:

$$\text{LDPE} > \text{HDPE} > \text{LLDPE} > \text{PP}.$$

As far as we are aware there are no data in the literature on the stability of PP. For the other polymers, our results are in agreement with the previously published results. Comparing the stability order of these four polymers, it is obvious that bubble instabilities can not be correlated with the simple shear rheological data. We recall that it is virtually impossible to predict the extensional properties from simple shear data: film blowing is controlled by the extensional flow behavior of the material and coupling effects between heat transfer and rheological properties. The more stable behavior of the LDPE is attributed to its strain hardening in elongational flow, as reported by Kanai and White (1984) and White and Yamane (1987). The elongational behavior of the other three polymers is not as well characterized, although there are indications that linear PEs and PP are strain thinning (Kanai and White, 1984; Hingmann and Marczinke, 1994). Strain hardening elongational properties have been reported for a HDPE at low elongational rates (Fleissner, 1988). The HDPE used in our experiments is the second most stable polymer. Obviously, more work is needed to clarify the importance of strain hardening coupled with cooling effects on film blowing stability.

Regions of multiple and non-existing solutions were detected for the LDPE as the *TUR* value was increased; a slight change in the cooling air flow rate would increase the *FLH* value to an upper steady state or decrease it to a lower steady state. Bubble instability at low *BUR* was observed with the LLDPE and the PP. The mechanism of bubble instability is believed to be primarily rheological in character. Die exit effects such as extrudate swelling as well as extensional properties may play an important role on bubble stability. As the *BUR* and/or the *TUR* are increased exit effects become negligible and bubble stability is increased.

For the HDPE, the LLDPE, and the PP the instability of the film blowing process (mainly *FLH* instability) increased with increasing *BUR* and *TUR* values and decreasing *FLH* values (the effect of decreasing *FLH* on the stability was clearly seen at high *TUR*). Interestingly, the stretch rate in this process, as measured by Kanai and White (1984) for HDPE , LDPE, and LLDPE, follows the same pattern, i.e. it increases with increasing *BUR*, decreasing *FLH*, and increasing *TUR*. Therefore, we speculate that as the stretch rate (and, hence, the tensile stress) increases and reaches a critical value, instability phenomena in film blowing start to appear. We assume that at critical stretch rate a local thinning of the tubular film may happen resulting in the instability of the bubble by a mechanism proposed by Fleissner (1988). This is briefly described below.

Because of the local thinning of the tubular film in the neck zone, which is accompanied by a decrease in the drawing force, melt is accumulated in the die region since

both mass flow rate of polymer and take-up velocity are constant. However, the thinner section can be drawn more easily and cooling is more rapid resulting in a shift down of the *FLH*. Meanwhile, mass accumulation inevitably causes a thickening of the film. The thicker film can no longer be easily stretched resulting in a higher tensile force and therefore the upward shift of the *FLH*. The higher tensile stress will again thin down the tubular film in the die region and this cycle will continue and finally cause the collapse of the bubble.

Helical instability was observed with all the polymers. It usually decreased with increasing *TUR* and it also depended on the bubble shape. Air drag forces play an important role on the helical instability. At low *TUR* values , the air drag forces are comparable to the viscous forces. As a consequence, the bubble is sensitive to the drag forces. As the drag forces can vary substantially along the length of the bubble, this may cause the forces acting on the bubble to be unbalanced and consequently, lead to helical instability. With increasing *TUR*, the viscous forces become predominant and this makes the bubble less sensitive to the drag forces.

Finally, the bubble was found to be more stable as the *FLH* value was increased, except in the case of the PP at low *TUR*. This is clearly in disagreement with the suggestion of Minoshima and White (1986) who have stated that increasing the *FLH* value decreases the range of stable conditions. However, our results show an upper limit above which the bubble becomes unstable.

We finally discuss our observations on bubble stability in light of the theoretical predictions of Cain and Denn (1988) who analyzed bubble stability to infinitesimal disturbances. As mentioned in a previous paragraph, helical instability can be attributed to the existence of air drag forces. However, this term was neglected in the analysis of Cain and Denn. Therefore, it should not be expected that helical instability be predicted by their analysis. For the conditions of fixed take-up velocity and constant amount of inflating air, they predicted the occurrence of instability at very low *BUR* (about 0.3) for a Newtonian fluid. Instability in film blowing of a Maxwell fluid was also predicted at very low *BUR*, but confined to a smaller region. This instability was totally suppressed with increasing relaxation time. This is qualitatively in agreement with our experimental observations. The HDPE has a higher relaxation time than the LLDPE, as shown in Figure 5. Figure 11 shows that bubble instability at low *BUR* was not observed with the HDPE, in agreement with the model predictions. On the other hand, Cain and Denn's analysis does not provide any realistic information on the occurrence of instability at high *BUR*. They have predicted instability at high *BUR* to occur at a thickness reduction in excess of 700 for a Newtonian fluid and at a thickness reduction of about 230 for a Maxwell fluid. Increasing relaxation time did not change significantly the thickness reduction at which instability at high *BUR* appeared. In contrast, we observed instabilities at high *BUR* (*FLH* instability) for the HDPE and the LLDPE at thickness reductions as low as about 20. In summary, our experimental results are in little agreement with the predictions of Cain and Denn (1988). This stresses the need for a more realistic rheological constitutive equation, with parameters characterizing the

elongational properties of polymers, and the necessity of heat transfer considerations in the analysis of the film blowing process. In a forthcoming article we will examine the elongational flow behavior of molten polymers in film blowing using a birefringence method.

2.6. Acknowledgment

The authors wish to acknowledge financial support received from the FCAR programme of the Province of Quebec and from NSERC. We are also thankful to the anonymous reviewers for their helpful comments.

2.7. Notation

D = bubble diameter, m

D_i = inner die diameter, m

D_o = outer die diameter, m

D_r = diameter range, m

G' = storage modulus, Pa

G'' = loss modulus, Pa

M_n = number-average molecular weight, kg/kmol

M_w = weight-average molecular weight, kg/kmol

M_z = z-average molecular weight, kg/kmol

P_l = position of the left bubble edge, m

P_r = position of the right bubble edge, m

V = nip rolls speed, m/s

w = mass flow rate of molten polymer at die exit, kg/s

Greek letters

η_0 = zero shear viscosity, Pa.s

η^* = complex viscosity, Pa.s

λ = relaxation time, s

ρ = density of molten polymer at die exit, kg/m^3

ω = frequency, rad/s

Abbreviation

BI = bubble instability

BUR = blow-up-ratio

DHI = degree of helical instability

FI = FLH instability

FLH = frost line height, m

HDPE = high density polyethylene

LDPE	=	low density polyethylene
LLDPE	=	linear low density polyethylene
MI	=	melt index, dg/min
PE	=	polyethylene
PH	=	partially helical
PP	=	polypropylene
TUR	=	take-up-ratio

2.8. Literature Cited

Ast, W., "Air Cooling on Blown Film Lines," *Kunstoffe*, **64**, 146 (1974).

Bird, R.B., R.C. Armstrong, and O. Hassager, *Dynamics of Polymeric Liquids*, 2nd Ed., Wiley-Interscience , New York, (1987).

Cain, J.J., and M.M. Denn, "Multiplicities and Instabilities in Film Blowing," *Polym. Eng. Sci.*, **28**, 1527 (1988).

Campbell, G.A., N.T. Obot, and B. Cao, "Aerodynamics in the Blown Film Process," *Polym. Eng. Sci.*, **32**, 751 (1992).

Fleissner, M., "Elongational Flow of HDPE Samples and Bubble Instability in Film Blowing," *Int. Polym. Process.*, **2**, 229 (1988).

Ghijsels, A., J.J.S.M. Ente, and J. Raadsen, "Melt Strength Behavior of PE and its Relation to Bubble Stability in Film Blowing," *Int. Polym. Process.*, **5**, 284 (1990).

Han, C.D., and J.Y. Park, "Studies on Blown Film Extrusion. III. Bubble Instability," *J. Appl. Polym. Sci.*, **19**, 3291 (1975).

Han, C.D., and R. Shetty, "Flow Instability in Tubular Film Blowing. 1. Experimental Study," *IEC Fundam.*, **16**, 49 (1977).

Hingmann, R., and B.L. Marczinke, "Shear and Elongational Flow Properties of Polypropylene Melts", *J. Rheol.*, **38**, 573 (1994).

Kanai, T., and J.L. White, "Kinematics, Dynamics and Stability of the Tubular Film Extrusion of Various Polyethylenes," *Polym. Eng. Sci.*, **24**, 1185 (1984).

Minoshima, W., and J.L. White, "Instability Phenomena in Tubular Film, and Melt Spinning of Rheologically Characterized High Density, Low Density and Linear Low Density Polyethylenes," *J. Non-Newt. Fluid Mech.*, **19**, 275 (1986).

Obijeski, T.J., and K.R. Pruitt, "Improving the Output and Bubble Stability of Thick Gauge Blown Film," *ANTEC 92*, 150 (1992).

Pearson, J.R.A., and C.J.S. Petrie, " A Fluid-Mechanical Analysis of the Film-Blowing Process," *Plastics & Polymers*, **38**, 85 (1970).

Sweeney, P.A., G.A. Campbell, and F.A., Feeney, "Real Time Video Techniques in the Analysis of Blown Film Instability," *Int. Polym. Process.*, 7, 229 (1992).

Sweeney, P.A., and G.A. Campbell, "Blown Film Stability," *ANTEC 93*, 461 (1993).

Terry, B.W., and K. Yang, " A New Method for Determining Melt Density as a Function of Pressure and Temperature," *SPE Journal*, **20**, 540 (1964).

White, J.L., and H. Yamane, "A Collaborative Study of the Stability of Extrusion, Melt Spinning and Tubular Film Extrusion of Some High-, Low- and Linear-Low Density Polyethylene Samples," *Pure and Applied Chem.*, **59**, 193 (1987).

Yeow, Y.L., "Stability of Tubular Film Flow: A Model of the Film-Blowing Process," *J. Fluid Mech.*, **75**, 577 (1976).

Table 1. Materials used in this study and main characteristics*

Polymer	Supplier	MI dg/min	Density kg/m^3	η_0 Pa.s	M_w kg/kmol	M_w/M_n	M_z/M_w
HDPE	Du Pont 16A	0.25	946	237,000**	140,000	7.0	10.0
LDPE	Novacor LF0222-B	2.2	922	10,000**	-	-	-
LLDPE	Du Pont 12J1	1.0	924	17,100**	100,000	5.8	3.4
PP	Himont 6631	1.8	902	3,030†	-	-	-

* The molecular characteristics of the LDPE and PP were not available;
** at 180 °C;
† at 240 °C.

Figure Headings

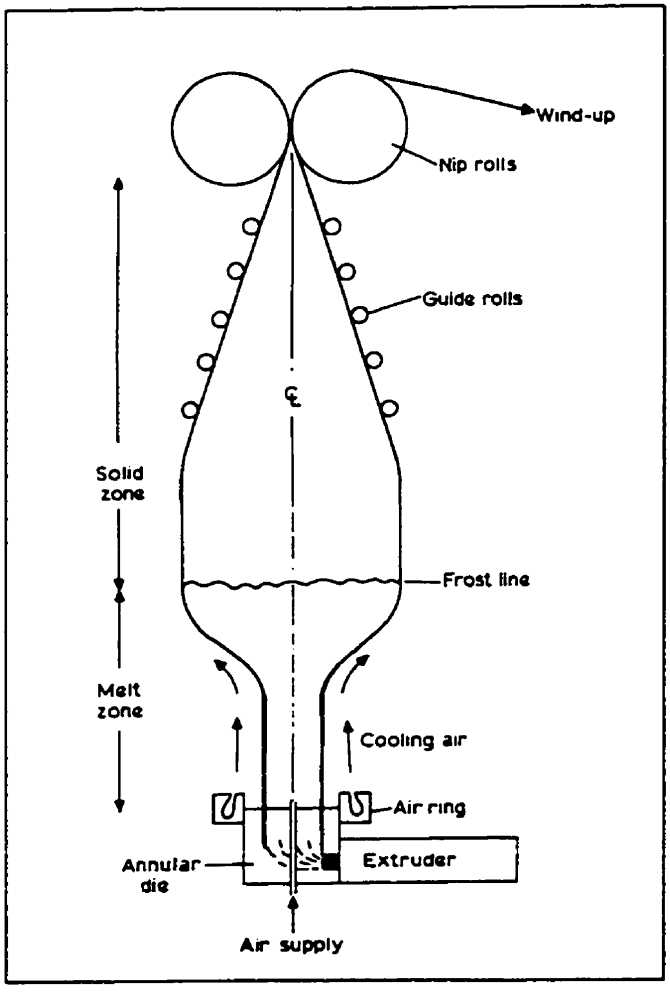

Figure 1. Blown film extrusion.

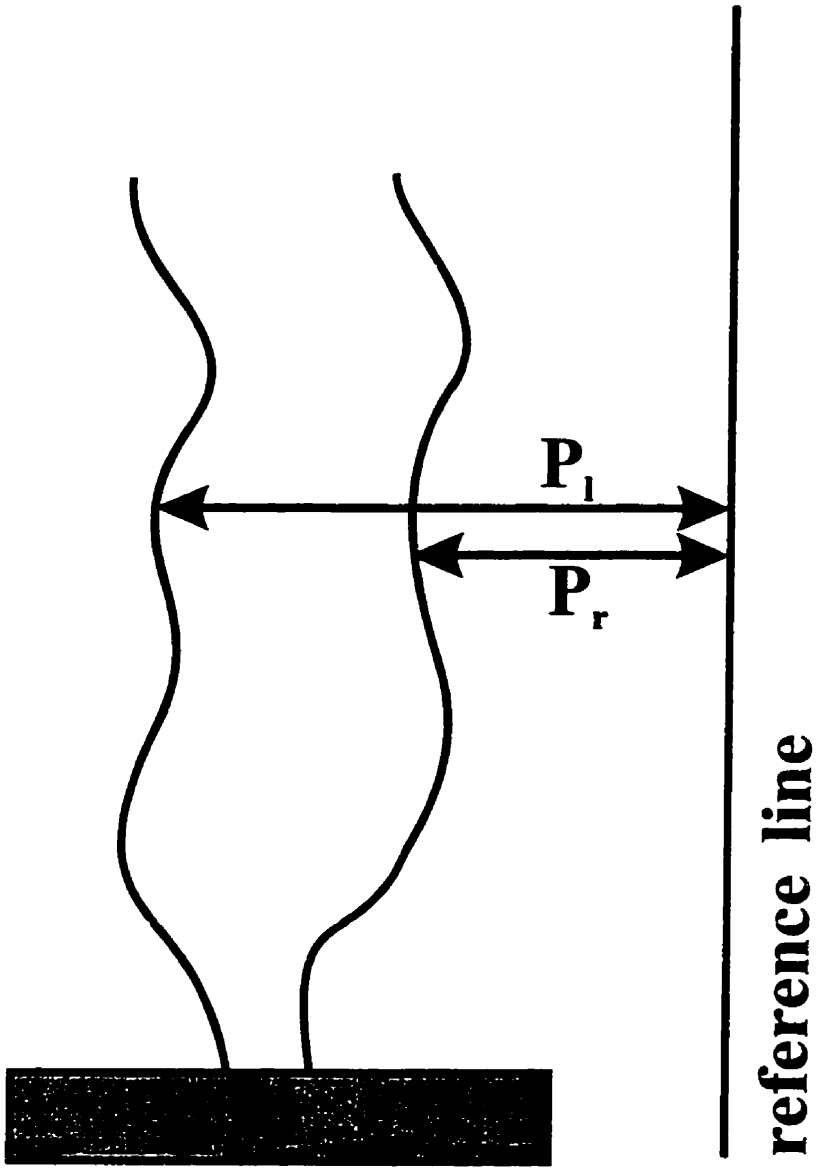

Figure 2. Bubble instability measurement.

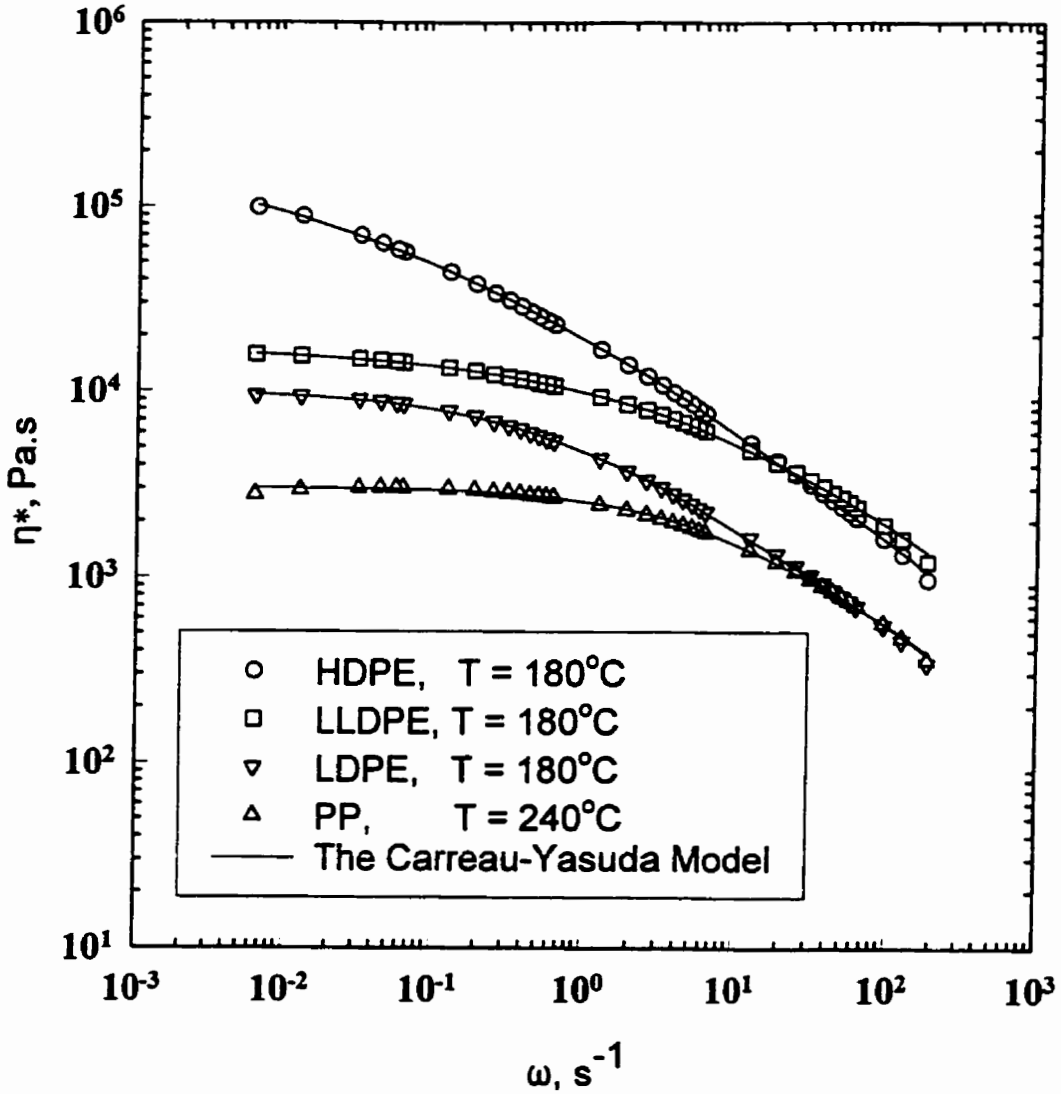

Figure 3. Complex viscosity data vs frequency for HDPE, LDPE and LLDPE at 180°C and for PP at 240°C.

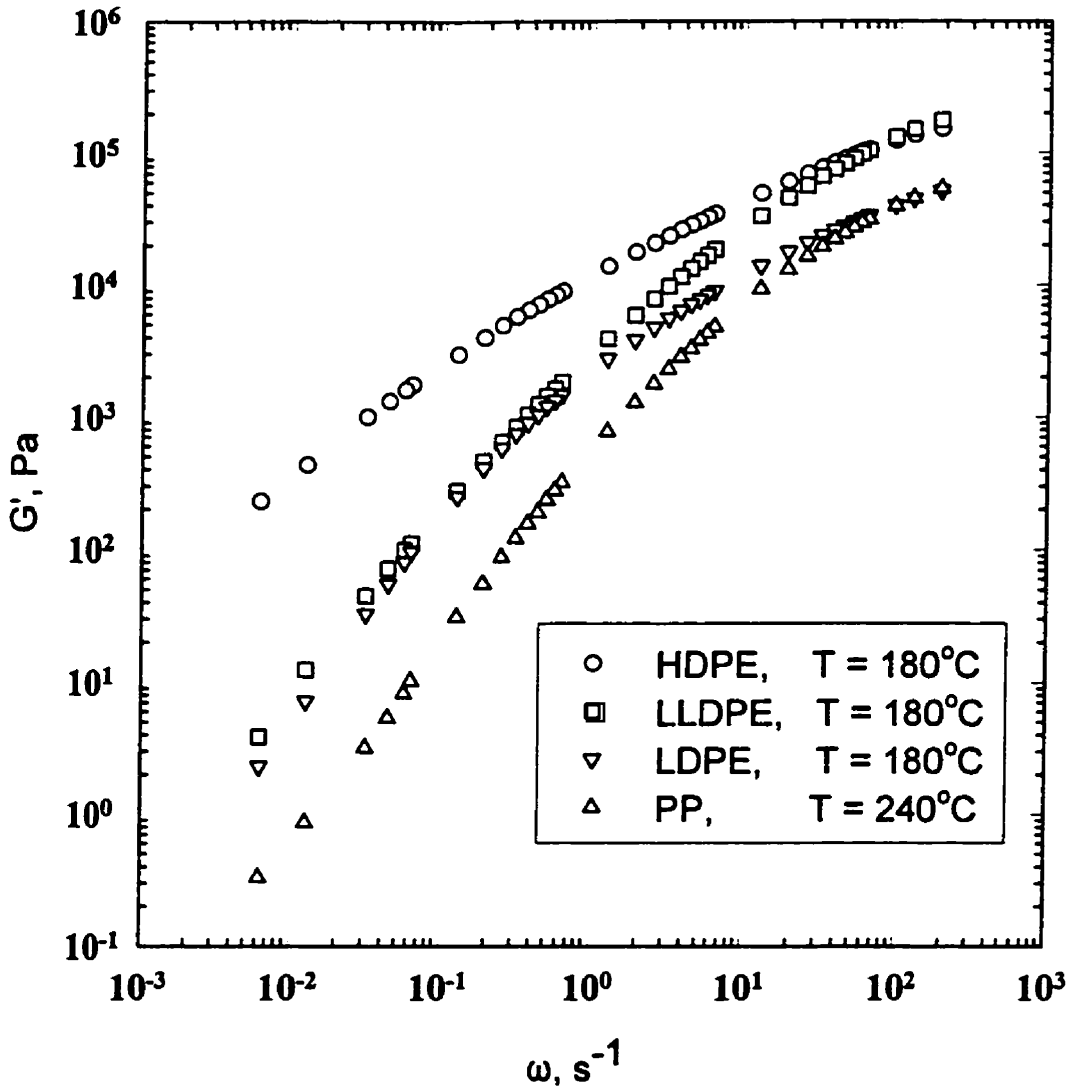

Figure 4. Storage modulus data vs frequency for HDPE, LDPE and LLDPE at 180°C and for PP at 240°C.

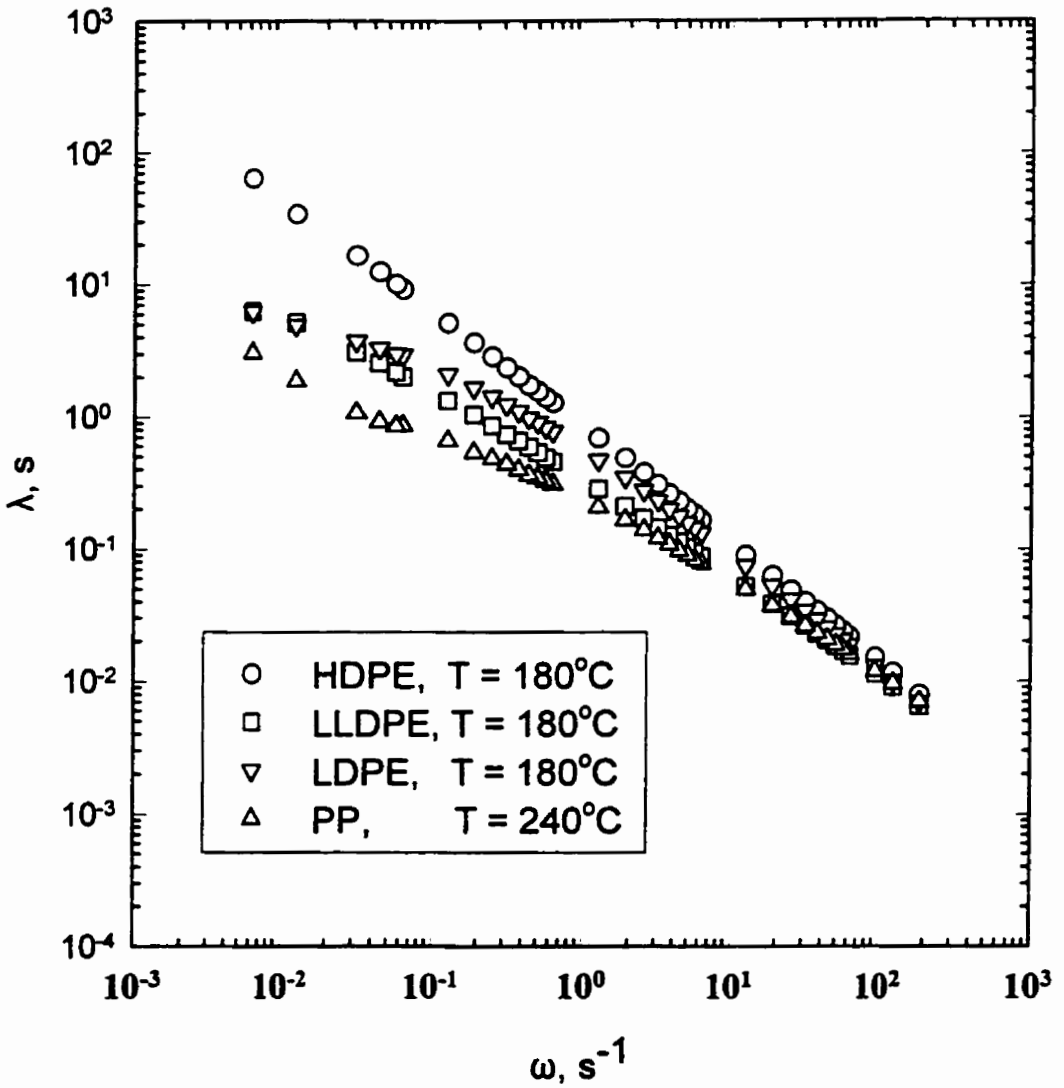

Figure 5. Relaxation time vs frequency for HDPE, LDPE and LLDPE at 180°C and for PP at 240°C.

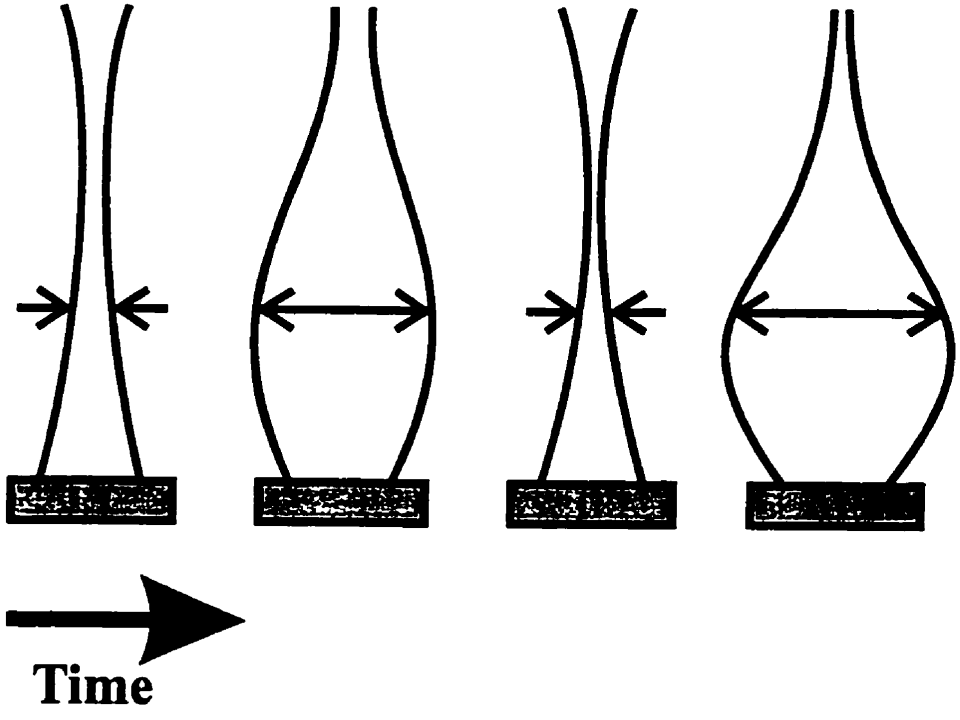

Figure 6. Bubble instability at low BUR.

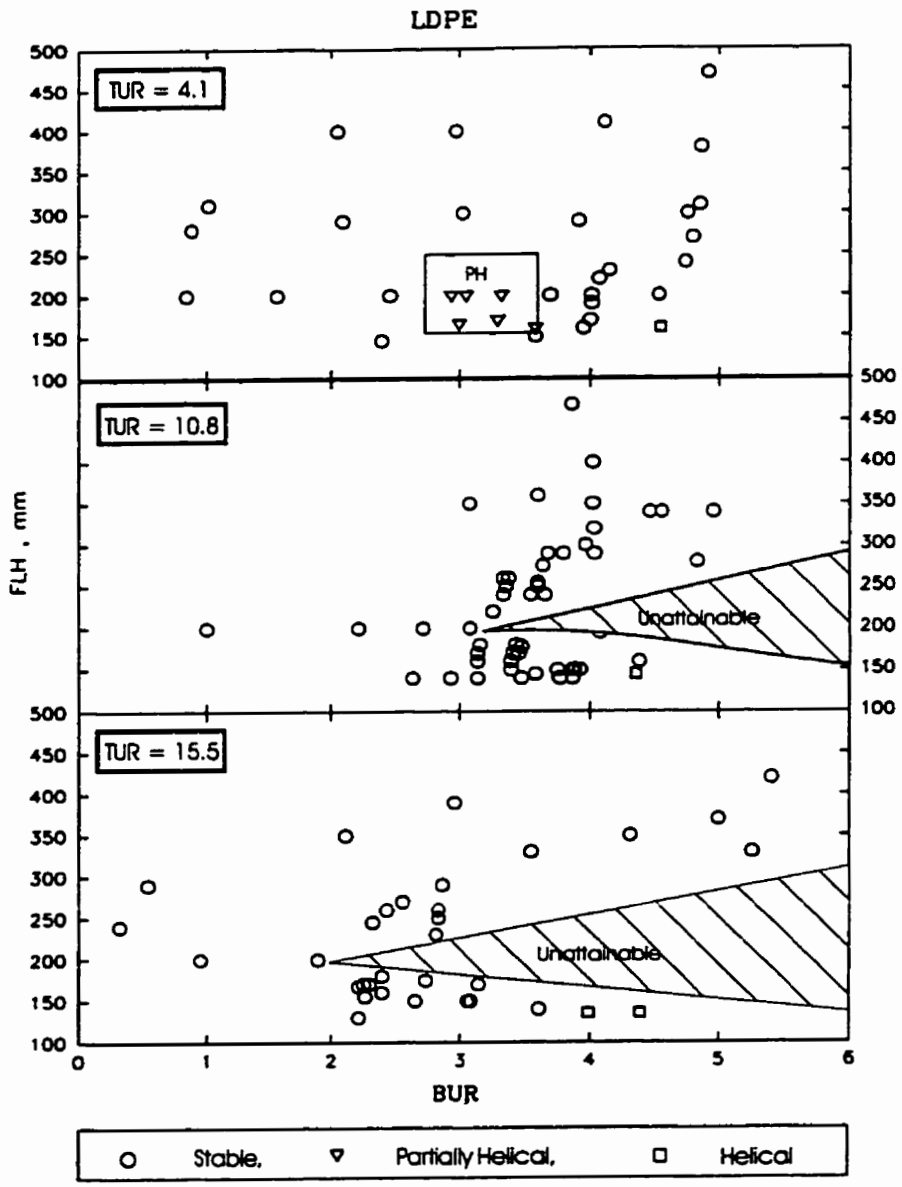

Figure 7. Bubble stability behavior of LDPE.

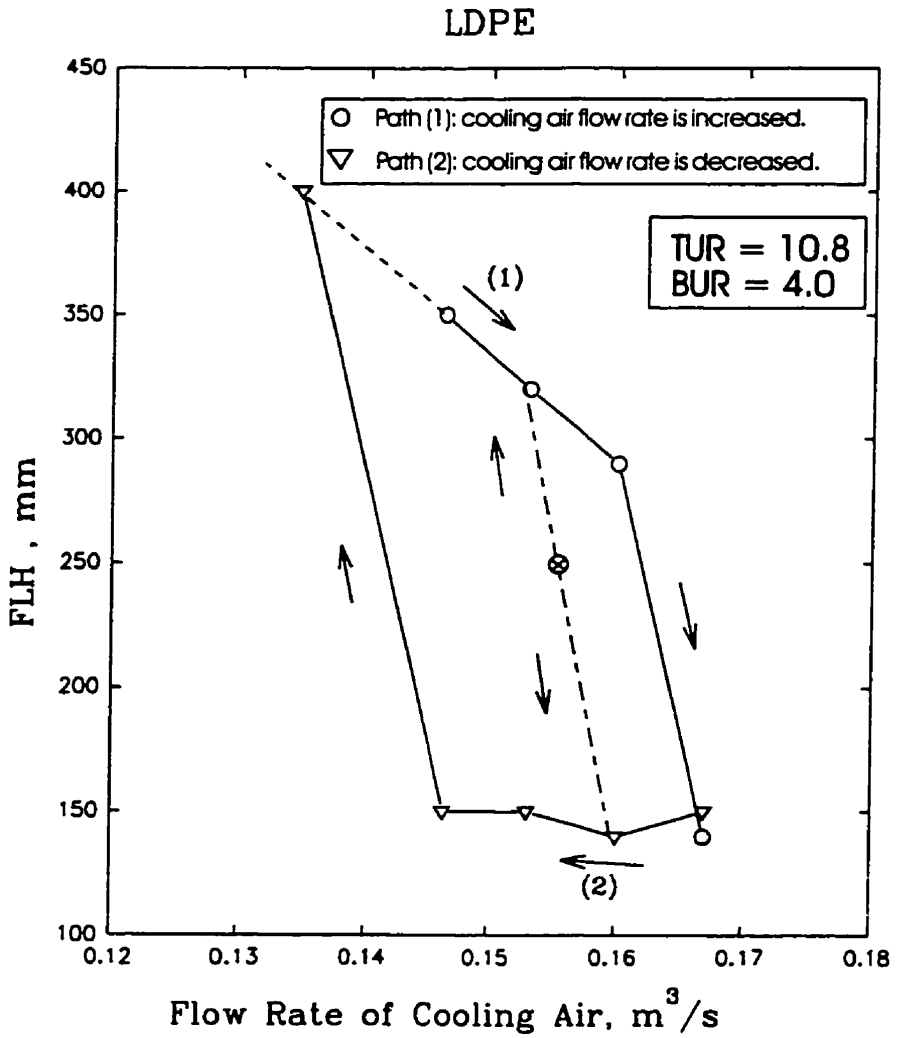

Figure 8. Multiple and non-existing solutions in film blowing of LDPE at TUR=10.8 and BUR=4.0.

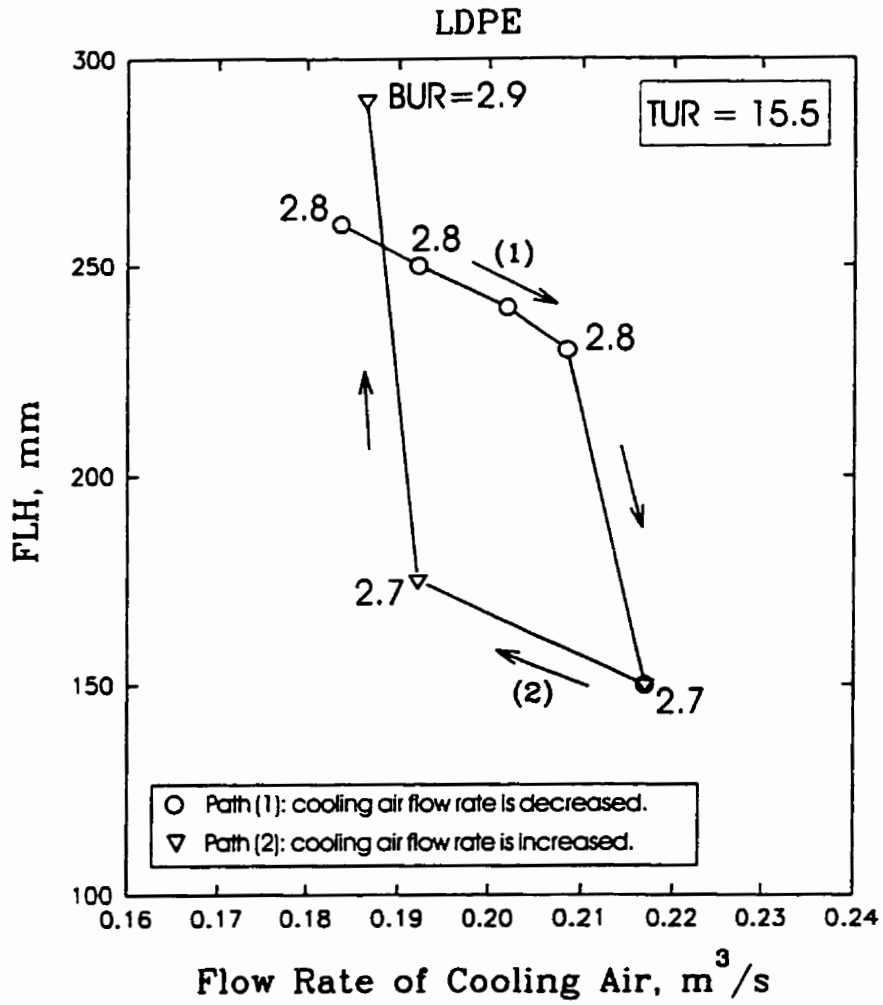

Figure 9. Multiple and non-existing solutions in film blowing of LDPE at TUR=15.5.

Numbers represent BUR values.

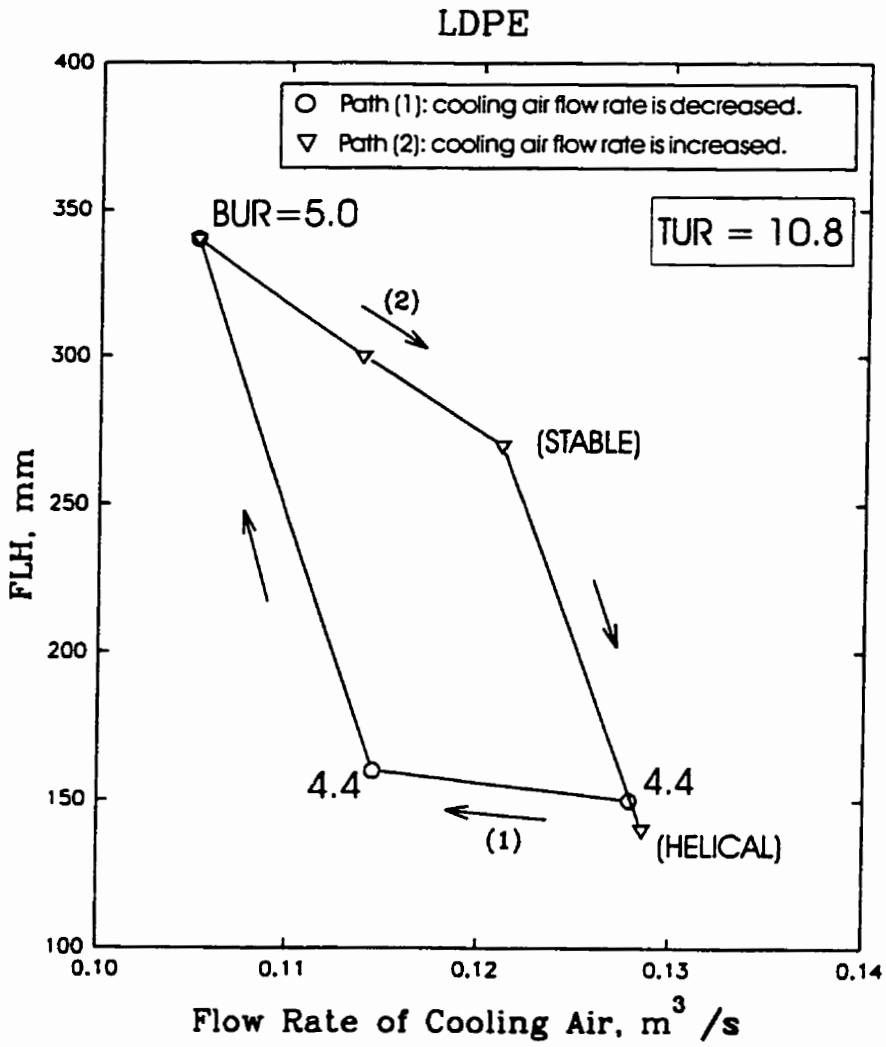

Figure 10. Multiple and non-existing solutions in film blowing of LDPE at TUR=10.8.

Numbers represent BUR values.

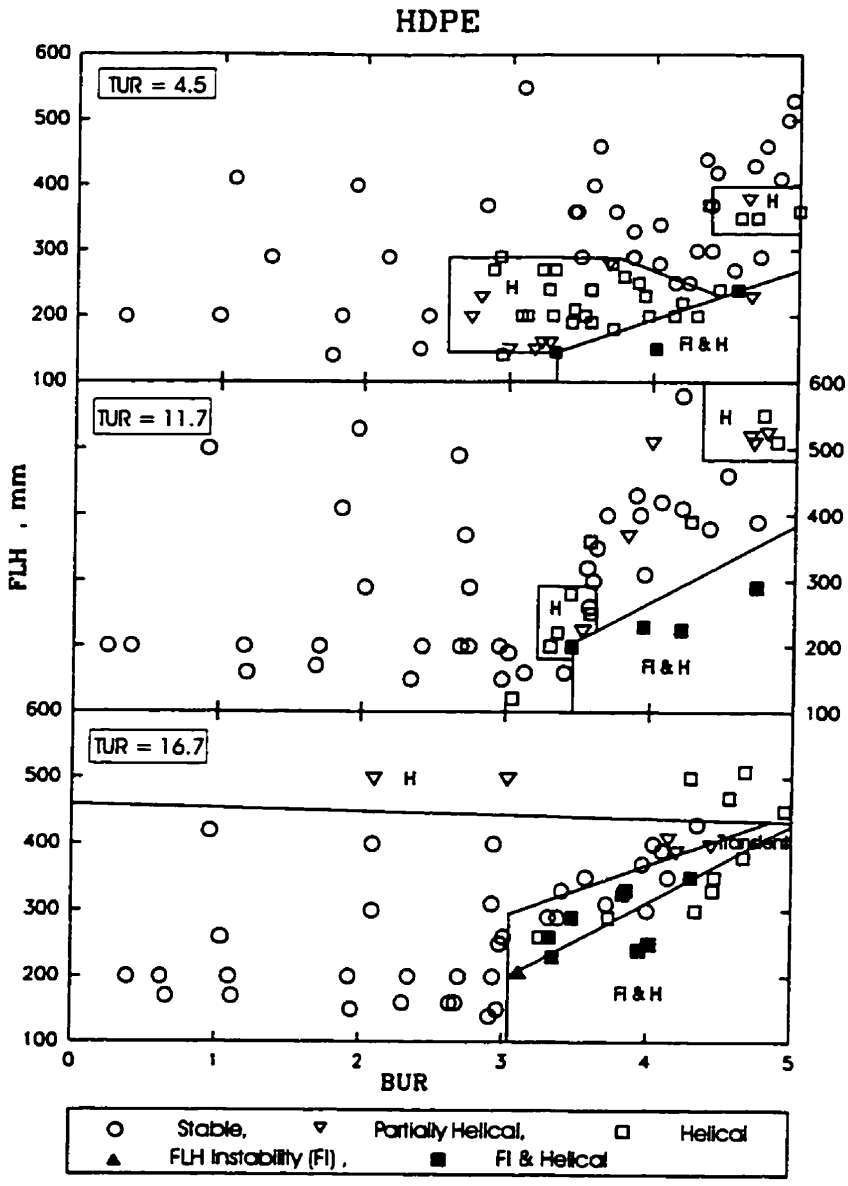

Figure 11. Bubble stability behavior of HDPE.

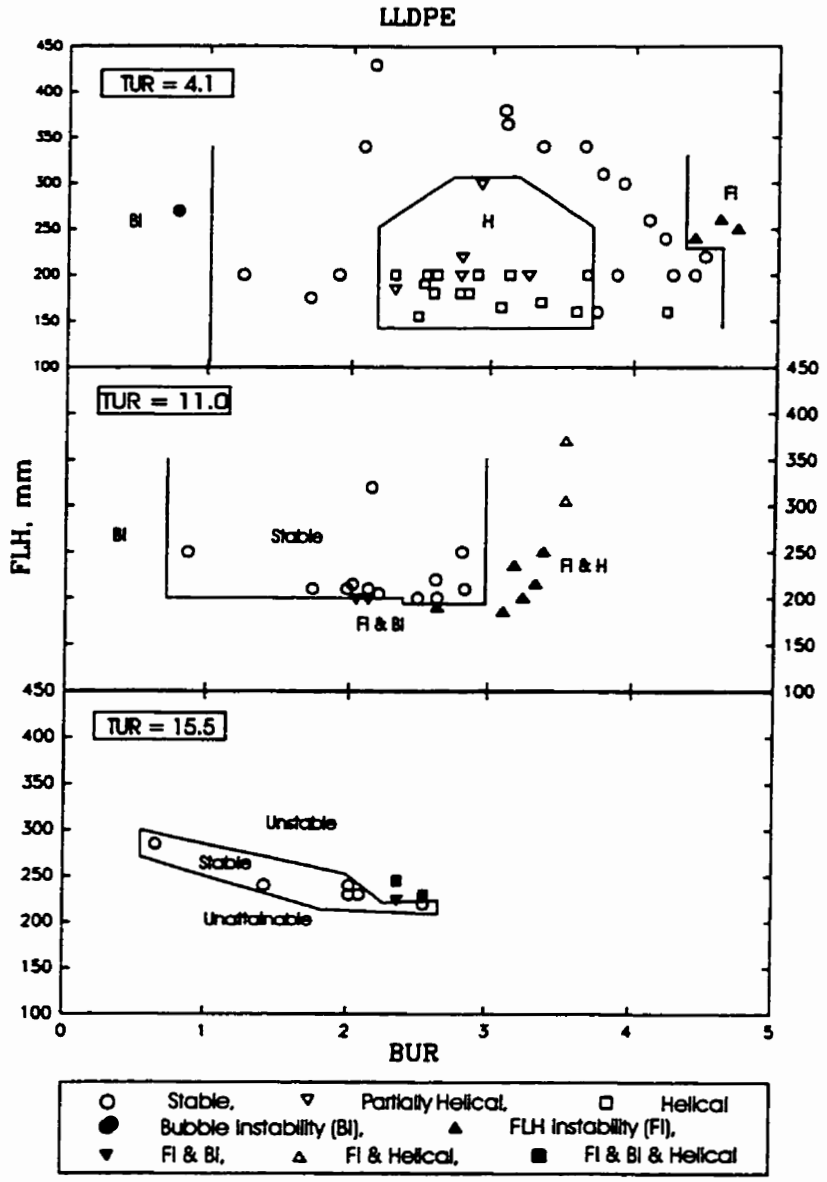

Figure 12. Bubble stability behavior of LLDPE.

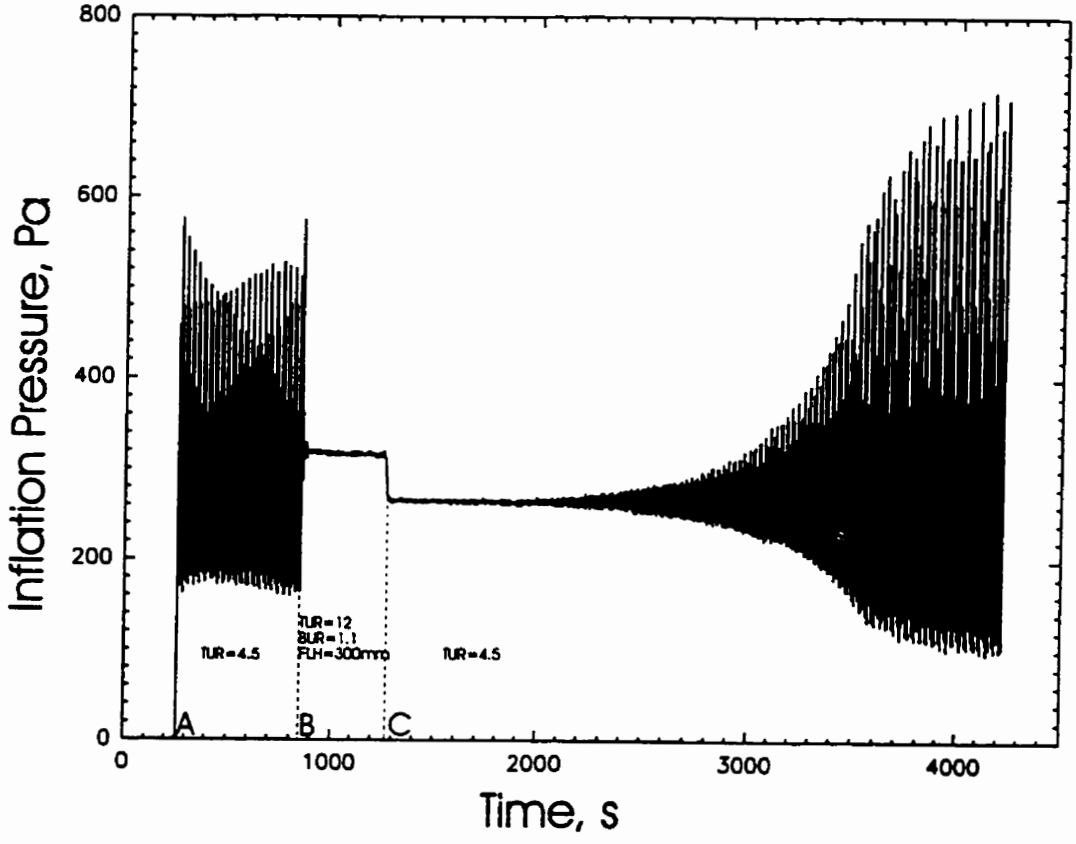

Figure 13. Bubble instability of LLDPE at low BUR.

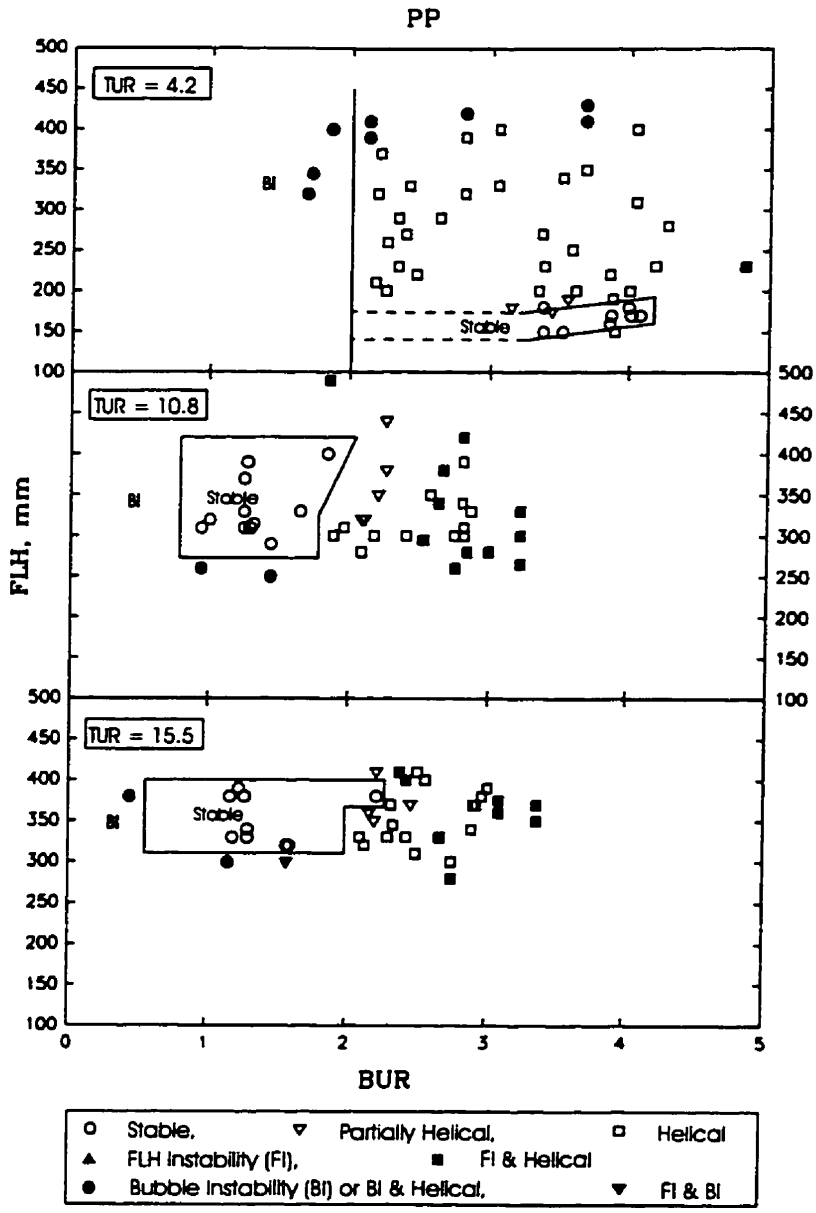

Figure 14. Bubble stability behavior of PP.

CHAPTER 3

SECOND ARTICLE:

APPLICATION OF BIREFRINGENCE TO FILM BLOWING

A. Ghaneh-Fard, P.J. Carreau, and P.G. Lafleur

Centre de recherche appliquée sur les polymères

(CRASP)

Department of Chemical Engineering

Ecole Polytechnique

PO Box 6079, Stn "Centre-Ville", Montreal, QC, H3C 3A7 CANADA

J. Plastic Film & Sheeting, January 1996, **12**, 68

Correspondence concerning this article should be addressed to P.J. Carreau.

3.1. Abstract

This paper presents a brief review of the flow birefringence technique and the analysis of the transmission of light through the blown film at oblique angle. The rheological application of the technique is based on the stress-optical law whose validity and restrictions are discussed. The technique is able to fully determine the stress tensor in the bubble by using different light paths. Preliminary results of the birefringence measurements are reported. The birefringence value is very low in the melt zone. However, it increases drastically in the vicinity of the frost line height where crystallization begins. The birefringence continues to increase above the frost line. It appears that the birefringence is highly affected by crystallization. The orientation of the crystalline phase is considerably higher than that of the molten polymer chains.

Key-Words: Film blowing, birefringence technique, molecular orientation, polyethylene.

3.2. Introduction

The film blowing process is one of the most important polymer processing operations. The process, schematically shown in Figure 1, has been extensively used over the years for the production of biaxially oriented, thin polymeric films. In blown film extrusion, the molten polymer is extruded through an annular die and the molten tube leaving the die is drawn upwards by the nip rolls. At the same time, air is introduced through an opening in the center of the die inflating the tube and forming a film bubble up to several times the diameter of the die. A cooling air ring, located just above the die directs air on the surface of the bubble.

The film blowing process is a very complex one; it involves interactions between fluid rheology, heat transfer and free surface kinematics. The film properties depend on the stresses, the rate of deformation and the thermal history encountered by the material during biaxial deformation. Depending on polymer rheology, pulling rate, blowing rate, and cooling conditions a specific level of orientation and stress-induced crystallization is developed in the film that determines the morphology of the film. This morphology then controls the ultimate optical and physical properties of the film. The extensional flow behavior of material plays an important role on the film blowing process. However, it is virtually impossible to predict the extensional properties from simple shear data. Our recent experimental results [1] show that bubble instabilities can not be correlated with the shear viscosity data: film blowing is controlled by the extensional flow behavior and heat transfer rate. There are several

publications [2-10] in the literature which discuss rheological aspects of the process from measurements of the rate of deformation and drawing force. The rate of deformation has been mostly measured by a tracer technique using a video camera. Recently Tas [9] and Michaeli and Schmitz [10] have employed the laser doppler velocimetry. The stress field in the bubble has been so far determined via force balances by measuring the bubble drawing force at the nip rolls using mechanical transducers. However, the bubble force measurement is influenced by different frictional forces during flattening of the film bubble, pinching-off and taking-up. This is the reason why the reliability of the stress data on blown film in the literature is questionable. On the other hand, the flow birefringence technique provides a non-contacting indirect measurement of the stresses occurring in the bubble, without disturbing the process. This article presents a brief review of the flow birefringence technique, an analysis of the transmission of light through blown film and results of preliminary experiments. Extensive results on birefringence measurements will be reported in a forthcoming article.

3.3. Birefringence Technique in Polymer Rheology

Birefringence or double refraction is the phenomenon observed when a light bdam passes through an optically anisotropic medium. If the linear density of the electrically charged particles of matter differs along the various directions in the body, the interaction of the light with the body will also differ with direction [11]. The incident light beam is resolved into two rays traveling at different speeds and polarized in two planes at right angle to each

other. In the case of polymer melts where the birefringence is much smaller than the absolute values of refractive indices, the two rays, so-called the ordinary and extraordinary rays, essentially follow the same path through the sample.

The flow birefringence technique is very useful for the investigation of stresses occurring in polymer flow. An advantage of this technique is that it does not disturb the flow field [14]. Other advantages, of this birefringence and other optical methods over classical mechanical methods, include faster responses, higher sensitivity to dilute components, and the ability to isolate the dynamics of separate constituents in the case of multi-component systems [11,16]. More importantly, spatially localized measurements can be carried out using optical methods. However, it should be mentioned that birefringence is an integrated effect along the direction of light beam. Therefore, only birefringence data in two dimensional fields without birefringence gradients in the direction of light beam can be collected. Optical methods require that the fluid under investigation be transparent. Another drawback of these methods is that they are indirect and stress-optical law has to be validated [12].

The rheological application of the birefringence method is based on the stress-optical law, which states that the deviatoric components of the refractive index tensor are proportional to those of the stress tensor; $n_{ij} = C\,\sigma_{ij}$, the proportionality, C, is called the stress-optical coefficient. In principle, the validity of the stress-optical law should be established for each polymer [11]. However, the stress-optical law has been proved valid for

many polymeric liquids and in different flow regimes such as steady and transient shear flow, uniaxial flow and biaxial extension [11-19]. In fact, the requirement is that both the stress and the refractive index are governed by the orientation distribution. This condition will be met as long as the flow does not change the orientation distribution, or the shape of a polymer coil, too far from the equilibrium Gaussian distribution. The failure of the stress-optical law observed for a high stress extensional flow is probably explained by chain stretching expected under these conditions. The orientation of polymer chains reaches a limiting value and the refractive index becomes constant but the polymer contribution to the stress continues to increase with the velocity gradient [11,16]. The stress-optical law will also fail when form contributions to the birefringence are present. Indeed, the form birefringence, in contrast to the intrinsic birefringence, does not arise from inherent anisotropy in the sample but rather it arises from anisotropic in the shape of constituents suspended in a medium whose refractive index is different from that of the constituents [16].

The situation in extensional experiments is not as complicated as it is in shear experiments because the directions of the principal axes are well defined. If the tensile stress, $\Delta\sigma = \sigma_{11} - \sigma_{22}$, is not too high (less than 10^6 Pa) one observes a linear stress-optical law given by [12] :

$$\Delta n = C\,\Delta\sigma \qquad \textbf{(1)}$$

where $\Delta n = n_{11} - n_{22}$ is the difference of the principal refractive indices between the stretch

and perpendicular directions, measured when the light beam is directed along axis 3. The following expression for the stress-optical coefficient, C, can be derived from theory of ideal rubber [12]:

$$C = \frac{2\ \pi}{45\ k\ T} \left(\frac{(n^2 + 2)^2}{n}\right) (\alpha_1 - \alpha_2) \qquad (2)$$

where n is the average refractive index of the material, k the Boltzmann constant, T the temperature and $\alpha_1 - \alpha_2$ the difference of polarizabilities in polymeric chains ,that is: C depends on the chemical structure of the polymer.

For a given polymer, the stress-optical coefficient is essentially independent of the molecular weight and its distribution [11,16]. It has been also found to be independent of the strain rate [19] and relatively insensitive to temperature [11,14,15,19], but may decrease with total strain [15].

3.4. Birefringence Measurement

There are a number of ways to measure birefringence [23]. In our experiments an optical train, shown schematically in Figure 2, was used, with a polarization modulation scheme based on a rotating half wave plate. The design of this optical train is outlined in Reference [21]. The elements of the apparatus are (1) a light source, which is a He-Ne gas

laser beam (λ = 632.8nm), (2) a polarization state generator (polarizer and rotating half wave plate), that defines the polarization of the light prior to transmission through the sample, (3) the blown film (sample), (4) a polarization state analyzer (circular polarizer), (5) a detector, and (6) a data acquisition system.

The birefringence measurement in film blowing faces several problems. Since it is practically impossible to place a light detector inside the bubble, the light has to be detected after passing through the two edges of the bubble. Hence, the bubble must be perfectly symmetrical and stable. However, this is a very difficult task to achieve. The other problem is that the film thickness has to be measured very accurately. Lastly, in the bubble inflating region the film is not perpendicular to the light direction, effect which should be taken into account in the analysis of the light transmission. This will be described in the next section. As far as we are aware there is only one study [20] in the literature dealing with the birefringence measurement in film blowing. That study was restricted to a blow-up-ratio of 1 to avoid the problem of oblique angle.

3.5. Analysis of the Light Transmission Through the Blown Film

The problem of the oblique direction of incident light was first analyzed by Stein [25]. Hongladarom and Burghardt [26] have recently employed the oblique transmission of light to fully determine the refractive index tensor in rheological investigations of polymeric liquids.

The analysis presented here is similar to their approach.

It is known that upon interactions of light with a material the polarization of the light is generally affected. This is detected by a polarimetry experiment. The polarization properties of light can be represented by Jones' or Stokes' vector, **A** or **S**, respectively. Normally this interaction can be described by the following linear relationships:

$$A_1 = J \cdot A_0 \tag{3}$$

and

$$S_1 = M \cdot S_0 \tag{4}$$

where **J** and **M** are the Jones and Mueller matrices and subscript (0) and (1) refer to the incident and exiting light respectively. The quantity which is measured in a polarimetry experiment is the light intensity. Hence, the Stokes vector is normally more convenient to use when analyzing a polarimetry experiment.

Our optical train consists of a cascade of optical elements, and each can be represented by a Jones or Mueller matrix. In order to analyze such an optical train the final Stokes vector of the light measured (S_f) will simply be the incident Stokes vector multiplied by the products of the Mueller matrix of each element in the train [21]:

$$S_f = M_{CP} \cdot M_S \cdot S_{PSG} \tag{5}$$

The Mueller matrix for the circular polarizer ($\mathbf{M}_{CP}$) and the Stokes vector generated by the polarization state generator (S_{PSG}) are tabulated in the literature [23]. Hence, to analyze the transmission of light through the blown film we need to derive the Mueller matrix for the blown film ($\mathbf{M}_S$). To do this we consider a light beam which is directed to the center of the bubble horizontally as shown in Figure 3.

The incident wave (light beam) gives rise to a reflected wave in the air and a transmitted (or refracted) wave in the first edge of the bubble (for simplicity the reflected wave is not shown in this figure). The refraction angle (θ_r) can be calculated by Snell's law:

$$\sin\theta_r = \frac{\sin\theta_i}{n} \qquad (6)$$

Here n is the average refractive index of the film and θ_i is the light incident angle (which is equal to the bubble inflation angle). The wave is then retarded by passing through the birefringent film of retardation δ and oriented at an angle of 0° with respect to axis 1. The incident wave from the film gives rise to a reflected wave in the film and a transmitted (or refracted) wave in the air. The wave experiences the same effects when traveling through the second edge of the bubble. Hence, the light beam totally experiences four refraction effects and two retardation effects. The Jones matrix of the sample (blown film) can be obtained by multiplication of the Jones matrices of the individual effects, that is:

$$J_S = \begin{bmatrix} t'_p & 0 \\ 0 & t'_s \end{bmatrix} \begin{bmatrix} e^{-i\frac{\delta}{2}} & 0 \\ 0 & e^{i\frac{\delta}{2}} \end{bmatrix} \begin{bmatrix} t''_p & 0 \\ 0 & t''_s \end{bmatrix} \begin{bmatrix} t'_p & 0 \\ 0 & t'_s \end{bmatrix} \begin{bmatrix} e^{-i\frac{\delta}{2}} & 0 \\ 0 & e^{i\frac{\delta}{2}} \end{bmatrix} \begin{bmatrix} t''_p & 0 \\ 0 & t''_s \end{bmatrix} \quad (7)$$

where t_p and t_s are the so-called Fresnel complex-amplitude transmission coefficients for the parallel (p) and the perpendicular (s) polarization respectively. They depend on the refractive indices of media and the light propagation angle [22]. Superscripts (′) and (″) refer to the air-film and the film-air interface respectively.

After matrix manipulations we obtain:

$$J_S = \begin{bmatrix} t'^2_p \, t''^2_p \, e^{-i\delta} & 0 \\ 0 & t'^2_s \, t''^2_s \, e^{i\delta} \end{bmatrix} \quad (8)$$

The number of coefficients are reduced by defining:

$$T_p = t'^2_p \, t''^2_p \qquad T_s = t'^2_s \, t''^2_s \quad (9)$$

We can express the Mueller Matrix for the blown system as [22]:

$$M_S = \begin{bmatrix} \frac{1}{2}(T_p^2 + T_s^2) & \frac{1}{2}(T_p^2 - T_s^2) & 0 & 0 \\ \frac{1}{2}(T_p^2 - T_s^2) & \frac{1}{2}(T_p^2 + T_s^2) & 0 & 0 \\ 0 & 0 & T_p T_s \cos(2\delta) & -T_p T_s \sin(2\delta) \\ 0 & 0 & T_p T_s \sin(2\delta) & T_p T_s \cos(2\delta) \end{bmatrix} \quad \textbf{(10)}$$

To derive the equation of light intensity we simply need to perform the matrix multiplication of Equation 5. The first element of the final Stokes vector is indeed the light intensity:

$$I = I_0 [\ 1 + A_2 \sin(4\omega t) + B_2 \cos(4\omega t)\ ] \quad \textbf{(11)}$$

where

$$A_2 = -\frac{2 T_p T_s}{T_p^2 + T_s^2} \sin(2\delta) \quad \textbf{(12)}$$

$$B_2 = \frac{T_p^2 - T_s^2}{T_p^2 + T_s^2} \quad \textbf{(13)}$$

Here I_0 is the incident light intensity. The coefficients A_2 and B_2 can be extracted by performing a fast Fourier transform. This analysis neglects imperfections in the optical elements. The retardation (δ) in Equation 12 is related to the birefringence (Δn) by the

following relation [24]:

$$\delta = \frac{2\ \pi\ \Delta n(\theta_r)\ d}{\lambda\ \cos\theta_r} \qquad (14)$$

where d is the thickness of the film and λ the wavelength.

In the case of film blowing in which the shear components of the stress tensor are assumed to be negligible, the refractive index tensor in the local rectangular Cartesian coordinate system (see Figure 3) will take the form

$$\boldsymbol{n} = \begin{bmatrix} n_{11} & 0 & 0 \\ 0 & n_{22} & 0 \\ 0 & 0 & n_{33} \end{bmatrix} \qquad (15)$$

where subscripts 1, 2, and 3 refer to the machine, normal, and transverse (tangential) directions respectively.

The refractive index tensor experienced by the light passing through the film can be obtained by a suitable coordinate frame rotation. The measured birefringence ($\Delta n\ (\theta_r)$) may then be calculated from:

$$\Delta n(\theta_r) = (\Delta_3)\ \cos^2\theta_r + (\Delta_2)\ \sin^2\theta_r \qquad (16)$$

Here, $\Delta_3 = n_{11} - n_{33}$ and $\Delta_2 = n_{22} - n_{33}$ are the two normal optical differences. Equation 16 shows that the birefringence varies as a function of the incident angle and includes contributions from the two normal optical differences. To determine these contributions, two independent values of incident angle are required. Extra data can be collected by using additional light paths, permitting a check of self-consistency of the measurements.

3.6. Experimental

3.6.1. Blown Film Extrusion and Materials

A 45 mm Killion single screw extruder with a helical blown film die (outer diameter = 50.82 mm and die gap at exit = 680 μm) was used in this study. The extrusion was carried out at a temperature of 180°C and a polymer flow rate of about 4.0 kg/h. To measure the film thickness, the whole process, i.e., screw rotation and nip rolls rotation, was stopped and the bubble was immediately solidified by blowing cooling air. The thickness profile was then measured on the frozen bubble by using a micrometer. This method was also used by Han and Park [2]. However, as suggested by Huang and Campbell [7], this may lead to some errors due to elastic recovery before freezing. More accurate thickness profile can be calculated via a mass balance using axial film velocity and bubble diameter profiles. A comparison of results using the two methods will be reported in a forthcoming article. The experimental procedure of the film blowing operations is detailed in our previous article [1]. Preliminary experiments

were carried out to demonstrate the ability of the birefringence technique for on-line characterization of structure development in film blowing.

Two different film-grade linear low density polyethylenes (LLDPE) were used in this study: Dowlex 2038 with octene co-monomer from Dow Chemical with a melt index of 1.0 dg/min and a density of 935 kg/m^3 and TUFLIN HS-7028 Natural 7 with butene co-monomer from Union Carbide with a melt index of 1.0 dg/min and a density of 918 kg/m^3.

3.6.2. Optical Train

The optical train, shown in Figure 2., was provided by Professor Fuller from Stanford University. The diode laser (Uniphase Corp.) emitted linear polarized light with a wavelength of 632.8 nm. The polarizer and the half-wave plate (Meadowlark Optics) were mounted in front of the diode laser. A saturated waveform could be obtained by rotating the polarizer in its housing relatively to the fixed diode laser which consequently changed the intensity of the laser beam. The rotation of the half-wave plate was accomplished by using an electromotor at a frequency of about 100 s^{-1}. An encoder mounted externally on the half wave device was used to register the rotation frequency. A hardware unit (Optical Analyzer Controller) transmitted this frequency. The circular polarizer (Meadowlark Optics) was placed in the housing of the detector. The laser diode and the detector were mounted on damped rods (Newport Corp.) to reduce noises in the signal. Data acquisition and control were carried out

by the ROA 1.8 software (supplied by Professor Fuller), implemented in the LabVIEW (National Instruments) , and installed on a personal computer equipped with a data acquisition board (National Instruments). The optical train was calibrated to correct for imperfections in the half-wave plate by using a polarizer as the sample. The calibration of the optical train was also done to correct the detector offset and phase offset of the waveform as well as non-zero baselines in the values of the coefficients multiplying the sin and cos harmonics of the signal (coefficients A_2 and B_2 in Equation 11). The birefringence measurement was first tested by using a quarter-wave plate as a standard sample; very good results were obtained.

3.7. Results

As seen by Equation 12, the signal produced by the optical train is proportional to $\sin(2\delta)$. Figure 4 shows the results for the thickness and $\sin(2\delta)$ along the length of the bubble in the case of the LLDPE from Union Carbide. A take-up-ratio (TUR) of 7.6, a blow-up-ratio (BUR) of 1.0 and a frost line height (FLH) of 300 mm were used in this experiment. We notice that the film thickness decreases rapidly to a final value at the FLH after which no change is observed. On the other hand, the retardation signal ($\sin(2\delta)$) first increases slowly and then increases rapidly until it reaches the maximum value of unity, which corresponds to $\delta = \pi/4$. Afterwards, the retardation exceeds the value of $\pi/4$, as shown by a decrease in the $\sin(2\delta)$ signal. This stresses the inherent problem in any birefringence measurement using monochromatic light. Since the signal produced by the optical train is a sinusoidal function

of the retardation, there can be ambiguity concerning the absolute value of the retardation. Hence, extreme care was taken in each experiment to make sure of the order of the retardation.

Using the thickness and retardation data, we calculated the in-plane birefringence (n_{11}-n_{33}) via Equation 14 and the results are shown in Figure 5. The birefringence increases very slowly up to the vicinity of the FLH where crystallization occurs. Then, it increases drastically even above the FLH where the thickness profile becomes flat. It appears that the contribution of the crystalline phase to the total orientation is much larger than that of the molten polymer. The birefringence is mainly developed during the crystallization process. Nagasawa et al. [20] observed the same trend for a high density polyethylene (HDPE), a Nylon 6 and a polybutene-1. As expected, the measured orientation angle, also reported in Figure 5, is about zero along the entire length of the bubble, indicating that the shear component of the stress tensor in 1-3 plane is negligible. These results justify our assumption that the orientation angle of the macromolecules in the film is zero. The analysis of the transmission of light at perpendicular angle through a sample oriented at non-zero angle can be found elsewhere [21].

The effect of BUR, at constant TUR and FLH values, on the birefringence profile is shown in Figure 6 for the LLDPE from Dow Chemical. For the experiment with BUR = 2.0, the maximum value of the bubble inflation angle, θ_i, was about 15°. Equation 6 then yields

θ_r =10.0° using a value of 1.49 for average refractive index of polyethylene [27]. Hence, we can see from Equation 16 that Δ_2 (= n_{22} - n_{33}) does not contribute more than 3% to the birefringence signal . The effect of the bubble inflation angle in the blowing zone is, therefore, assumed to be negligible: the birefringence measured by the light beam can be approximated with the in-plane birefringence. No noticeable differences between the birefringence values are observed in the melt zone, i.e., amorphous phase, for the experiments conducted at two different BUR values. However, it appears that the ultimate value of the birefringence decreases with increasing BUR indicating that the film becomes less anisotropic, as expected. This is in contrast with the findings of Butler and Patel [28] who carried out off-line measurements of the birefringence of the end product film of a LLDPE. They found no significant effect of BUR on the in-plane birefringence.

Figure 7 illustrates the results of the birefringence measurement for the two different LLDPEs at the same operating conditions. The birefringence profiles for two materials become somewhat different once the crystallization process begins. Ultimately, the Dowlex 2038 LLDPE reaches a higher value. This can be explained by noticing that the Dowlex 2038 LLDPE has a higher density.

3.8. Discussions and Conclusions

The flow birefringence is a non-contacting technique which can be effectively used for

on-line rheological investigation of a polymeric process. Its rheological applications are based on the stress-optical law whose restrictions were discussed. The transmission of light through the blown film at oblique angle was analyzed. The birefringence varies as a function of the incident angle and includes the contributions from the two normal optical differences.

Preliminary birefringence measurements for the film blowing of two LLDPEs illustrate that the orientation is mainly developed during the crystallization process. However, the orientation of the molecules in the molten state may have a significant effect on the direction of the crystal growth. The birefringence data below the onset of crystallization can be used to calculate the elongational viscosity providing that the stress-optical law is valid. Interpretation of the birefringence data in terms of the molecular orientation is quite difficult for semi-crystalline polymers like polyethylenes. This becomes even much more complicated when one is dealing with a biaxial extensional flow as it is the case with film blowing. Indeed, the birefringence is a measure of the total molecular orientation of a system. For semi-crystalline polymers, the birefringence results from the orientation of amorphous and crystalline phases as well as from the form birefringence. A knowledge of the intrinsic birefringence of the crystalline and amorphous regions of a semi-crystalline polymer is essential if information on the separate contributions to the total measured birefringence is to be obtained from the measured birefringence. The form birefringence has been found to contribute 5-10% of the total birefringence in polyethylenes [29]. This effect is usually neglected.

Extensive birefringence measurements are being carried out on different polyolefin resins for typical blown film conditions to clarify the influence of material parameters and process conditions on the birefringence. The results will be reported in a forthcoming article.

3.9. Acknowledgments

The authors wish to acknowledge financial support received from the FCAR programme of the Province of Quebec and from NSERC. We are also thankful to Professor G.G. Fuller from Stanford University, Professor W.R. Burghardt and Mr. K. Hongladarom from Northwestern University and Dr. A. Ajji from National Research Council of Canada for providing us with helpful information on the analysis of the transmission of light beam.

3.10. Notation

A	=	Jones Vector.
C	=	Stress-optical coefficient (m^2/N).
d	=	Film Thickness (m).
I	=	Light intensity.
J	=	Jones matrix.
k	=	Boltzmann constant (1.381×10^{-23} J/K).
M	=	Mueller matrix.

$\mathbf{n}$, n_{ij}	=	Refractive index tensor.
n	=	Average refractive index.
Δn	=	Birefringence.
$\mathbf{S}$	=	Stokes vector.
T	=	Temperature (K).
t	=	Time (s).
t_p	=	Fresnel transmission coefficient for parallel polarization.
t_s	=	Fresnel transmission coefficient for perpendicular polarization.

Greek letters

α_1, α_2	=	Polarizabilities.
δ	=	Retardation.
θ_i	=	Incident angle of light (or Bubble inflation angle).
θ_r	=	Refraction angle of light.
λ	=	Wavelength (m).
ω	=	Rotation frequency of half-wave plate (1/s).

Subscripts

(CP)	=	Circular polarizer.

(f)	=	Final.
(PSG)	=	Polarization state generator.
(S)	=	Sample.
(0)	=	Incident.
(1)	=	Exiting.

Superscripts

(')	=	Air-film interface.
(")	=	Film-air interface.

Abbreviations

BUR	=	Blow-up-ratio.
FLH	=	Frost line height (m).
LLDPE	=	Linear low density polyethylene.
TUR	=	Take-up-ratio.

3.11. References

1. Ghaneh-Fard, A., P.J. Carreau, and P.G. Lafleur, (1996) "Study of Instabilities in Film Blowing," *AIChE J.*, **42**, pp.1388-1396.
2. Han, C.D., and J.Y. Park, (1975) "Studies on Blown Film Extrusion. I. Experimental Determination of Elongational Viscosity," *J. Appl. Polym. Sci.*, **19**, pp.3257-3276
3. Wagner, M.H., (1978) "Experimental Investigations into the Analysis of the Film Blowing Process," *Kunststoffe*, **68**, pp.15-17.
4. Gupta, R.K., A.B. Metzner, and K.F. Wissbrun, (1982) "Modelling of Polymeric Film-Blowing Processes," *Polym. Eng. Sci.*, **22**, pp.172-181.
5. Winter, H.H., (1983) "A Collaborative Study on the Relation Between Film Blowing Performance and Rheological Properties of Two Low-Density and Two High-Density Polyethylene Samples," *Pure & Appl. Chem.*, **55**(6), pp.943-976.
6. Kanai, T., and J. L. White, (1984) "Kinematics, Dynamics and Stability of the Tubular Film Extrusion of Various Polyethylenes," *Polym. Eng. Sci.*, **24**, pp.1185-1201.
7. Huang, T.A., and G.A. Campbell, (1985) "Deformational History of LLDPE/LDPE Blends on Blown Film Equipment," *Advances in Polymer Technology*, **5**(3), pp181-192.
8. Huang, T.A., and G.A. Campbell, (1986) "Deformational and Temperature History Comparison for LLDPE and LDPE Elements in the Bubble Expansion Region of Blown Films," *J. Plastic Film & Sheeting*, **2**, pp.30-39.

9. Tas, P.P., (1994) *Film Blowing: from Polymer to Product*, Ph.D. Dissertation, EindhovenUniversity of Technology, The Netherlands.

10. Michaeli, W., and G. Schmitz, (1995) "Investigation of Blown Film Extrusion Using the Laser Doppler Velocimetry," *ANTEC '95*, pp.181-185.

11. Dealy, J.M., and K.F. Wissbrun, (1990) *Melt Rheology and Its Role in Plastics Processing: Theory and Application*, New York, Van Nostrand Reinhold.

12. Janeschitz-Kriegl, H., (1983) *Polymer Melt Rheology and Flow Birefringence*, Berlin, Springer-Verlag.

13. Wales, J.L.S., (1976) *The Application of Flow Birefringence to Rheological Studies of Polymer Melts*, The Netherlands, Delft University Press.

14. Van Aken, J.A., and H. Janeschitz-Kriegl, (1980) "New Apparatus for the Simultaneous Measurement of Stresses and Flow Birefringence in Biaxial Extension of Polymer Melts," *Rheol. Acta*, **19**, pp.744-752.

15. Osaki, K., N. Bessho , T. Kojimoto, and M. Kurata, (1979) "Flow Birefringence of Polymer Solutions in Time-Dependent Field," *J. Rheol.*, **23**, pp.457-475.

16. Fuller, G.G., (1990) "Optical Rheometry," *Annu. Rev. Fluid. Mech.*, **22**, pp.387-417

17. Kimura, S., K. Osaki, and M.Kurata, (1981) "Stress Relaxation of Polybutadiene at Large Deformation. Measurements of Stress and Birefringence in Shear and Elongation," *J. Polym. Sci.: Polym. Physics Edition*, **19**, pp.151-163.

18. Subramanian, R., D.R. Wilson, and J.J.C. Picot (1992) "Flow Birefringence in Polymer Rheology," *Polym. Eng. Sci.*, **32**, pp.573-578.

19. Koyoma, K., and O. Ishizuka, (1989) "Birefringence of Polyethylene Melt in Transient Elongational Flow at Constant Strain Rate," *J. Polym. Sci.: Part B, Polym. Physics*, **27**, pp.297-306.

20. Nagasawa, T., T. Matsumura, S. Hoshino, and K. Kobayashi, (1973) "Film Forming Process of Crystalline Polymer. I. Factors Inducing a Molecular Orientation in Tubular Blown Film," *Applied Polymer Symposium*, **20**, pp.275-293.

21. Fuller, G.G., and K.J. Mikkelsen, (1989) "Optical Rheometry Using Rotary Polarization Modulator," *J. Rheol.*, **33**, pp.761-769.

22. Azzam, R.M.A., and N.M. Bashara, (1979) *Elipsometry and Polarized Light*, Amsterdam, North-Holland Publishing Company.

23. Fuller, G.G., (1994) "Optical Rheometry: Optical Methods for Structure and Dynamics," Short course presented for the Society of Rheology at the 66th Annual Meeting, Philadelphia, PA.

24. Born, M., and Wolf, E., (1965) *Principles of Optics*, 3rd. Edn., Oxford, Pergamon Press.

25. Stein, R.S., (1957) "Measurement of Birefringence of Biaxially Oriented Films," *J. Polym. Sci.*, **24**, pp.383-396.

26. Hongladarom, K., and W.R. Burghardt, (1994) "Measurement of the Full Refractive Index in Sheared Liquid Crystalline Polymer Solutions," *Macromolecules*, **27**, pp.483-489.

27. Brandrup, J., and E.H. Immergut (Eds), (1975) *Polymer Handbook*, 2nd. Edn.,

Toronto, John Wiley.

28. Butler, T.I., and R. Patel, (1993) "Blown Film Bubble Forming and Quenching Effects on Film Properties," *J. Plastic Film & Sheeting*, **9**, pp.181-200.

29. Samuels, R.J., (1974) *Structured Polymer Properties*, Toronto, John Wiley.

Figure Headings

Figure 1. Film blowing process.

Figure 2. Optical train for birefringence measurement: L- light source, P- polarizer, RH- rotating half-wave plate, CP- circular polarizer, D- detector, DA- data acquisition.

Figure 3. Transmission of light through the blown film; n is the average refractive index of film ,δ is the retardation, and θ_i and θ_t are the incident and refraction angles respectively. a) general view, b) details of light path.

Figure 4. Thickness and sin(2δ) along the length of the bubble for the Union Carbide LLDPE with TUR = 7.6, BUR = 1.0, and FLH = 300 mm.

Figure 5. Birefringence (n_{11}- n_{33}) and orientation angle along the length of the bubble for the Union Carbide LLDPE with TUR = 7.6, BUR = 1.0, and FLH = 300 mm.

Figure 6. Birefringence (n_{11}- n_{33}) along the length of the bubble for the two BUR values with TUR = 7.6, FLH = 300 mm; Dowlex 2038 LLDPE.

Figure 7. Birefringence (n_{11}- n_{33}) along the length of the bubble for the two LLDPE studied with TUR = 7.6, BUR = 1.0, and FLH = 300 mm.

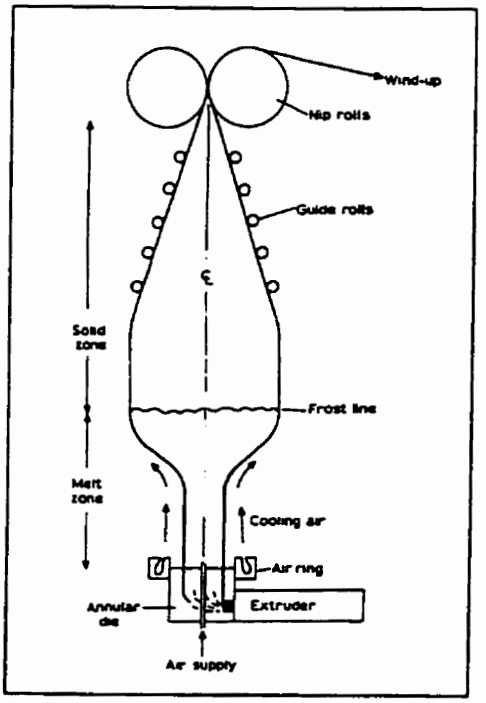

$$BUR = \frac{\text{final bubble diameter}}{\text{die diameter}}$$

$$TUR = \frac{\text{take-up velocity}}{\text{extrudate velocity at die exit}}$$

Figure 1. Film blowing process.

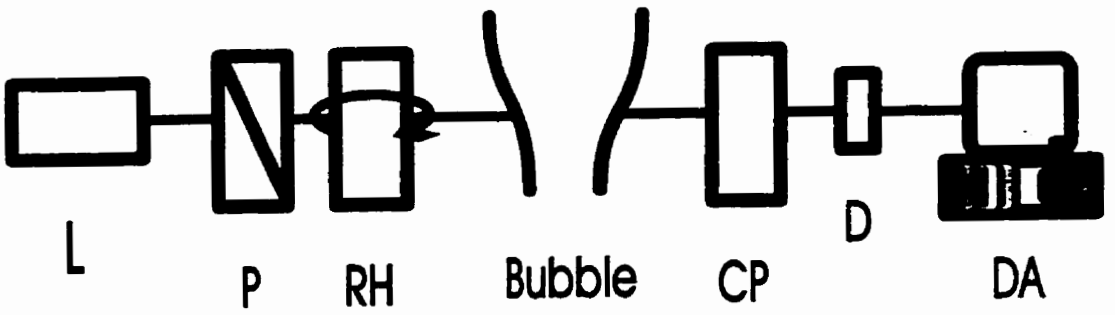

Figure 2. Optical train for birefringence measurement: L- light source, P- polarizer, RH- rotating half-wave plate, CP- circular polarizer, D- detector, DA- data acquisition.

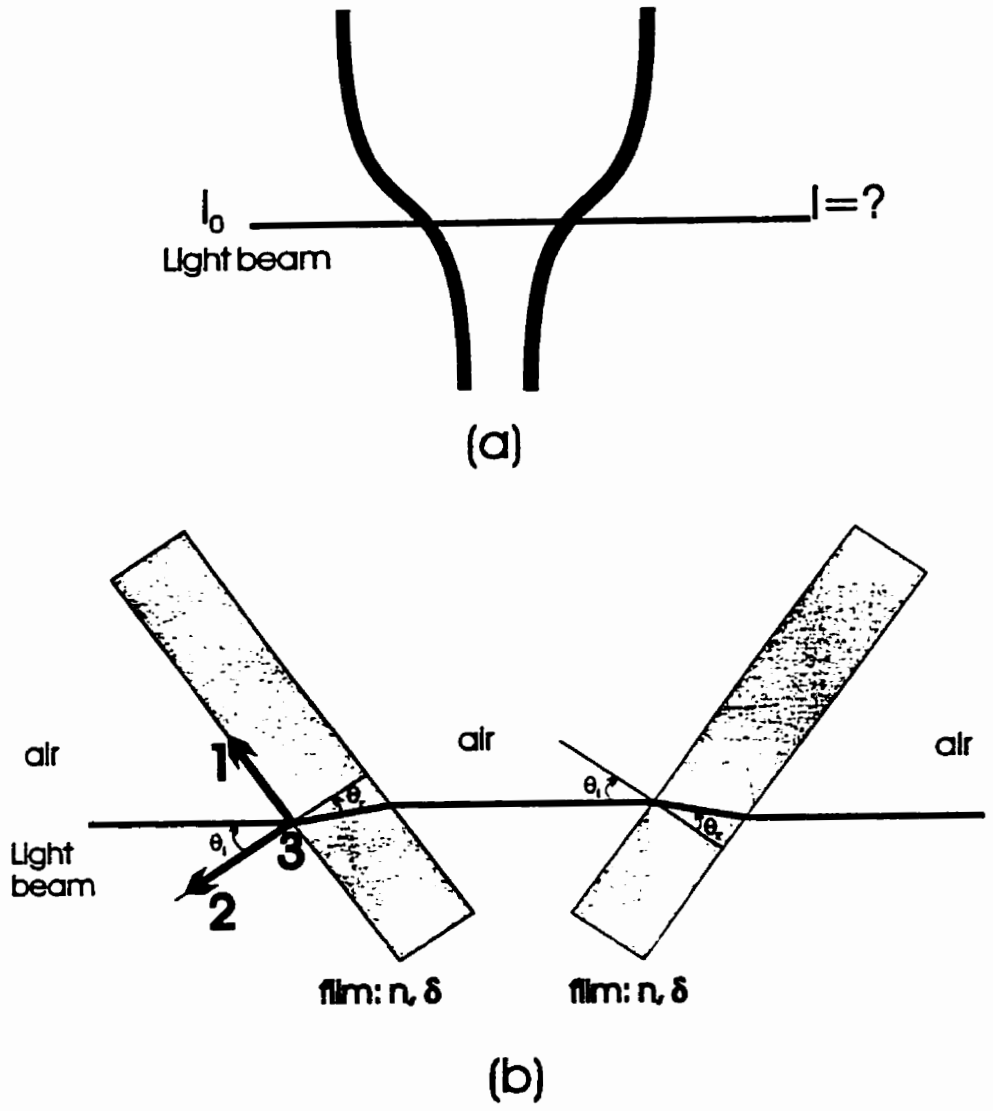

Figure 3. Transmission of light through the blown film; n is the average refractive index of film ,δ is the retardation, and θ_i and θ_r are the incident and refraction angles respectively. a) general view, b) details of light path.

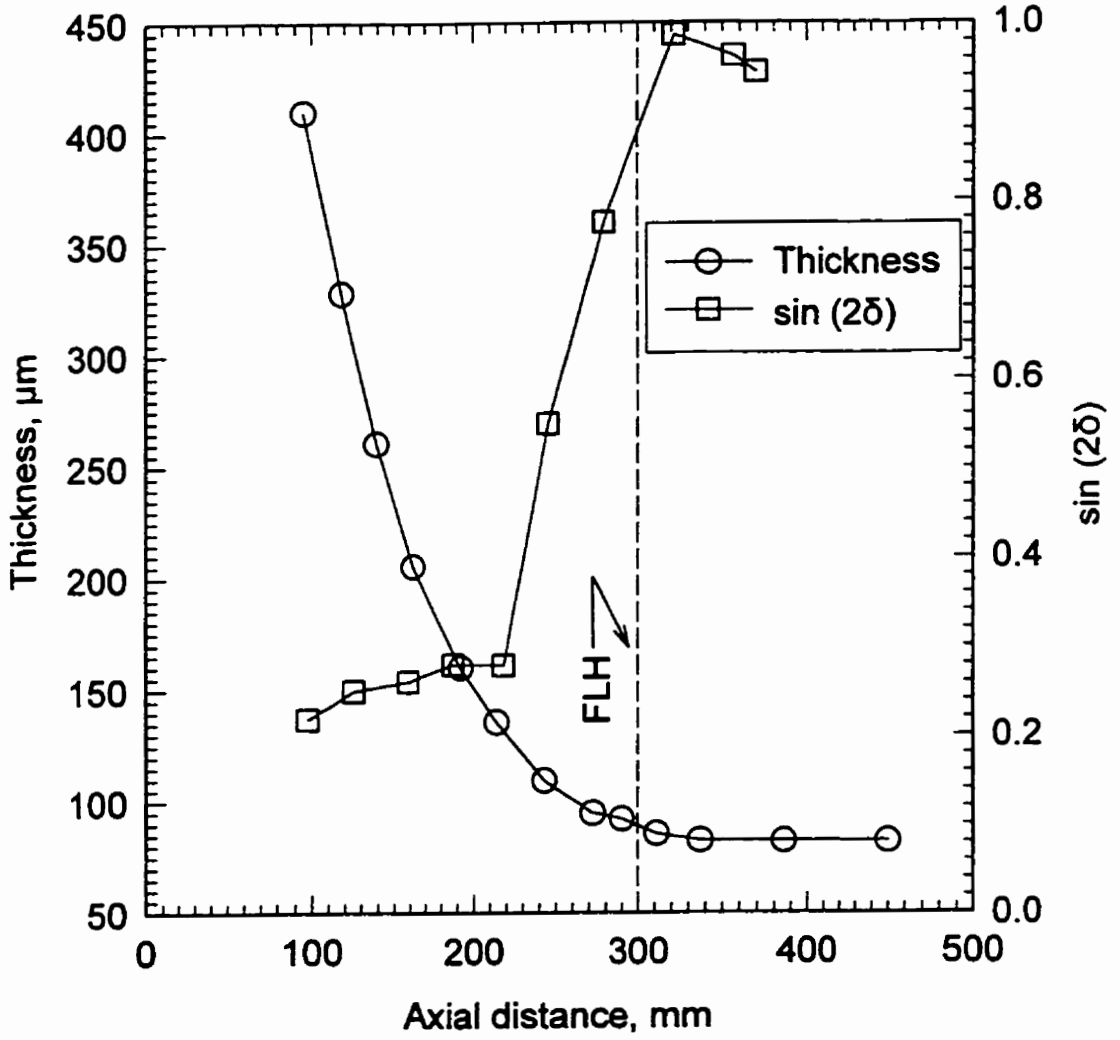

Figure 4. Thickness and sin(2δ) along the length of the bubble for the Union Carbide LLDPE with TUR = 7.6, BUR = 1.0, and FLH = 300 mm.

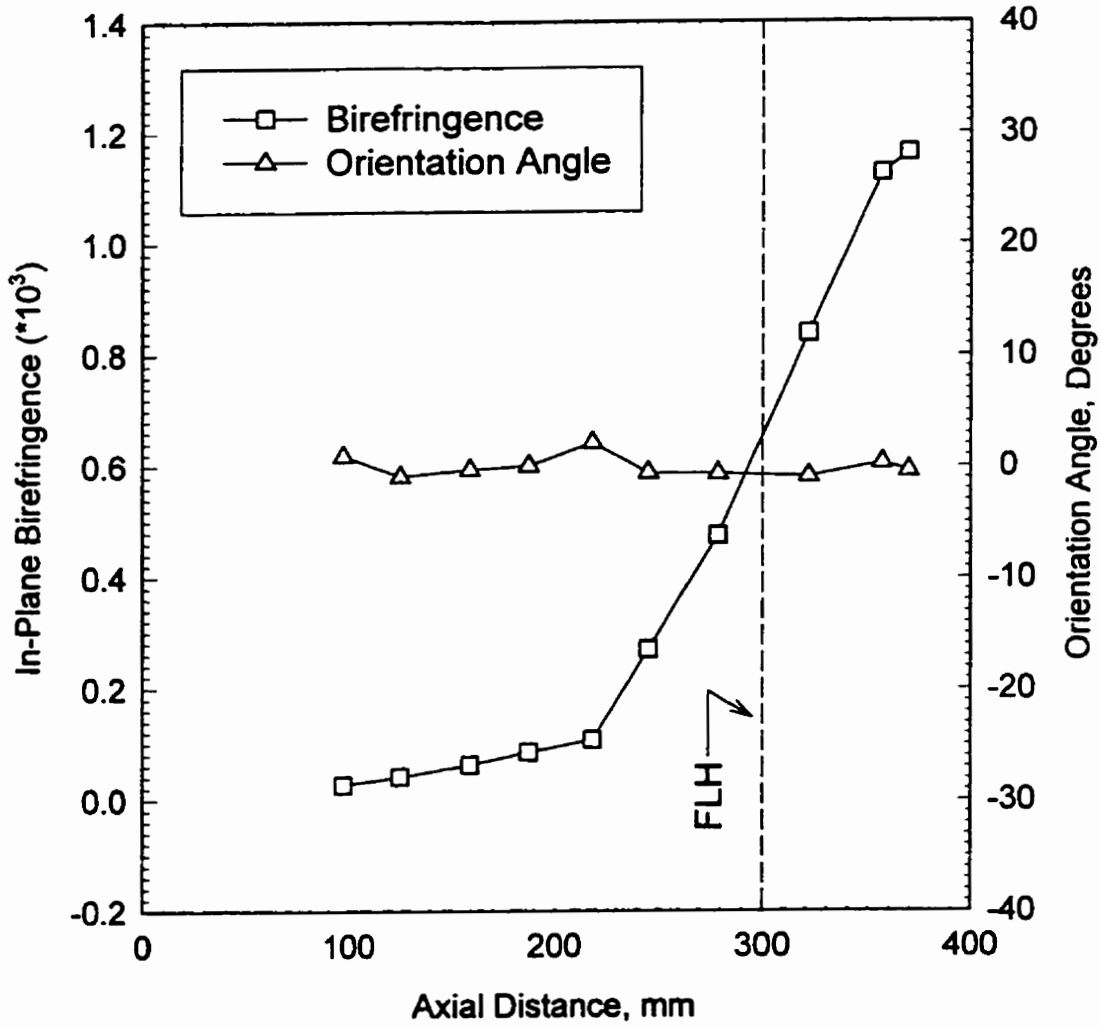

Figure 5. Birefringence (n_{11}- n_{33}) and orientation angle along the length of the bubble for the Union Carbide LLDPE with TUR = 7.6, BUR = 1.0, and FLH = 300 mm.

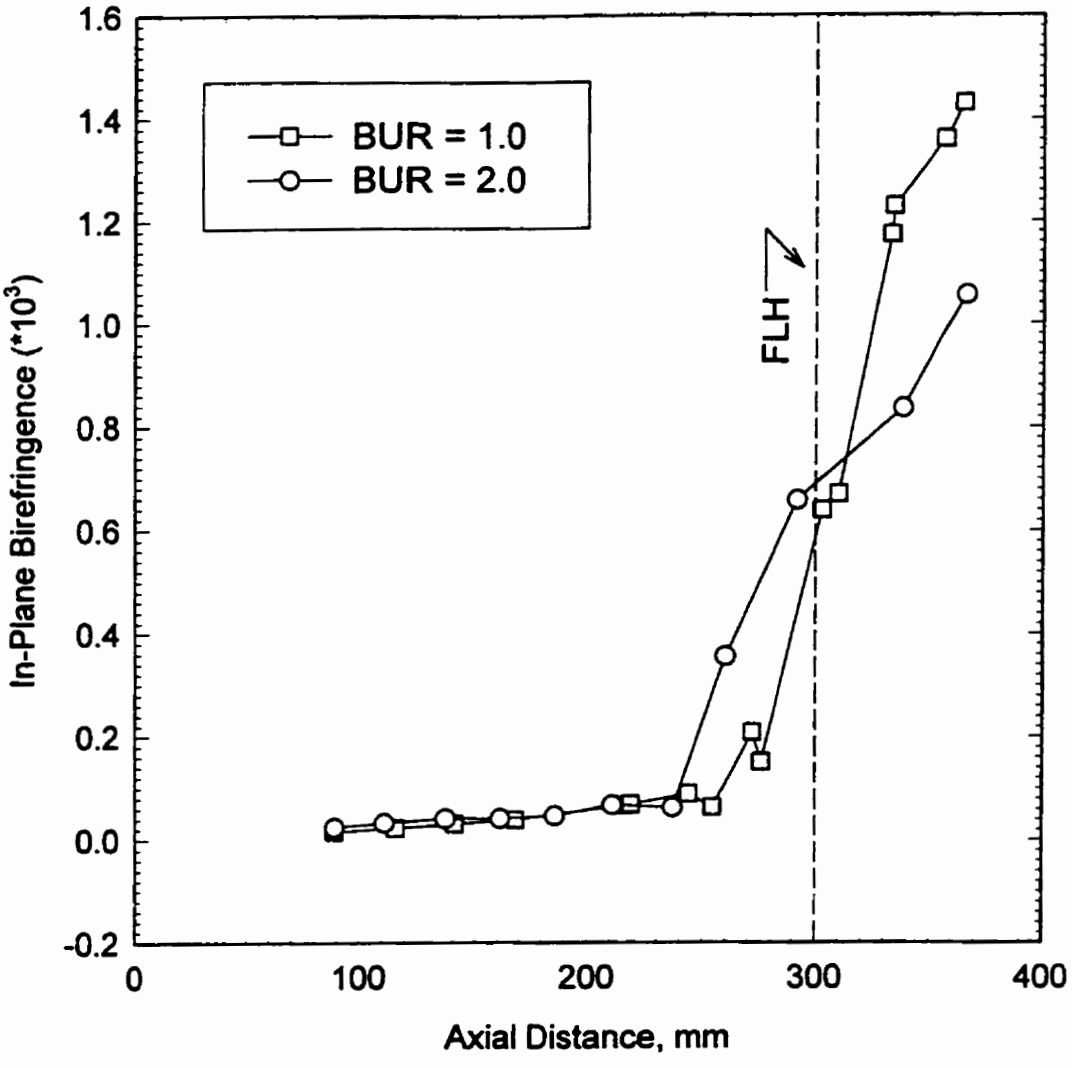

Figure 6. Birefringence (n_{11}- n_{33}) along the length of the bubble for the two BUR values with TUR = 7.6, FLH = 300 mm; Dowlex 2038 LLDPE.

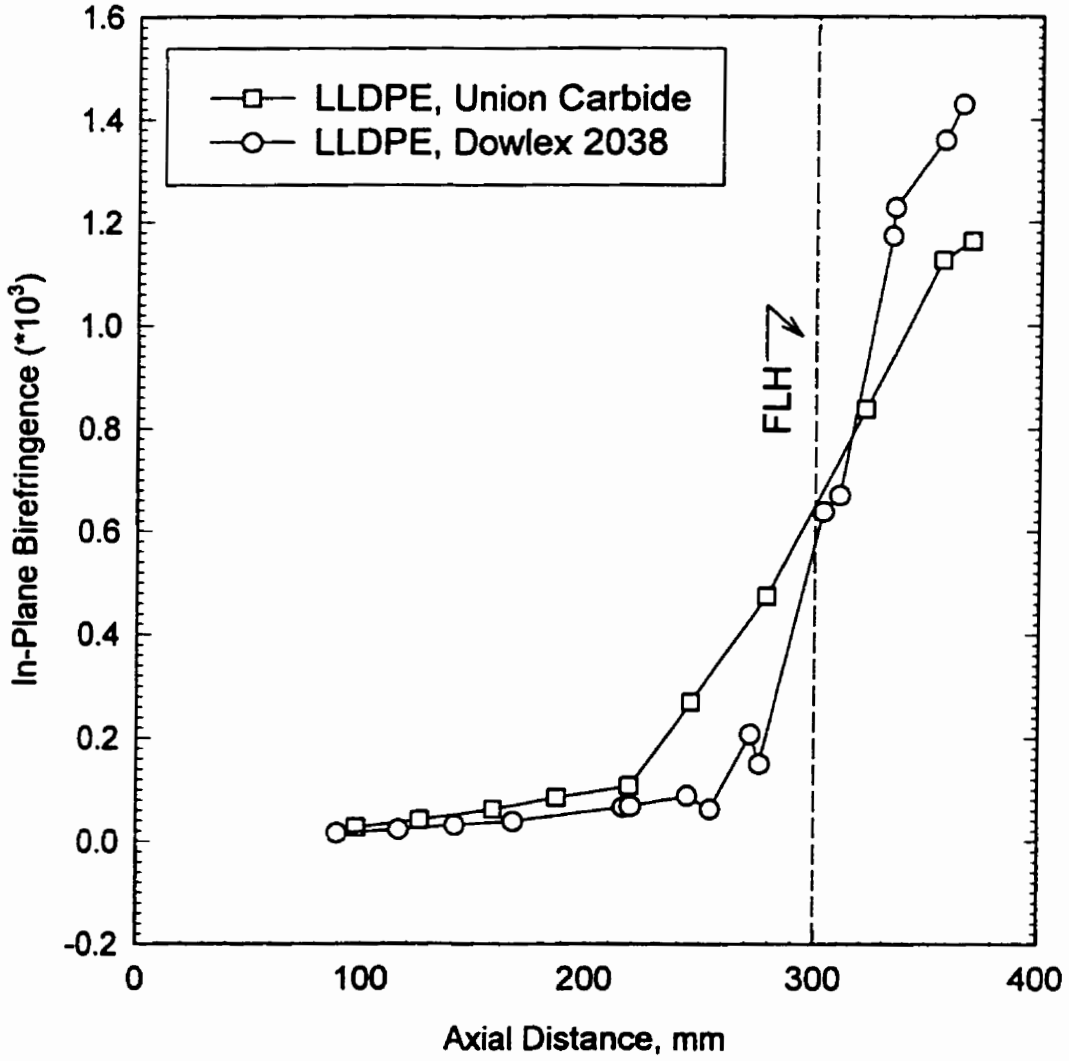

Figure 7. Birefringence (n_{11}- n_{33}) along the length of the bubble for the two LLDPE studied with TUR = 7.6, BUR = 1.0, and FLH = 300 mm.

CHAPTER 4

THIRD ARTICLE:

ON-LINE BIREFRINGENCE MEASUREMENT IN FILM BLOWING OF A LINEAR LOW DENSITY POLYETHYLENE

A. Ghaneh-Fard, P.J. Carreau, and P.G. Lafleur

Centre de recherche appliquée sur les polymères

(CRASP)

Department of Chemical Engineering

Ecole Polytechnique

PO Box 6079, Stn "Centre-Ville", Montreal, QC, H3C 3A7 CANADA

Submitted for publication in *Int. Polym. Process.*

September, 1996

Correspondence concerning this article should be addressed to P.J. Carreau.

4.1. Abstract

Blown film properties depend on the thermo-mechanical history experienced by molten polymer during biaxial deformation. In this study on-line birefringence measurements along the length of the bubble in film blowing of a linear low density polyethylene (LLDPE) were carried out in order to assess the stress level in the melt zone and total orientation in the solid zone. Bubble temperature measurements were carried out to find out the onset and the end of crystallization. Strain rates were also determined from bubble diameter and axial velocity measurements. We have focused on the effects of key processing parameters on the thermo-mechanical history of polymers. The relations between the birefringence and temperature profiles are described. The birefringence value is shown to be very small in the molten zone and increases rapidly as crystallization proceeds. The birefringence of the solidified film is strongly dominated by the crystalline phase contribution. Stresses in the molten blown film were calculated using the data of birefringence and pressure inside the bubble. The birefringence technique appears to be a promising but limited tool to determine stresses occurring in film blowing.

Key-words: film blowing, birefringence technique, molecular orientation, crystallization, linear low density polyethylene.

4.2. INTRODUCTION

Polymeric films are usually manufactured by the film blowing process. Molten polymer is extruded through an annular die and the molten tube leaving the die is drawn upwards by the nip rolls. At the same time, air is introduced through an opening in the center of the die inflating the tube. Biaxial stretching takes place in the melt before the point at which the polymer is solidified at the frost line. This two-directional orientation makes blown film extrusion much more attractive than flat film extrusion, since it allows the film properties to be precisely controlled by adjusting the axial drawing velocity and amount of air inside the bubble.

It is well-established that molecular orientation and stress-induced crystallization in a fabricated blown film influence its mechanical and physical properties. For semi-crystalline polymers like polyethylenes, the orientation of both the crystalline and amorphous phases are controlling the film properties. Several methods have been used by different researchers for characterizing the molecular orientation of blown films [1-18]. These include wide angle X-ray scattering (WAXS), small angle X-ray scattering (SAXS), transmission electron microscopy (TEM), scanning electron microscopy (SEM), infrared dichroism, Raman spectroscopy, thermal shrinkage, birefringence, and sonic modulus measurements. The abilities, merits, and demerits of these techniques can be found in the above-mentioned references. Birefringence is a measure of total molecular orientation in the sample. It is a

relatively quick and easy method, which could also be very useful for the investigation of stresses occurring in the melt zone of film blowing. The birefringence data can be used to calculate the components of the stress tensor using the stress-optical law. Advantages of the flow birefringence technique over classical mechanical methods are discussed in a previous article [19].

The purpose of the present study is to report experimental results of on-line birefringence as well as strain rate and bubble temperature measurements in film blowing of a linear low density polyethylene (LLDPE). We examine the effects of key process variables on strain rate, bubble temperature, and birefringence profiles. The stresses are calculated using the birefringence and pressure inside the bubble data. This article represents a continuation of our recent studies [19-20] on the film blowing process.

4.3. BACKGROUND

4.3.1. Kinematics, Dynamics, and Energy Balance in Film Blowing

In the film blowing process, three different flow regions exist, as shown in Figure 1-a: (1) Shear flow region. This is the region inside the die where the polymer melt undergoes an uni-dimensional steady shear flow, assuming negligible entrance and exit effects. (2) Transition region. This region, which is near the die exit, consists of both the confined flow

in the die and the extensional flow in the extrudate swell region. In the die, the flow is essentially shearing, with the extensional component just being developed. In the extrudate swell region, the flow becomes mainly extensional, with the shearing flow rapidly decreasing. Consequently, the flow field is very complicated in the transition region, at the die exit. (3) Pure extensional flow region. This is the region between the transition region and the frost line height in which free surface non-uniform biaxial extensional flow takes place. The deformation regime lies somewhere between biaxial extension and planar extension. In the neck zone, below the inflation region, the deformation is very close to planar extension. The following analysis is restricted to the extensional flow region.

The first effort at the modeling of film blowing was made by Pearson and Petrie [21-22], who used the thin shell approximation. The film thickness is assumed to be small compared to the radii of curvature of the bubble; the curved film can be approximated as a plane. This, therefore, allows one to use local rectangular Cartesian coordinates, as illustrated in Figure 1-b. It is also assumed that the shear components of the deformation rate are negligible, and the strain rate tensor may then be written as

$$\dot{\gamma} = \begin{bmatrix} \dot{\gamma}_{11} & 0 & 0 \\ 0 & \dot{\gamma}_{22} & 0 \\ 0 & 0 & \dot{\gamma}_{33} \end{bmatrix} \qquad (1)$$

The strain rate in the machine direction (direction 1) is given by [23] :

$$\dot{\gamma}_{11} = 2 \frac{dv_z}{dz} + 2 v_z \left(\frac{dr}{dz}\right) \frac{d\theta}{dz} \qquad (2)$$

where v_z is the film velocity in the z-direction , r the bubble radius, and θ the bubble inflation angle, the angle that the film makes with the z-direction. The strain rate in the transverse direction (direction 3) is obtained by:

$$\dot{\gamma}_{33} = 2 \frac{v_z}{r} \left(\frac{dr}{dz}\right) \qquad (3)$$

From the continuity equation for incompressible material we have:

$$\dot{\gamma}_{22} = - (\dot{\gamma}_{11} + \dot{\gamma}_{33}) \qquad (4)$$

The film thickness profile can be calculated from the macroscopic mass balance:

$$h = \frac{w \cos\theta}{2 \pi \rho r v_z} \qquad (5)$$

Here, w is the mass flow rate of polymer and ρ the density of polymer. Therefore, from the measured axial film velocity, the bubble radius, and the bubble inflation angle profiles, the components of the strain rate tensor as well as the film thickness can be calculated.

Assuming that the effects of surface tension, air drag and inertial force are negligible, a force balance in the pulling direction on the film between some arbitrary position z, where the local geometric parameters are r and θ, and the frost line height Z leads to the relation [24]:

$$2\,\pi\,r\,\cos\theta\,\sigma_{11}\,h + \pi\,\Delta P\,(R_f^2 - r^2) + 2\,\pi\,\rho\,g\int_z^Z r\,h\,\sec\theta\,dz = F_Z \quad (6)$$

and a force balance perpendicular to the film direction yields [25]:

$$\frac{\Delta P}{h} = \frac{\sigma_{11}}{R_1} + \frac{\sigma_{33}}{R_3} - \rho\,g\,\sin\theta \quad (7)$$

where σ_{11} denotes the normal stress in the machine direction, σ_{33} the normal stress in the transverse direction, ΔP the pressure difference across the bubble, R_f the final bubble radius, g the gravity acceleration, F_Z the bubble drawing force at the frost line height, and R_1 and R_3 are the radii of curvature in the machine and transverse directions respectively. ΔP is equal to the pressure inside the bubble considering the atmospheric pressure as zero. The bubble drawing force at the nip rolls can be measured by means of a mechanical transducer which can then easily be translated to F_Z. From the measurements of the bubble drawing force, the pressure difference across the bubble, the geometry of bubble, and the density of polymer, one may calculate the stress field in the film. However, as mentioned in our previous publication [19], the impact of the energy loss by frictional forces during flattening, pinching-off and taking-up of the film bubble on the drawing force is difficult to evaluate. Consequently, the measurement of the force applied to the bubble can only be made indirectly by calibrating the equipment.

Considering a vertical segment of the bubble, dz and assuming that the heat conduction in the film and heat convection inside the bubble are negligible, a differential energy balance can be written as [26]:

$$\rho\, C_p\, Q \cos\theta \frac{dT}{dz} = -2\,\pi\, r\, [\, h_c\, (T - T_c) + \epsilon\, k\, (T^4 - T_s^4)] + Q\, \Delta H_f \cos\theta \frac{dX}{dz} \qquad \textbf{(8)}$$

where C_p is the specific heat of the polymer melt, Q, the volumetric polymer flow rate, T, the mean temperature of the film, h_c , the heat transfer coefficient, T_c , the cooling air temperature, ϵ, the emissivity, k, the Stefan Boltzmann constant, T_s, the temperature of the surroundings, ΔH_f, the heat of crystallization, and X the degree of crystallinity.

4.3.2. Microstructure Development in Film Blowing

In film blowing the molten polymer is subjected to different stress fields that develop at various stages of the process. The stresses are the rheological responses to deformation and therefore are the combined result of the processing conditions and the melt rheology. First, as the melt flows through the annular die, it is subjected to shearing stresses, resulting in a partial molecular orientation in the machine direction (MD). Upon leaving the die, this orientation may be partially relaxed but further orientation of the macromolecules will occur as a result of biaxial stretching. The level of extensional stresses will then increase with increasing viscosity due to cooling. Depending on the cooling rate of the melt a second relaxation process may also take place, causing reorientation of macromolecules [3]. In the

vicinity of the frost line height the melt under stress starts to crystallize.

Polyethylene forms lamellar crystals upon crystallization. In the absence of stress and under steady state crystallization conditions, the lamellae are organized in larger superstructures, called spherulites. The crystallization of blown film under stress will, however, form a different morphology. The row nucleated crystalline structure, first proposed by Keller and Machin [27], is widely accepted to describe the crystalline phase structure of polyethylene blown films [2-5,7,8,10-12,15,16]. The stretched chains are oriented in the MD and act as nucleation surfaces. From these aligned nuclei chain folded lamellae grow radially, forming stacked lamellae with their normals in the MD. At low stresses, the lamellae may be twisted resulting in random a- and c-axis orientation in the stress direction and b-axis orientation perpendicular to this direction. In a study of the crystalline structure of a low density polyethylene (LDPE), Kwack and Han [12] have concluded that below a stress value of about 10^5 Pa, the crystalline structure is spherulitic. They have suggested that the row nucleated structure could be observed when the magnitude of the applied stress exceeds about 10^7 Pa.

Simpson and Harrison [16] have recently investigated the effects of processing conditions on crystalline and amorphous morphologies. They have found that increasing the take-up ratio (TUR) causes lamellae to become more perfectly stacked and amorphous orientation to increase in the MD. Increasing the blow-up ratio (BUR) increases lamellar

disorder and amorphous orientation in the transverse direction (TD). Increasing the frost line height (FLH) causes no significant changes in crystalline and amorphous morphologies. van Gurp et al. [15] have found that with increasing extrusion temperature the twisting of the lamellae increases. Resin rheological properties can be related to the orientation [11]. Linear low density polyethylene (LLDPE), due to its strain softening behavior, exhibits the lowest stress orientation, while LDPE, due its strain hardening behavior, exhibits an intermediate stress orientation.

Many parameters influence the morphology development of blown films in a very complex way. It is still a controversial issue to what extend blown film structure and properties are affected by flow kinematics. For example, Patel et al. [17] observed that the die land length had no significant effect on the blown film structure, as measured by birefringence and shrinkage techniques as well as determined by mechanical properties. Their conclusion was that the shear flow in the blown film die had an insignificant effect on the blown film structure and properties. In contrast, the results of Tas [18] showed that the modeling of film blowing was influenced by the shear flow in the die. Stresses calculated in the machine direction, ignoring the shear flow in the die, were much lower than the experimentally determined stresses. He then stated that the shear flow in the die influences the ultimate film properties.

4.3.3. Blown Film Characterization by Birefringence Technique

The only published study, prior to our efforts, dealing with on-line birefringence measurement in film blowing was carried out by Nagasawa et al. [1,2]. They observed a rapid increase in birefringence upon crystallization for high density polyethylene (HDPE), polybutene-1, and Nylon 6. We have observed the same trend in our preliminary results on two LLDPE resins [19]. Nagasawa et al. [2] have speculated that the initial increase in the birefringence would be followed by a decrease in its value during the crystallization process. They attributed the increase in the birefringence to the formation of central core of the rod-like structure in the MD. The subsequent decrease of the birefringence was interpreted as the formation of the outer part of the rod in which lamellae grew in the TD with twisting. In our previous [19] and present experiments, we have never observed such subsequent decreases.

Off-line birefringence measurement has been used to evaluate the total molecular orientation in blown films by few researchers [6-9,11,13,14,17]. Stein's tilting technique [28] was generally used for measuring out-of-plane birefringences in these studies. White and co-workers [6-9] measured the birefringences of polystyrene (PS), polypropylene (PP), HDPE, LLDPE, and LDPE blown films. They obtained positive values for the in-plane birefringence of polyethylene resins indicating a greater orientation magnitude in the MD. Measuring the bubble tension force and pressure inside the bubble, they stated that the birefringence of solidified film and principal stress difference at the FLH data could reasonably be correlated

for the investigated polymers. Using birefringence data of LLDPE and LDPE films, Ashizawa et al. [9] obtained negative values for the amorphous orientation factors, suggesting that the chains in the amorphous phase tended to be normal to the surface. The in-plane birefringence results of Haber and Kamal [11] on different polyethylenes mostly exhibited a negative birefringence. They attributed the negative birefringence to the amorphous chains orienting in the TD. Their conclusion was then dismissed by Simpson and Harrison [16]. With the help of infrared dichroism and thermal shrinkage techniques, they argued that the amorphous phase was predominantly oriented in the MD. The birefringence of different LLDPE blown films was measured by Kalyon and Moy [13]. Both negative and positive birefringence were reported. Patel and coworkers [14,17] have carried out off-line birefringence measurements of a LLDPE at different processing conditions and obtained negative in-plane birefringence values for most samples. In summary, the published results so far do not appear to be consistent. However, the different trends observed in these studies may be due to experimental difficulties and/or use of different resins and processing conditions.

4.4. THEORETICAL FORMULATION OF BIREFRINGENCE MEASUREMENT

We have presented the analysis of the transmission of light through the blown film elsewhere [19]. It was shown that the birefringence varied as a function of the incident angle of light and included contributions from two normal optical differences. We can determine these normal optical differences by directing the light beam at different off-center positions

on the bubble at the same axial distance, which provides different values of the incident angle. Therefore, we need to extend the analysis of the transmission of light to a more general form in which the light beam is directed to the bubble off-center and horizontally as shown in Figure 2. In this figure, θ_i is the bubble inflation angle, ϕ_i the off-center angle of incidence, and θ_r and ϕ_r are the components of the refraction angle.

For our optical train, described in a previous article [19], the equation of light intensity will take the form

$$I = I_0 \left[1 + A_2 \sin(4\omega t) + B_2 \cos(4\omega t) \right] \qquad \textbf{(9)}$$

Here I_0 is the incident light intensity, and ω the rotation frequency of half-wave plate. The coefficients A_2 and B_2 are related to the retardation and the orientation angle of the film as well as the so-called Fresnel coefficients and can be extracted by performing a fast Fourier transform.

The retardation (δ) is related to the birefringence (Δn) according to

$$\delta = \frac{2 \pi \Delta n(\theta_r, \phi_r) h}{\lambda \cos\theta_r \cos\phi_r} \qquad \textbf{(10)}$$

where h is the thickness of the film and λ the wave length .

The shear components of the stress tensor are normally assumed to be negligible in film blowing. Therefore, we neglect the off-diagonal components of the refractive index tensor. By a suitable coordinate frame rotation of this refractive index tensor, the birefringence ($\Delta n\ (\theta_r, \phi_r)$) and the orientation angle (α) may be calculated, yielding:

$$\Delta n\ (\theta_r, \phi_r) = (\cos^2\theta_r \sin^2\phi_r - \sin^2\theta_r \sin^2\phi_r)(\Delta_1) + \cos^2\theta_r \cos^2\phi_r (\Delta_3) + \sin^2\theta_r \cos^2\phi_r (\Delta_2) \qquad (11)$$

$$\tan 2\alpha = \frac{2 \sin\theta_r \sin\phi_r \cos\theta_r (\Delta_1)}{\Delta n(\theta_r, \phi_r)} \qquad (12)$$

Here, $\Delta_1 = n_{11} - n_{22}$, $\Delta_2 = n_{22} - n_{33}$, and $\Delta_3 = n_{11} - n_{33} = \Delta_1 + \Delta_2$ are the normal optical differences.

4.5. EXPERIMENTAL

4.5.1. Blown Film Extrusion and Material

A 45 mm Killion single screw extruder with a helical blown film die (outer diameter = 50.82 mm and die gap at exit = 680 μm) was used in this study. The experimental procedure of the film blowing operations is detailed elsewhere [20]. The effects of the key process variables including extrusion temperature, molten polymer flow rate, take-up ratio (TUR), blow-up ratio (BUR), and frost line height (FLH) on the measurements were investigated. The TUR is defined as the ratio of the take-up velocity to the extrudate velocity

at the die exit, the BUR as the ratio of the final bubble diameter to the die diameter. The FLH is defined in this study as the distance from the die where the bubble diameter profile becomes flat, as shown in Figure 1. A detailed summary of the film blowing experiments is presented in Table 1.

A linear low density polyethylene (LLDPE), TUFLIN HS-7028 Natural 7, from Union Carbide with a melt index of 1.0 dg/min and a density of 918 kg/m^3 was used in this study. The densities of the molten LLDPE at different temperatures were measured using an Instron capillary rheometer, replacing the capillary by a plug. The pressure inside bubble (P_i) was measured with a pressure transducer and the results are reported in Table 1.

4.5.2. Measurement of Strain Rates

The velocity profile was measured by a standard tracer technique, similar to that employed by previous authors [23,26,29-32]. A colored tracer was gently pushed on the polymer surface. A super VHS video camera system with a shutter speed of 30 frames/second was employed to trace the progress of the tracer on the bubble. The recorded tape was played back through a video cassette recorder with frame advance capabilities. The video signal was then passed into a computer, equipped with image analyzer hardware and software. At specified frame interval, i.e. time interval, the distance of the tracer from a reference line was measured. The axial velocity was obtained by numerically differentiating the collected time-

distance data. A central difference derivative formula [33] was used. Also, the bubble diameter profile was simply determined using video pictures of the bubble.

4.5.3. Measurement of Thickness Profile

Two methods were used to measure the thickness profile of the film along the length of the bubble. First, the thickness profile was calculated from the mass balance equation (Equation 5) by using the measured velocity and diameter profiles. In the second method, the whole process, i.e., screw rotation and nip rolls rotation, was stopped and the bubble was immediately solidified by blowing the cooling air. The thickness profile was then measured on the frozen bubble by using a micrometer.

According to Equation 5 the film thickness depends on density which varies along the length of the bubble. In our experiments, the temperature ranged from about 140^{0}C at the air ring face to about 90^{0}C above the FLH and therefore the temperature dependence of the density was neglected. The error resulting from this constant density assumption in thickness calculations should not be more than 4%. It was observed that both thickness profiles, i.e., measured on the solidified bubble and calculated from the mass balance, came down to the same value above the FLH. However, as one goes towards the die exit, the difference between these two profiles becomes more pronounced. This behavior, which was also observed by Haung and Campbell [31], may be attributed to the elastic recovery after the

pulling of the bubble is stopped. The calculated thickness profiles, believed to be more accurate, were used to calculate birefringence in all the experiments.

4.5.4. Measurement of Bubble Temperature

The temperature measurements were carried out by using an infrared pyrometer (IRCON 3400). The instrument absorbs the infrared radiation in a wavelength of 3.43 μm. The temperature reading with this wavelength represents the surface temperature of the bubble [34]. The instrument was calibrated with the help of a constant-temperature paraffin oil bath and a thermometer. During the experiments the emittance was set to 0.96 on the front panel. We have neglected the emittance dependence on the film thickness. This may cause a maximum error of 2°C within the range of our experimental conditions (see IRCON Operation Manual, 1987).

4.5.5. Measurement of Birefringence

The birefringence measurements were carried out using an optical train with a polarization modulation scheme based on a rotating half wave plate. The apparatus is described in details elsewhere [19].

4.6. RESULTS

4.6.1. Strain Rates

Typical results on the bubble diameter and the axial film velocity along the length of the bubble are shown in Figure 3. Fifth order polynomials were used to fit the velocity and diameter data. The strain rates were then calculated from Equations 2 and 3 by taking the derivatives of these functions. The same procedure has been used by Tas [18].

The machine and transverse direction strain rates for different operating conditions are shown in Figure 4. The general feature of the profiles are similar to those observed by previous authors; both MD and TD strain rates have small values at the die exit region. Then, they go through maxima in the bubble blowing zone and finally decrease to zero at the FLH. The maxima of strain rates increase with decreasing the FLH and increasing the TUR but the increase in the MD strain rate is more pronounced. Increasing the extrusion temperature has no significant effect on both the MD and TD strain rates. The magnitude of the TD strain rate is increased with increasing the BUR, as expected. The magnitude of the MD strain rate is not affected by the BUR. However, it appears that the position of the maximum of the MD strain rate somewhat shifts towards the die exit. Finally, Figure 4 shows that the magnitude of both the MD and TD stain rates drastically increase with increasing the flow rate of molten polymer at almost constant TUR. This can be easily explained by noticing that both film

velocity and its gradient increase for constant FLH with increasing polymer flow rate.

4.6.2. Bubble Temperature

The bubble temperature profiles for the different operating conditions investigated are shown in Figures 5. In general, the bubble temperature decreases almost linearly up to the point where the crystallization process begins. The temperature profile becomes almost flat during the crystallization process. The plateau corresponds to a heat balance between the rate of heat generation by crystallization and the rate of heat removal, as indicated by Equation 8. Once crystallization is completed, the temperature profile decreases almost linearly. No noticeable change in the temperature plateau was observed by varying the processing conditions; the temperature at the plateau was in between 105 °C and 107 °C. However, is was observed that the length of the plateau changed with varying the FLH; decreasing the FLH, by increasing the cooling air flow rate, decreased the length of the plateau. This, also observed by Kanai and White [26], indicates that the crystallization kinetics depend on the cooling rate of the bubble. The other processing parameters did not show any significant effect on the length of the plateau.

Figure 5 also shows the effects of the processing conditions on the bubble temperature in the melt zone. The bubble temperature decreased with decreasing FLH, BUR, and extrusion temperature but did not change with TUR and polymer flow rate. We may

expect such results from the heat balance equation, Equation 8. Decreasing the FLH value was accomplished by increasing the cooling air flow rate, i.e., increasing the heat transfer coefficient. Also, at lower FLH locally larger surface area is available for heat transfer. When increasing TUR, the FLH tends to increase. Therefore, the cooling air flow rate has to be slightly increased to keep the FLH constant. On the other hand, the bubble radius slightly decreased with increasing TUR. Apparently, these two effects counterbalance each other (see equation 8) and no significant effect of the TUR on the bubble temperature is observed in the range of the TUR studied. When increasing BUR, the FLH tends to decrease. Hence, the cooling air flow rate was lowered to maintain a constant FLH and consequently the temperature increased in the neck zone, as shown in Figure 5-c. Finally, the effect of increasing the polymer flow rate counterbalanced the effect of increasing the cooling air flow rate, required to keep the FLH constant, and no differences in temperature were observed for the two polymer flow rate values studied (Figure 5-e).

4.6.3. Birefringence Measurements

For on-center light beam, i.e., $\phi_i = 0$, Equation 11 reads:

$$\Delta n(\theta_r) = \cos^2\theta_r \, \Delta_3 + \sin^2\theta_r \, \Delta_2 \qquad \textbf{(13)}$$

Within our range of experimental conditions, the maximum value of the bubble inflation angle, θ_i, was about 17°. The maximum value of θ_r, obtained from Snell's law, is about 11.3° using

a value of 1.49 for the refractive index of polyethylene [35]. Therefore, the contribution of the out-of-plane birefringence (Δ_2) is less than 4% and the on-center light beam is assumed to give the in-plane birefringence (Δ_3). In this article the results of the in-plane birefringence measurements, which provide information about the difference between the MD and the TD orientations, will be presented.

For all experiments the in-plane birefringence values obtained were positive indicating that the MD orientation was always greater than the TD orientation within conditions investigated. The results are shown in Figure 6. In general, the birefringence values are very low in the melt zone, i.e., before the beginning of the plateau in the temperature profile. In this region slight increases in the n_{11} - n_{33} values are usually observed indicating that the MD orientation increases with increasing axial tension. Then, slight decreases in the n_{11} - n_{33} values are observed for most experiments. These decreases may indicate that the TD orientation increases faster than the MD orientation in the bubble inflating region. The other possible explanation is that it may result from the relaxation of molecular orientation. The relaxation process has already been speculated by Maddams and Preedy [3]. Afterwards, as illustrated in Figure 6, the in-plane birefringence drastically increases during crystallization. The large increase in orientation during crystallization has been attributed to oriented nucleation and growth processes [7,8]. Finally, we notice that the birefringence values continue to increase even after the end of the plateau in the temperature profile is reached. In other words, it appears that even in the completely solid zone some orientation development is going on. This

increase in the birefringence may indicate that the solidified film is still undergoing slight stretching. Nagasawa et al. [2] suggested that the observed behavior may result from temperature gradient along the bubble. As shown in Figure 5, the bubble temperature decreases after the completion of the crystallization process. As they reported, the birefringence of polyethylene film oriented at higher temperature increased with decreasing temperature, while keeping the original length. Another possible explanation for this behavior is that there might be still some crystallization of low molecular-weight material after the end of the plateau in the temperature profile , causing an increase in the birefringence.

The effect of the FLH on the birefringence profile is illustrated in Figure 6-a. The birefringence is increased with decreasing the FLH in the melt zone. We notice that the influence of decreasing the FLH on the n_{11} - n_{33} and the difference between MD and TD strain rates in the melt zone are qualitatively consistent. We can also see that the birefringence value for the two experiments finally reaches, more or less, the same value above the FLH, at an axial distance of about 350 mm. Simpson and Harrison [16] have previously stated that the FLH causes no significant changes in crystalline and amorphous morphologies.

Figure 6-b shows the influence of the TUR on the birefringence profile. In the melt zone the differences between the two profiles, in the range of TUR studied, are not significant. The higher value of birefringence at higher TUR in the solidified film suggests that the MD orientation increases with TUR, as expected. This result is in agreement with data

of Nagasawa et al. [1] for HDPE.

The influence of the BUR value on the birefringence profile is shown in Figure 6-c. The n_{11}-n_{33} value in the melt zone, i.e., amorphous phase, increases with decreasing the BUR, as expected. This is also supported by the results of the strain rate measurements, shown in Figure 4. A lower BUR increases the difference between the MD and TD orientations and results in a higher value of the final birefringence. The results of White and co-workers [7,9] also showed that an increase of the BUR will result in a decrease of the in-plane birefringence of the end product film of polyethylenes.

Figure 6-d illustrates that increasing the extrusion temperature, keeping the other processing parameters constant, has almost no influence on the birefringence in the melt zone, but yields much lower final values of n_{11} - n_{33} leading to a less anisotropic film. This is in agreement with the results of Butler and Patel [14], who found that increasing the extrusion temperature decreases the difference between n_{11} and n_{33} of the end product film. However, it should be mentioned that they have obtained negative values for the in-plane birefringence.

Finally, we see from Figure 6-e that in the melt zone the birefringence slightly decreases as the polymer flow rate decreases. The birefringence profile in the melt zone is almost flat in the case of low polymer flow rate. Apparently, a higher final birefringence may be achieved with decreasing the polymer flow rate. This is an unexpected result but can be

possibly explained by a decrease of the crystallinity level with increasing cooling rate. Finally, it should be mentioned that the final birefringence values reported in Figure 6 might not be the same values if measured off-line. As the pulling of the film is stopped, some orientation may be relaxed. Therefore, the comparison between our results and off-line measurements results reported in the literature should be made with caution.

The out-of-plane birefringences, which represent the magnitudes of both the MD and TD orientations, can be determined via Equation 11 by directing additional light beam at different positions. It is required that the bubble be completely stable and uniform along the bubble circumference. However, noticeable thickness variations were observed in our experiments. Kalyon and Moy [13] have also previously observed significant thickness and birefringence variations along the bubble circumference in blown films of different LLDPE resins. The circumferential variations in birefringence may come from non-uniform crystallization around the bubble due to non-uniform cooling rate. One has to overcome these experimental difficulties in order to obtain reliable out-of-plane birefringence data.

4.6.4. Machine and Transverse Stresses

Applying the stress-optical law, we can now translate the birefringence data into stresses. The stress-optical law is given by:

$$n_{11} - n_{33} = C\,(\sigma_{11} - \sigma_{33}) \qquad \textbf{(14)}$$

The theory of ideal rubber predicts that the stress and refractive index are linearly related [36]. It has widely been observed that the law is valid for many polymeric liquids and in different flow conditions [19]. Since stresses in film blowing are not too high, we are quite confident that the stress-optical law can be applied in the melt zone of this process, even though it has not been yet verified experimentally for film blowing. As soon as crystallization is initiated, the theory of rubber elasticity is no longer applicable. Therefore, it is obvious that the stress-optical law is not appropriate for semi-crystalline polymers below the crystallization temperature. Nevertheless, White and co-workers [7,8] have shown that the birefringence of solidified film might be correlated with normal stress difference at the FLH. The stress-optical coefficient, C, for PE was taken to be 2.1×10^{-9} m^2/N [36]. The MD and TD stresses can be calculated via Equations 7 and 14, using the birefringence and the pressure data.

Figure 7 shows the effects of the processing conditions on the MD and TD normal stresses in the molten film. In general, the stresses monotonously increase along the axial length. For all the processing conditions , the MD stress is always greater than the TD stress which obviously resulted from positive birefringences. Both the MD and TD stresses considerably increases with decreasing FLH, increasing TUR, and increasing polymer flow rate; the increases are more pronounced at higher axial distances. With increasing BUR (Figure 7-c), a higher TD stress is obtained in the bubble inflating zone but it is slightly lower at low axial distance. The MD stress is somewhat higher at low BUR. Finally, Figure 7-d displays that increasing the extrusion temperature decreases the stresses, as expected.

We finally analyze our stress data assuming a Newtonian behavior. The relationships between stresses and deformations for non-uniform biaxial stretching of a Newtonian fluid can be written as [25]:

$$\sigma_{11} = \eta (\dot{\gamma}_{11} - \dot{\gamma}_{22}) = \eta (2 \dot{\gamma}_{11} + \dot{\gamma}_{33}) \qquad \textbf{(15)}$$

$$\sigma_{33} = \eta (\dot{\gamma}_{33} - \dot{\gamma}_{22}) = \eta (2 \dot{\gamma}_{33} + \dot{\gamma}_{11}) \qquad \textbf{(16)}$$

As shown before, a lower bubble temperature and higher strain rates are obtained at lower FLH. Consequently, the Newtonian model predicts considerably higher stress values at lower FLH. This is consistent with our stress data, reported in Figure 7-a. Using the peak values of strain rate data in Figure 4-b and the maximum stresses in Figure 7-b, we note that the predictions of the Newtonian model on the effect of the TUR are quite comparable with the measured stress data. The strain rates and the bubble temperature are affected by decreasing the BUR. In the neck zone, the bubble temperature is lower for the lower BUR value but the strain rates are not much different. Hence, the higher stresses are predicted from the Newtonian model, in agreement with our measurements. The model also correctly predicts an increase in the TD stress with increasing the BUR in the bubble inflating zone. Note that the agreement is only qualitative. On the effect of the extrusion temperature, the higher stresses observed at lower extrusion temperature can simply be attributed to the temperature effects on viscosity, predictable from the Newtonian model. Finally, using the peak values of the strain rate data in Figure 4-e and the maximum stresses in Figure 7-e, we

note that the Newtonian model overpredicts the effect of the polymer flow rate. This indicates that the dependence of viscosity on strain rate and the melt deformation history inside and outside the die (viscoelastic properties) can not be ignored in dealing with the film blowing process.

4.7. CONCLUDING REMARKS

Our experimental data reveal the effects of key processing parameters including TUR, BUR, FLH, extrusion temperature, and polymer flow rate on the strain rate, temperature, and birefringence profiles along the length of the bubble for the LLDPE studied. Both MD and TD normal stresses can be determined by on-line birefringence measurements.

It was observed that both the MD and TD strain rates increased with increasing TUR and polymer flow rate and decreasing FLH. The magnitude of the TD strain rate was increased with increasing BUR. The results demonstrate that the TUR is not sufficient to define the film blowing process; one also needs to specify the polymer flow rate.

It was also observed that processing conditions had no noticeable effect on the temperature at the plateau in the crystallization zone. However, the length of the plateau changed with varying FLH. The bubble temperature in the melt zone decreased with decreasing FLH, BUR, and extrusion temperature. The results are interpreted in the light of

the energy balance equation.

In all experiments only a very low birefringence was observed in the melt zone. There was a large increase in the birefringence upon crystallization. This is attributed to oriented nucleation and growth processes. The increase in the birefringence was observed even after the completion of the apparent crystallization. This behavior may be an indication of continued stretching and/or further crystallization in the solid zone. These results indicate that the birefringence of the solidified film is strongly dominated by the crystalline phase contribution.

The stress data in the molten film were calculated using the birefringence, pressure, bubble diameter, and film velocity data. Both the MD and TD normal stresses increase considerably with decreasing FLH, increasing TUR, and increasing polymer flow rate and slightly with decreasing extrusion temperature. With increasing BUR, a higher TD stress is obtained. The stress data were compared with the predictions of a simple Newtonian fluid. The trends of our data are qualitatively well predicted. However, it is shown that the dependence of viscosity on strain rate and the melt deformation history inside and outside the die should not be ignored in dealing with the film blowing process. Extensive experiments on different resins and operating conditions are being carried and will be reported in a forthcoming publication.

4.8. ACKNOWLEDGMENT

The authors would like to acknowledge financial support received from the FCAR programme of the Province of Quebec and from NSERC. We are also thankful to Union Carbide for supplying the polymer used in this study.

4.9. REFERENCES

1. Nagasawa, T., T. Matsumura, S. Hoshino, and K. Kobayashi (1973) "Film Forming Process of Crystalline Polymer. I. Factors Inducing a Molecular Orientation in Tubular Blown Film," *Applied Polymer Symposium*, **20**, 275.

2. Nagasawa, T., T. Matsumura, and S. Hoshino, (1973) "Film Forming Process of Crystalline Polymer. II. Microstructure," *Applied Polymer Symposium*, **20**, 295.

3. Maddams, W.F., and J.E. Preedy, (1978) "X-Ray Diffraction Orientation Studies on Blown Polyethylene Films. I. Preliminary Measurements," *J. Appl. Polym. Sci.*, **22**, 2721.

4. Maddams, W.F., and J.E. Preedy, (1978) "X-Ray Diffraction Orientation Studies on Blown Polyethylene Films. II. Measurements on Films from a Commercial Blowing Unit," *J. Appl. Polym. Sci.*, **22**, 2739.

5. Maddams, W.F., and J.E. Preedy, (1978) "X-Ray Diffraction Orientation Studies on

Blown Polyethylene Films. III. High-Stress Crystallization Orientation," *J. Appl. Polym. Sci.*, **22**, 2751.

6. Choi, K., J.L. White, and J.E .Spruiell (1980) "Orientation Development in Tubular Film Extrusion of Polystyrene," *J. Appl. Polym. Sci.*, **25**, 2777.

7. Choi, K., J.E. Spruiell, and J.L. White, (1982) "Orientation and Morphology of High-Density Polyethylene Film Produced by the Tubular Blowing Method and its Relationship to Process Conditions," *J. Polym. Sci.: Polym. Phys. Ed.*, **20**, 27.

8. Shimomura, Y., J.E. Spruiell, and J.L. White, (1982) "Orientation Development in the Tubular Film Extrusion of Polypropylene," *J. Appl. Polym. Sci.*, **27**, 2663.

9. Ashizawa, H., J.E. Spruiell, and J.L. White, (1984) "An Investigation of Optical Clarity and Crystalline Orientation in Polyethylene Tubular Film," *Polym. Eng. Sci.*, **24**, 1035.

10. Picot, J.J.C., (1984) "Molecular Orientation in Film Extrusion of High-Density Polyethylene," *Polym. Eng. Sci.*, **24**, 415.

11. Haber, A., and M.R. Kamal, (1987) "Morphology and Orientation in Polyethylene Tubular Blown Films," *SPE ANTEC'87*, 446.

12. Kwack, T.H., and C.D. Han, (1988) "Development of Crystalline Structure during Tubular Film Blowing of Low-Density Polyethylene," *J. Appl. Polym. Sci.*, **35**, 363.

13. Kalyon, D.M., and F.H. Moy, (1988)"Ultimate Properties of Blown Films of Linear Low Density Polyethylene Resins as Affected by Alpha-Olefin Comonomers," *Polym. Eng. Sci.*, **28**, 1551.

14. Butler, T.I., and R. Patel, (1993) "Blown Film Bubble Forming and Quenching Effects on Film Properties," *J. Plastic Film & Sheeting*, **9**, 181.

15. van Gurp, M., B.J. Kip, J.P.C. van Heel, and S. de Boer, (1994) "On the Development of Orientation in LDPE Blown Films," *J. Plastic Film & Sheeting*, **10**, 156.

16. Simpson, D.M., and I.R. Harrison, (1994) "A Study of the Effects of Processing Parameters on the Morphologies and Tensile Modulus of HDPE Blown Films: Application of Composite Theories on a Molecular Level to Characterize Tensile Modulus," *J. Plastic Film & Sheeting*, **10**, 302.

17. Patel, R.M., T.I. Butler, K.L. Walton, and G.W. Knight, (1994) "Investigation of Processing-Structure-Properties Relationships in Polyethylene Blown Films," *Polym. Eng. Sci.*, **34**, 1506.

18. Tas, P.P., (1994) *Film Blowing: from Polymer to Product*, Ph.D. Dissertation, Dept. Mech. Eng., Eindhoven University of Technology, The Netherlands.

19. Ghaneh-Fard, A., P.J. Carreau, and P.G. Lafleur, (1996) "Application of Birefringence to Film Blowing," *J. Plastic Film & Sheeting*, **12**, 68.

20. Ghaneh-Fard, A., P.J. Carreau, and P.G. Lafleur, (1996) "Study of Instabilities in Film Blowing," *AIChE J.*, **42**, 1388.

21. Pearson, J.R.A., and C.J.S. Petrie, (1970) "The Flow of a Tubular Film. Part 1. Formal Mathematical Representation," *J. Fluid Mech.*, **40**, 1.

22. Pearson, J.R.A., and C.J.S. Petrie, (1970) "A Fluid-Mechanical Analysis of the Film-

Blowing Process," *Plast. Polym.*, **38**, 85.

23. Gupta, R.K., A.B. Metzner, and K.F. Wissbrun, (1982) "Modeling of Polymeric Film-Blowing Processes," *Polym. Eng. Sci.*, **22**, 172.

24. Han, C. D., and J.Y. Park, (1975) "Studies on Blown Film Extrusion. I. Experimental Determination of Elongational Viscosity," *J. Appl. Polym. Sci.*, **19**, 3257.

25. Agassant, J.-F., J. Avenas, J.-Ph. Sergent, and P.J. Carreau, (1991) *Polymer processing: Principles and Modeling*, New York, Hanser Publisher.

26. Kanai, T., and J. L. White, (1984) "Kinematics, Dynamics and Stability of the Tubular Film Extrusion of Various Polyethylenes," *Polym. Eng. Sci.*, **24**, 1185.

27. Keller, A., and M.J. Machin, (1967) "Oriented Crystallization in Polymers," *J. Macromol. Sci.*, **Part B, 1**, 41.

28. Stein, R.S., (1957) "Measurement of Birefringence of Biaxially Oriented Films," *J. Polym. Sci.*, **24**, 383.

29. Farber, R., and J.M. Dealy, (1974) "Strain History of the Melt in Film Blowing," *Polym. Eng. Sci.*, **14**, 435.

30. Wagner, M.H., (1978) "Experimental Investigations into the Analysis of the Film Blowing Process," *Kunststoffe*, **68**, 15.

31. Huang, T.A., and G.A. Campbell, (1985) "Deformational History of LLDPE/LDPE Blends on Blown Film Equipment," *Advances in Polymer Technology*, **5**, 181.

32. Huang, T.A., and G.A. Campbell, (1986) "Deformational and Temperature History Comparison for LLDPE and LDPE Elements in the Bubble Expansion Region of

Blown Films," *J. Plastic Film & Sheeting*, **2**, 30.

33. Griffiths, D.V., and I.M. Smith (1991) *Numerical Methods for Engineers*, CRC Press, Boston.

34. Cao, B., P. Sweeney, and G.A. Campbell, (1990) "Simultaneous Surface and Bulk Temperature Measurement of Polyethylene During Film Blowing," *J. Plastic Film & Sheeting*, **6**, 117.

35. Brandrup, J., and E.H. Immergut (Eds), (1975) *Polymer Handbook*, 2nd Edn., Toronto, John Wiley.

36. Janeschitz-Kriegl, H., (1983) *Polymer Melt Rheology and Flow Birefringence*, Berlin, Springer-Verlag.

Table 1. Film blowing conditions and pressure measurements.

Exp. No.	T* (°C)	w (kg/h)	BUR	TUR	FLH (mm)	h_f** (μm)	P_i (Pa)
1	180	3.89	2.0	7.6	250	38	252.1
2	180	3.89	2.0	7.6	200	38	303.8
3	180	3.89	2.0	5.5	250	55	243.5
4	180	3.89	1.4	7.6	250	53	279.0
5	220	3.89	2.0	7.6	250	38	210.9
6	220	1.90	2.0	7.0	250	41	109.9

* Extrusion temperature;

** Final film thickness.

FIGURE HEADINGS

Figure 1. Bubble geometry, a): different flow regions in film blowing, b): local rectangular Cartesian coordinate system, moving with the bubble.

Figure 2. Transmission of light through the blown film, n_1 and $\underline{n}$ are the average refractive indices of air and film, and δ is the retardation. a) general view, b) details of light path through the film.

Figure 3. Axial film velocity and bubble diameter profiles for experiment No. 1. Solid lines are the results of curve fitting using fifth order polynomial functions.

Figure 4. Strain rates in MD and TD. a) effect of FLH, b) effect of TUR, c) effect of BUR, d) effect of extrusion temperature, e) effect of polymer flow rate.

Figure 5. Bubble temperature profiles along the length of the bubble. a) effect of FLH, b) effect of TUR, c) effect of BUR, d) effect of extrusion temperature, e) effect of polymer flow rate.

Figure 6. In-plane birefringence profiles along the length of the bubble. a) effect of FLH, b) effect of TUR, c) effect of BUR, d) effect of extrusion temperature, e) effect of polymer flow rate.

Figure 7. Stresses in MD and TD. a) effect of FLH, b) effect of TUR, c) effect of BUR, d) effect of extrusion temperature, e) effect of polymer flow rate.

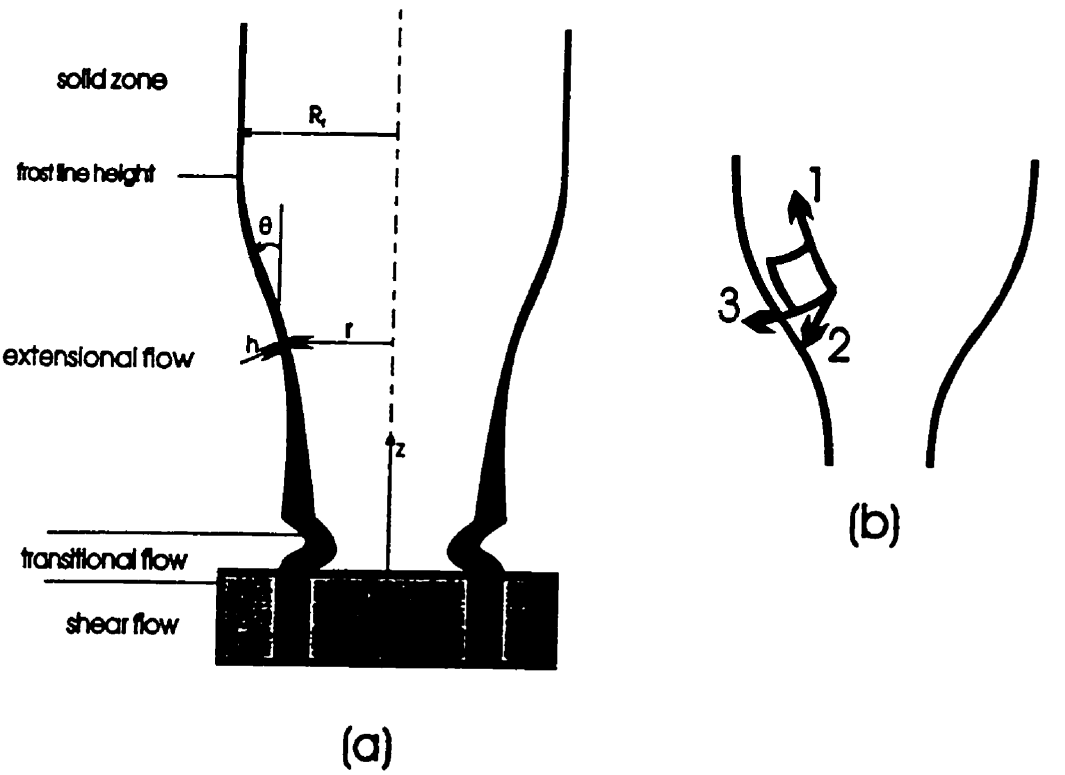

Figure 1. Bubble geometry, a): different flow regions in film blowing, b): local rectangular Cartesian coordinate system, moving with the bubble.

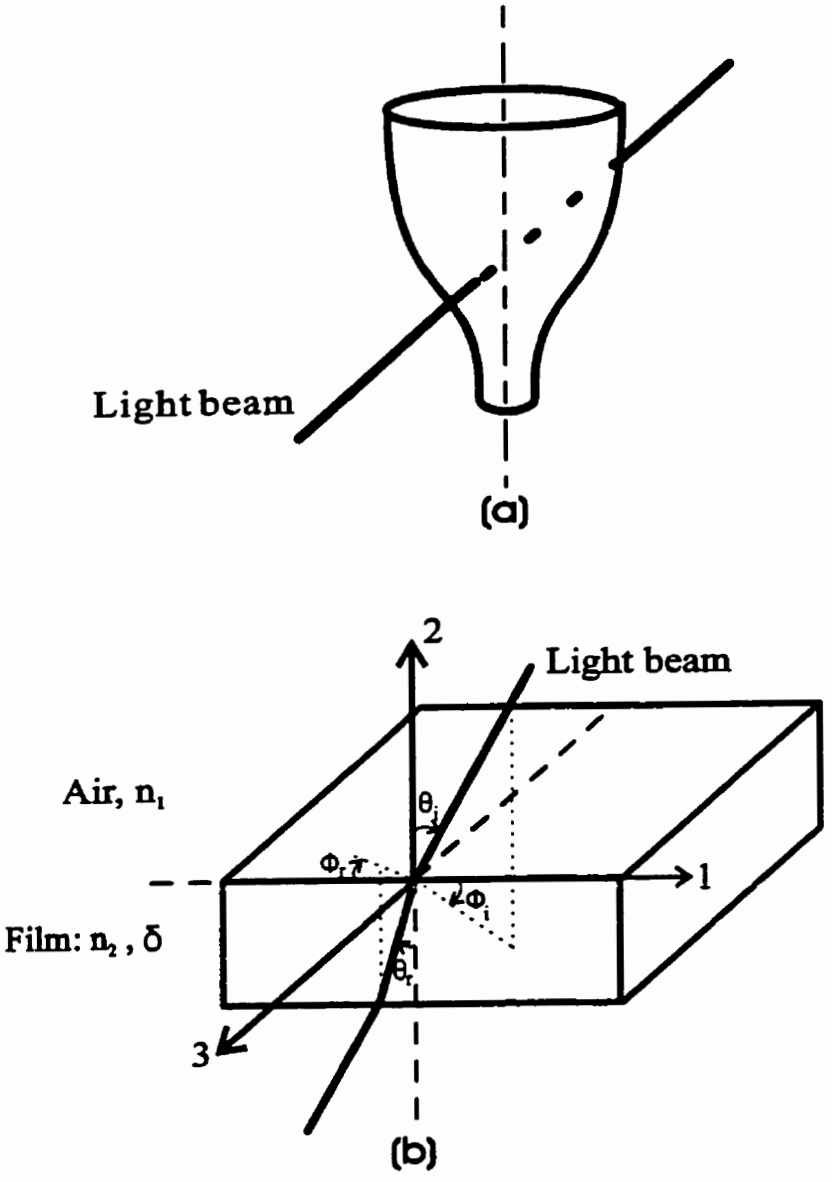

Figure 2. Transmission of light through the blown film, n_1 and n_2 are the average refractive indices of air and film, and δ is the retardation. a) general view, b) details of light path through the film.

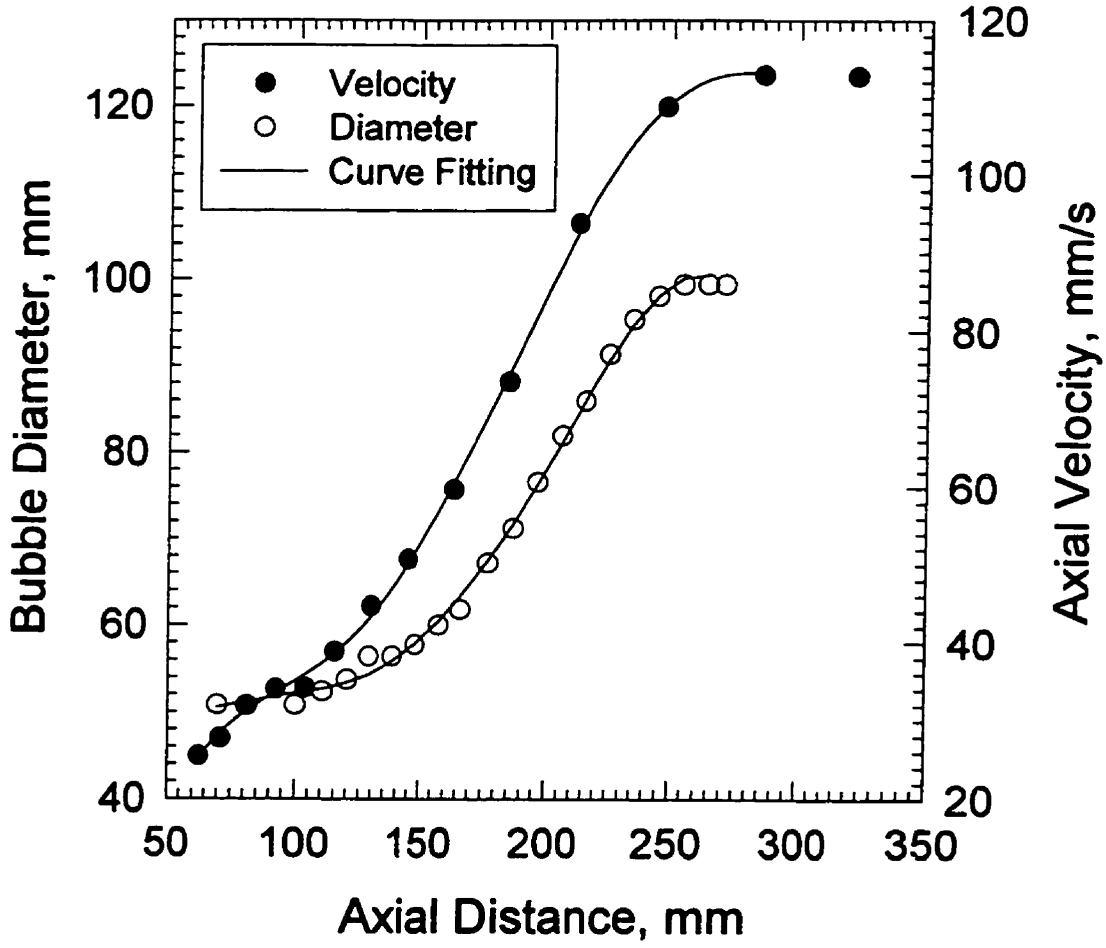

Figure 3. Axial film velocity and bubble diameter profiles for experiment No.1. Solid lines are the results of curve fitting using fifth order polynomial functions.

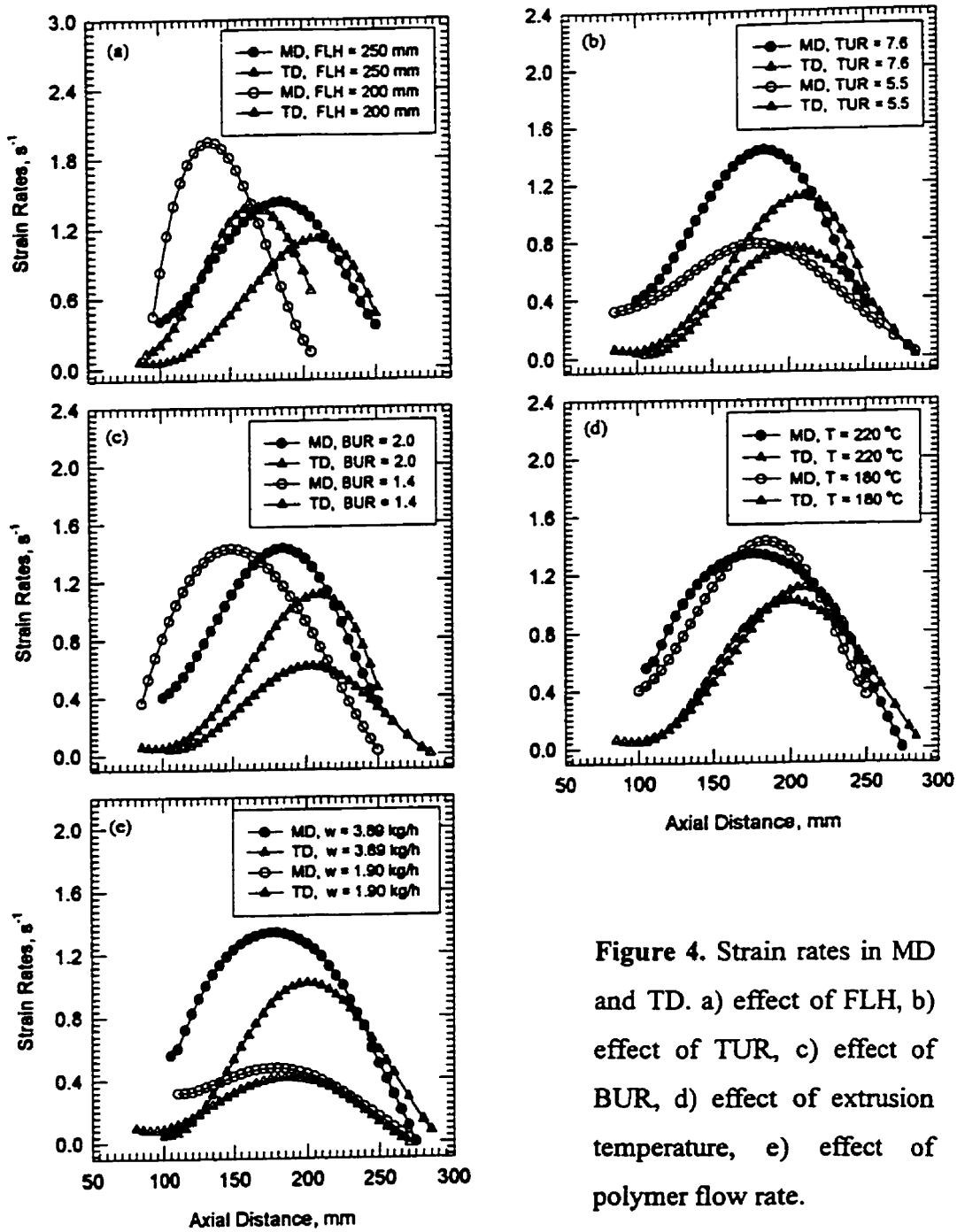

Figure 4. Strain rates in MD and TD. a) effect of FLH, b) effect of TUR, c) effect of BUR, d) effect of extrusion temperature, e) effect of polymer flow rate.

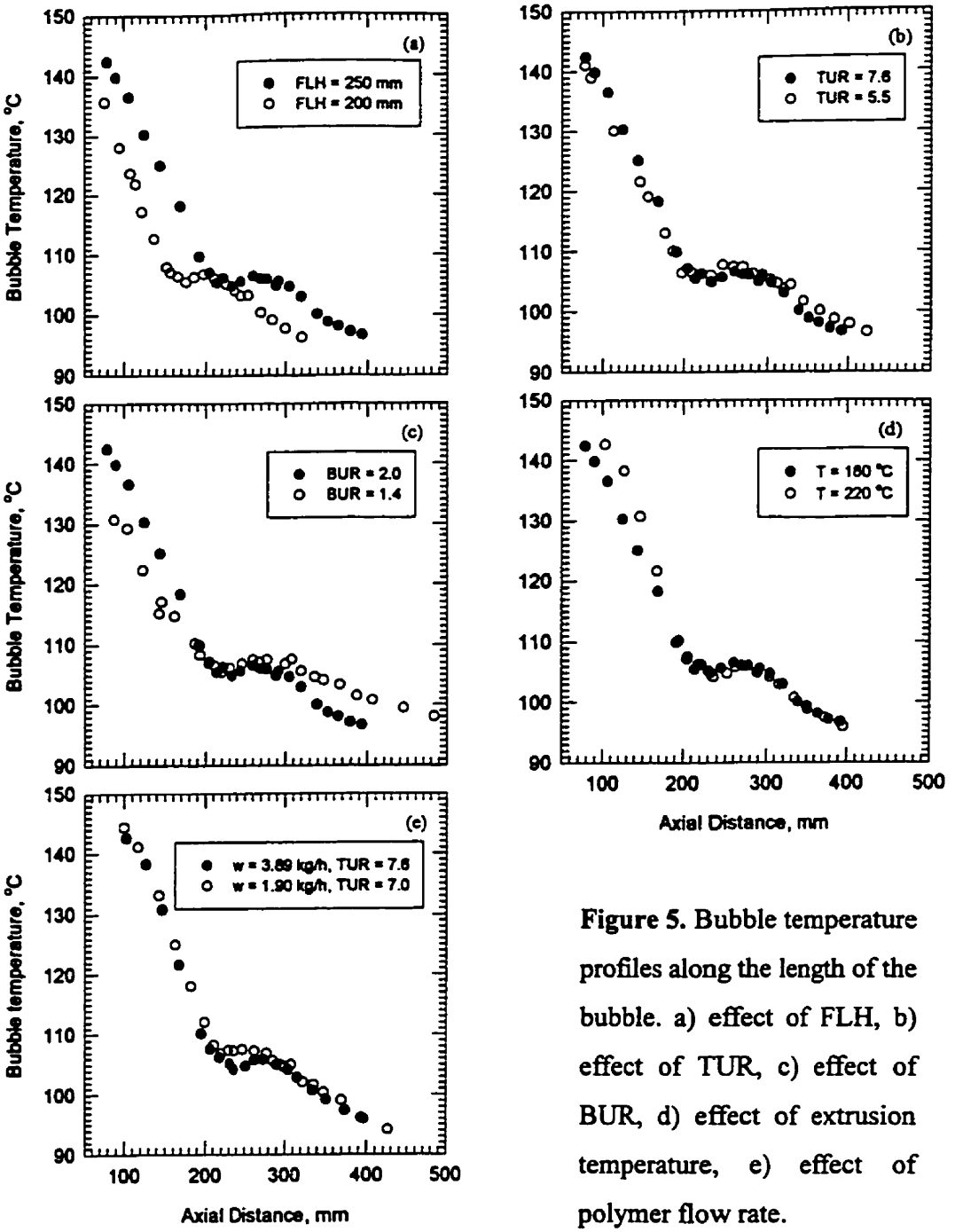

Figure 5. Bubble temperature profiles along the length of the bubble. a) effect of FLH, b) effect of TUR, c) effect of BUR, d) effect of extrusion temperature, e) effect of polymer flow rate.

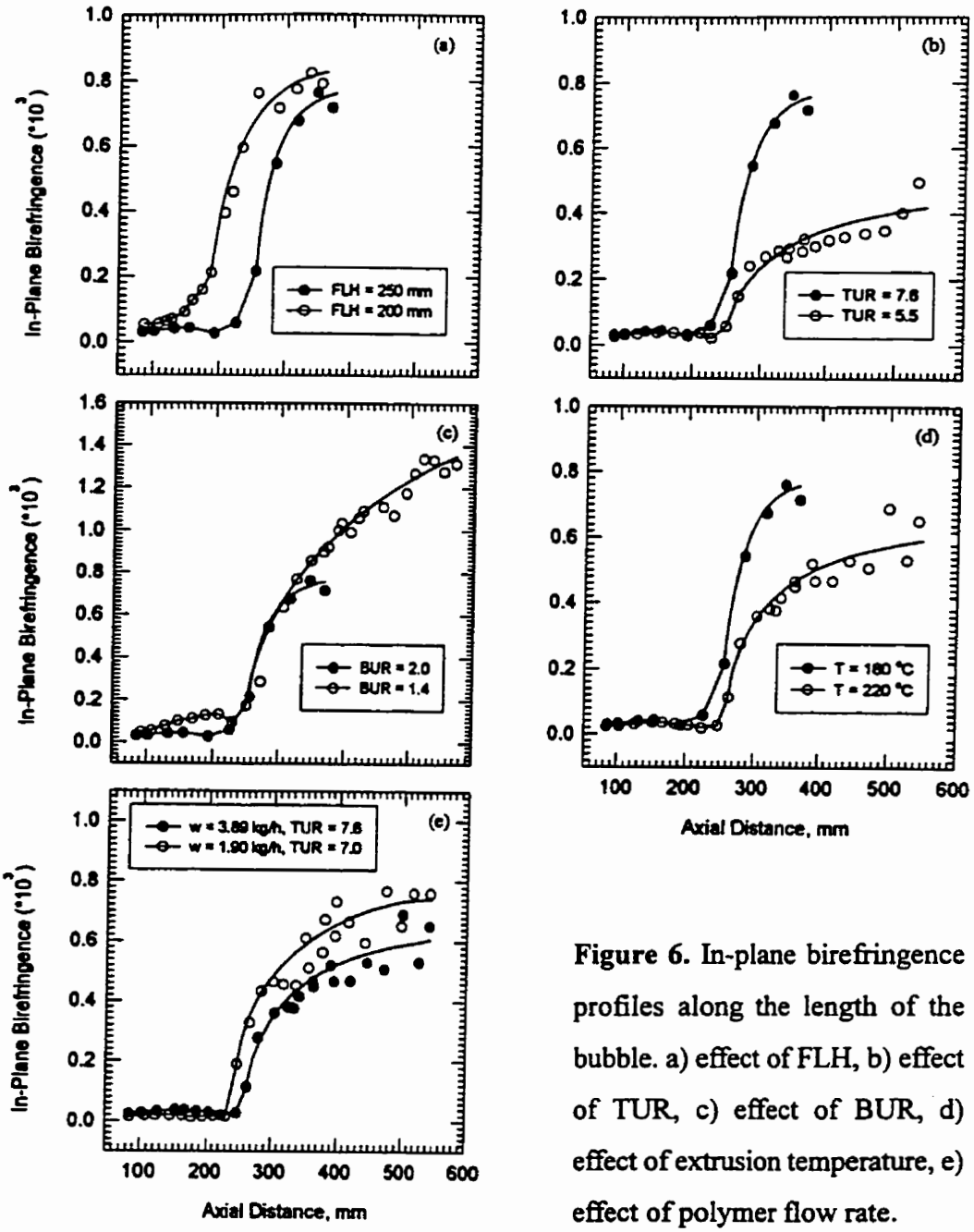

Figure 6. In-plane birefringence profiles along the length of the bubble. a) effect of FLH, b) effect of TUR, c) effect of BUR, d) effect of extrusion temperature, e) effect of polymer flow rate.

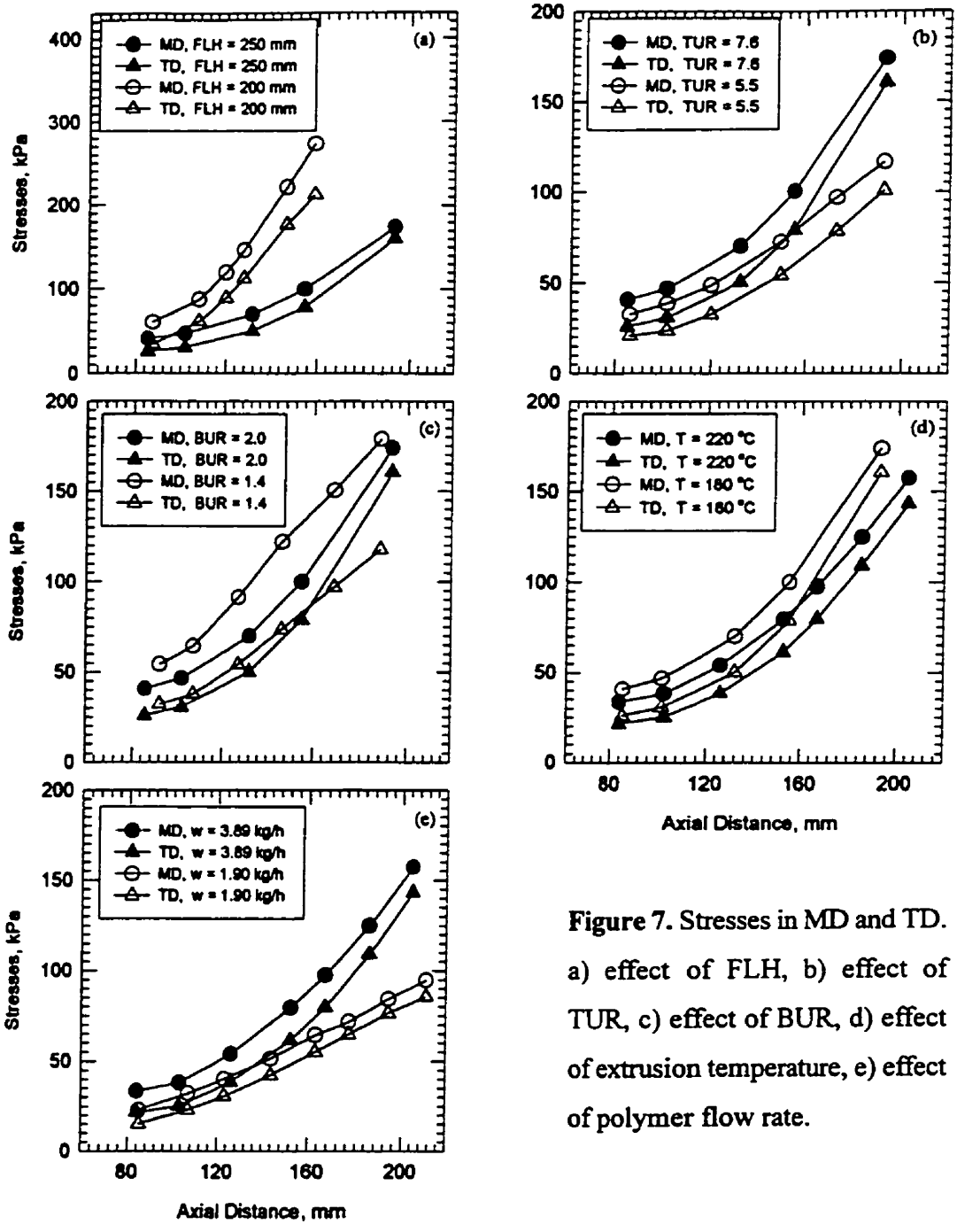

Figure 7. Stresses in MD and TD. a) effect of FLH, b) effect of TUR, c) effect of BUR, d) effect of extrusion temperature, e) effect of polymer flow rate.

CHAPTER 5

FOURTH ARTICLE:

STUDY OF KINEMATICS AND DYNAMICS OF FILM BLOWING OF DIFFERENT POLYETHYLENES

A. Ghaneh-Fard, P.J. Carreau, and P.G. Lafleur

Centre de recherche appliquée sur les polymères

(CRASP)

Department of Chemical Engineering

Ecole Polytechnique

PO Box 6079, Stn "Centre-Ville", Montreal, QC, H3C 3A7 CANADA

Submitted for publication in *Polym. Eng. Sci.*

October, 1996

Correspondence concerning this article should be addressed to P.J. Carreau.

5.1. Abstract

An extensive experimental study of the effects of material characteristics and processing parameters on the kinematics and dynamics of film blowing is presented. Three polyethylene resins, a high density polyethylene (HDPE), a low density polyethylene (LDPE), and a linear low density polyethylene (LLDPE) were investigated. The convergent flow analysis of Cogswell was used to characterize the elongational flow behavior of the polymers. Strain rates and pressure inside the bubble (P_i) have been determined over a wide range of film blowing conditions. Moreover, on-line bubble temperature and birefringence measurements have been carried out along the length of the bubble. The experimental results reveal that the three polymers display different behaviors. The LLDPE requires the highest P_i value and the LDPE, the lowest. Consistent with this, the LLDPE shows the lowest in-plane birefringence and the LDPE, the highest. Interactions between various process parameters affecting the P_i value are characterized. Bubble instability is correlated to the apparent uniaxial elongational viscosity and P_i. The most stable polymer (LDPE) has the highest elongational viscosity and requires the lowest P_i. Stresses have been calculated with the help of the birefringence and P_i data. The stress and strain rate data were used to calculate an apparent non-uniform biaxial elongational viscosity of the melts, but could not be correlated through any simple constitutive equation.

Key-words: film blowing, kinematics, dynamics, processing conditions, polymer rheology, birefringence technique, polyethylene.

5.2. INTRODUCTION

Film blowing is one of the most important process in polymer industry and is used to produce most of the polyethylene (PE) films. It is a complex non-isothermal and non-uniform biaxial extensional process involving interactions between melt rheology, heat transfer, and aerodynamics. Ultimate film properties are controlled by molecular orientation and stress-induced crystallization. Molecular orientation is developed preliminary in the blown film die but mainly in the bubble forming zone. There are several publications [1-9] in the literature which discuss kinematics and dynamics of film blowing from measurements of the rate of deformation, drawing force, and pressure inside the bubble. However, many aspects have not received any treatment and some of the experimental observations appear to lead to contradictory conclusions. Strain rates in film blowing have been extensively measured by different authors. Nevertheless, the effects of some processing parameters on strain rates have not been yet investigated. Although the pressure inside the bubble is an important parameter, only a few scattered data can be found in the literature [3,5,6,8]. The most difficult parameter to measure in film blowing is the bubble drawing force, information rarely found in the literature. It is widely believed that final film properties can be predicted from stresses, deformations, and thermal history encountered by the melt during biaxial deformation. However, the relationships between these parameters are far from being understood, mostly because of lack of sufficient and reliable data.

The objective of the present study is to compare the behavior of a series of PE resins from kinematics and dynamics points of view. The effects of film blowing conditions on strain rates and pressure inside the bubble are extensively examined. Some interactions between film blowing variables are characterized. The results of on-line bubble temperature and birefringence measurements for some film blowing conditions are also presented. Stresses are calculated with the help of the birefringence and pressure data and used together with the strain data to calculate an apparent non-uniform biaxial elongational viscosity of the polymers which is compared to the extensional flow behavior obtained using the convergent flow analysis of Cogswell [10]. This article represents a part of our continued efforts [11-13] to achieve a better understanding of the film blowing process.

5.3. BACKGROUND

5.3.1. Kinematics and Dynamics

The kinematics and dynamics of film blowing are described in details elsewhere [13]. We present only the main equations here. The strain rate in the machine direction is given by:

$$\dot{\gamma}_{11} = 2\,\frac{dv_z}{dz} + 2\,v_z\,(\frac{dr}{dz})\,\frac{d\theta}{dz} \qquad (1)$$

where v_z is the axial film velocity , r the bubble radius, and θ the bubble inflation angle. The strain rate in the transverse direction is obtained from:

$$\dot{\gamma}_{33} = 2\,\frac{v_z}{r}\,(\frac{dr}{dz}) \qquad (2)$$

A force balance in the pulling direction on the film leads to the relation:

$$2\,\pi\,r\,\cos\theta\,\sigma_{11}\,h + \pi\,\Delta P\,(R_f^2 - r^2) + 2\,\pi\,\rho\,g\int_z^z r\,h\,\sec\theta\,dz = F_Z \qquad (3)$$

and a force balance perpendicular to the film yields:

$$\frac{\Delta P}{h} = \frac{\sigma_{11}}{R_1} + \frac{\sigma_{33}}{R_3} - \rho\,g\,\sin\theta \qquad (4)$$

where σ_{11} denotes the stress in the machine direction, σ_{33} the stress in the transverse direction, ΔP the pressure difference across the bubble, h the film thickness, R_f the final bubble radius, ρ the density of polymer, g the gravity acceleration, F_Z the bubble drawing force at the frost line height, and R_1 and R_3 are the radii of curvature in the machine and transverse directions respectively.

5.3.2. Cogswell's Convergent Flow Analysis

The measurement of the elongational viscosity still continues to pose a challenge to rheologists due to experimental difficulties. Commercially available Meissner-type extensional rheometers have only a limited range of operation. An alternative method of determining

uniaxial elongational viscosity is using the convergent flow analysis of Cogswell [10]. The method is relatively simple and quick. More importantly, one can obtain elongational viscosity data at high strain rates, relevant to real polymer processing conditions. It is assumed in the analysis that the viscosity under simple tension is independent of stress. Also, the total pressure drop in a converging die is taken to be the sum of that due to shear flow and that due to extensional flow.

The convergent flow analysis has been used by several researchers to measure the elongational viscosity [14-17]. Shroff et al. [14] noted that the convergent flow analysis yields quick and reliable extensional data in a wide range of strain rates and temperatures. Laun and Schuch [15] compared the converging flow elongational viscosities of various polyethylene and polystyrene resins with directly measured steady state viscosities and found a good agreement in some cases but did not give any general rule on the range of agreement. Covas and Carneiro [16] have shown that the convergent flow analysis is able to correctly predict the relative behavior of the different materials but quantitatively shows considerable inaccuracy which may come from the assumptions made in the analysis.

5.4. EXPERIMENTAL

5.4.1. Materials

Three different polyethylene resins were used in this study: a high density polyethylene

(HDPE), a low density polyethylene (LDPE), and a linear low density polyethylene (LLDPE). The HDPE was supplied by Petromont, the LLDPE by Union Carbide, and the LDPE by Novacor. The densities, melt indices (*MI*) and zero shear viscosities of the three polymers are summarized in Table 1.

5.4.2. Rheological Measurements

The dynamic rheological properties, storage and loss moduli, G' and G'', complex viscosity, η^*, were measured using a CSM Bohlin rheometer in a concentric disk configuration under a dry nitrogen atmosphere. The frequency used ranged from 0.001 Hz to 20 Hz and the applied stress was adjusted to maintain the experiments in the linear domain. Measurements were carried out at a temperature of 180°C. Concentric disks of diameter equal to 25 mm with a gap between 1 and 1.2 mm were used for all measurements.

The shear viscosity was measured by an Instron capillary rheometer with a capillary die (D = 760 μm and L/D = 41.4). The barrel diameter of the rheometer was 9.53 mm. The measurements were carried out at a temperature of 180 °C throughout. The shear viscosities were calculated following the Rabinowitch procedure. A long die was used in order to neglect end effects or Bagley correction.

A 45-mm Killion single-screw extruder with a coni-cylindrical (convergent) die was

used to measure the elongational viscosity, following the convergent flow analysis of Cogswell [10]. The characteristics of the 30° conical die were: diameter at the entry = 45 mm, diameter at the exit = 1.6 mm, and length = 37.4 mm. The melt temperature was set at 180°C and monitored at the entry of the die by using a moving thermocouple. The maximum variations of the melt temperature across the die were observed to be ±2 °C. The densities of the molten polymers were measured using an Instron capillary rheometer, replacing the capillary by a plug, and used to calculate the volumetric flow rates.

5.4.3. Blown Film Extrusion

The same extruder as used for the converging flow experiments was employed to produce blown films. A helical blown film die (outer diameter = 50.91 mm and die gap at exit = 920 μm) was used in this study. The experimental procedure of the film blowing operations is detailed in our recent publication [11]. Extensive experiments were carried out in order to investigate the effects of material characteristics and key process variables, that is: extrusion temperature, molten polymer flow rate, take-up ratio (TUR), blow-up ratio (BUR), and frost line height (FLH), on the dynamics and kinematics of the process.

Displacements were measured by a standard tracer technique and used to determine axial velocities and strain rates. The thickness profile was calculated from the mass balance equation by using the velocity and diameter profiles. The bubble temperature measurements

along the length of the bubble were carried out by using an infrared pyrometer (IRCON 3400). The emittance dependence on the thickness was taken into account. The birefringence measurements in the melt zone were carried out by using an optical train with a polarization modulation scheme based on a rotating half wave plate. The pressure inside the bubble was determined with a pressure transducer. Experimental details of these measurements can be found elsewhere [12,13].

5.5. RESULTS

5.5.1. Rheological Measurements

The complex viscosities, η^*, for the three polymers used in this study at a temperature of 180 °C are shown in Figure 1. At low frequencies, the HDPE has the highest viscosity and the LLDPE, the lowest. The HDPE does not depict a plateau in the low frequency region. At high angular frequencies, the LLDPE has the highest viscosity and the LDPE, the lowest. The zero shear viscosities (η_0) were determined using the Carreau-Yasuda model [18] and are reported in Table 1.

Figure 1 also includes the results of the steady shear viscosity (open symbols) obtained from the capillary rheometer. For the LLDPE, the dynamic and the steady shear viscosities match quite well at corresponding shear rate and frequency indicating that the Cox-Merz rule

[19] is fairly satisfied. For the HDPE and the LDPE, the shear viscosities are somewhat higher than the complex viscosities; the violation of the Cox-Merz rule being more pronounced for the LDPE. Cogswell [20] discussed the relationship between steady shear and dynamic viscosity. He has stated that the differences between steady shear and dynamic viscosity measurements were indicating of the nonlinear response of the material to irrotational (extensional) flows. Shroff and Shida [21] noted that with increasing branching for PE resins the differences between steady shear and dynamic viscosity increase. Our observations are in line with theirs. Nevertheless, it should be mentioned that there are reports in the literature [22,23] showing that branched polyethylenes exhibit a better agreement with the Cox-Merz rule while linear polyethylenes tend to violate it. Obviously, further work is required to find out the range of validity of Cox-Merz rule for polyolefins.

Figure 2-a reports the uniaxial elongational viscosities of the three polymers calculated from the convergent flow analysis. The capillary shear data were used to calculate the shear flow contribution to the total pressure drop. We were not able to produce elongational data at lower elongational strain rates due to apparatus limitations. The uniaxial elongational viscosities are presented in terms of an effective rate of deformation defined as:

$$\dot{\bar{\gamma}} = \sqrt{\frac{1}{2} II_{\dot{\gamma}}} = \sqrt{3}\ \dot{\varepsilon} \qquad (5)$$

where $II_{\dot{\gamma}}$ is the second invariant of the rate-of-deformation tensor and $\dot{\varepsilon}$ the uniaxial

elongational strain rate. Since the shear rate changes continuously in the convergent die, a truly steady state may not be attained. Hence, the calculated viscosity is an apparent one. Our data indicate that the elongational viscosity of the LDPE is much higher than that of the HDPE and the LLDPE at lower strain rates and that it decreases as the strain rate increases and reaches, more or less, the same level as the elongational viscosity of the HDPE at higher strain rates. The HDPE shows slightly higher viscosity than the LLDPE, however, the difference might be within experimental errors. The elongational viscosity of the HDPE and the LLDPE do not vary much with the strain rate. Figure 2-b compares the Trouton ratio, that is: the ratio of the elongational viscosity to the shear viscosity, for the three polymers investigated. The Trouton ratio for the LDPE far exceeds the prediction for a Newtonian fluid or expected from the theory of linear viscoelasticity, that is: $\eta_E/\eta=3$, while the LLDPE does not deviate much from this theory. The Trouton ratio for the HDPE is in between that of the other melts. The remarkable deviations of the LDPE from the linear behavior may be due to its strain hardening behavior. Although strain hardening is not shown in our data, it very likely occurs at lower strain rates. As far as we are aware there are no data in the literature on the elongational viscosities in the range of strain rate studied. The assessment of the available data in the literature, described in a previous section, indicates that the absolute values of converging flow elongational viscosities must be viewed with caution. Nevertheless, our data should be useful for comparing the relative elongational behavior of the polymers.

5.5.2. Bubble Temperature, Diameter, and Axial Velocity

The bubble temperature profiles along the length of the bubble for the PE resins studied and at typical film blowing conditions are shown in Figure 3. As reported in our recent publication [13], the temperature decays almost linearly until it reaches a plateau. Once crystallization is completed, the temperature decreases almost linearly. The temperatures at the plateau are about 124 °C, 108 °C, and 97 °C for the HDPE, the LLDPE, and the LDPE respectively. Obviously, the LDPE requires the highest cooling air flow rate and the HDPE the lowest for the same FLH. The length of the plateau is not noticeably different for the LLDPE and the LDPE. The HDPE shows a much broader plateau. The temperature profiles were used to determine the point at which crystallization begins.

Typical results on the bubble diameter and the axial film velocity along the length of the bubble for the three PE resins and at the same blowing conditions are shown in Figure 4. The axial velocity and bubble diameter profiles represent the elongational rheological response of the melts to the imposed take-up speed. The bubble shape is determined by the local force balances. We note that the three PE resins have quite different behaviors; the behavior of the LDPE is far different from the others. For the HDPE, the axial velocity is very low in the neck zone. Afterwards, it increases very rapidly in the bubble inflating region and then becomes constant somewhat before the FLH. In this study, the FLH is defined as distance from the die exit where the bubble diameter profile becomes flat. Figure 4 shows that the axial

velocity for the LDPE is very high compared with the HDPE in the neck zone. Then, it increases smoothly until the FLH at which it becomes constant. The velocity profile of the LLDPE is in between those of the other PE resins but closer to that of the HDPE.

The results for the bubble diameter are reported in Figure 4. We note that the bubble diameter profiles demonstrate the same trend as the axial velocity profiles; the HDPE is inflated in a shorter distance and, on the other hand, the LDPE is inflated in a longer distance, that is: the inflation takes place in a smoother manner. Again, the behavior of the LLDPE is in between those of the other two polymers. These trends are in agreement with the results reported in the literature [6].

We observed that, in most cases, the film velocity of the HDPE became constant somewhat, say about 20 mm, before the FLH, which was almost the beginning of the plateau in the bubble temperature profile (see Figure 3). Decreasing the extrusion temperature from 220 °C to 150°C did not affect either the bubble diameter or the film velocity significantly. However, a noticeable effect of the extrusion temperature on the film velocity was observed for the LDPE. As the extrusion temperature decreased, the axial distance at which plateauing of the velocity profile occurred shifted towards the die exit.

The bubble diameter and axial velocity data were smoothed by fitting into polynomial functions. Fifth order polynomials were used to fit the entire range of the bubble diameter

data of the three polymers and the axial velocity data of the LDPE. However, we could not obtain a good fitting of fifth order polynomials for the axial velocity data of the HDPE and the LLDPE. This was achieved by breaking the data into two parts. Second order polynomials were used to fit the first part of the data in which we had slow increase in the film velocity. The second part of the data in which we had rapid increase in the film velocity and then levelling off the film velocity was fitted into fifth order polynomials.

5.5.3. Strain Rates

The machine and transverse directions (MD and TD respectively) strain rates were calculated from equations 1 and 2 by taking the derivatives of the smoothed bubble diameter and axial velocity data. Figure 5 compares the MD and TD strain rates of the three PE resins. The sudden jumps in the MD strain rates for the HDPE and the LLDPE at almost 150 mm are due to the use of two different polynomial expressions, as explained in the previous section. For the HDPE, the MD strain rate is first very small, then increases drastically and reaches a maximum and finally decreases to about zero at the FLH. The LLDPE shows quite the same MD strain rate profile except that the maximum is lower and that it has higher strain rates at low axial distances. The MD strain rate profile of the LDPE is very different from the others: it decreases smoothly until it becomes zero above the FLH. The maximum in the MD strain rate of the LDPE may probably occur very close to the die exit where we could not make any measurements because of the air ring.

The TD strain rates of the polymers are not as different as the MD strain rates. The maximum in the TD strain rate of the HDPE is somewhat higher than the others and for the LDPE it occurs earlier than the others. Note that for the LDPE, the TD strain rate exceeds the MD strain rate in the region of bubble expansion. Such results were also observed by Farber and Dealy [1].

5.5.3.1. Effect of the Processing variables

We have discussed the effects of the film blowing parameters on the strain rates of the LLDPE elsewhere [13]. In this article, the effects on the HDPE and the LDPE will be shown and compared with the results of Kanai and White [6]. The effect of the BUR is depicted in Figure 6. Increasing BUR from 1.5 to 2.5 does not noticeably affect the MD strain rate for the LDPE. For the HDPE, the maximum in the MD strain rate occurs earlier as the BUR decreases but its magnitude remains almost unchanged. For both polymers, the TD strain rate increases with increasing BUR; the effect being more pronounced with the LDPE. The effect of the FLH is shown in Figure 7. For the HDPE, both the MD and TD strain rates increase with decreasing FLH but the increase in the MD strain rate is much more pronounced. In contrast with our results, Kanai and White [6] reported that the TD strain rate increased with increasing FLH for a HDPE. For the LDPE, no significant effect on the MD strain rate is observed above the axial distance of about 100 mm. The TD strain rate increases as the FLH decreases. As shown in Figure 8, increasing the extrusion temperature does not significantly

affect the TD strain rates of the two resins and the MD strain rate of the HDPE, but for the LDPE the MD strain rate pattern changes considerably with temperature. Much higher MD strain rate are observed at lower temperatures. The effect of the TUR and the polymer flow rate on the strain rates for the HDPE and the LDPE was also investigated. Both the MD and the TD strain rates considerably increased with increasing TUR and/or polymer flow rate, as it was the case for the LLDPE [13]. The results are not reported here.

5.5.4. Pressure Inside the Bubble (P_i)

5.5.4.1. Effect of TUR

Figure 9 shows the effect of the TUR on the P_i value for the three PE resins at the two different extrusion temperatures. For some experimental points, error bars are shown, indicating a good reproducibility in the measurements. The three polymers depict quite different behaviors. For the LLDPE, the P_i value increases with increasing TUR at both extrusion temperatures of 220 °C and 150 °C. For the HDPE, it increases very slightly at the higher extrusion temperature but decreases slightly at the lower extrusion temperature with increasing TUR. Finally, for the LDPE, it decreases with increasing TUR at both extrusion temperature. The differences between the P_i values for the three polymers at low TUR are small. However, they become very large at high TUR; the LLDPE showing the highest P_i and the LDPE, the lowest. Our results are not in agreement with the findings of Kanai and White

[6] who observed that the P_i value increased with increasing TUR for all PEs and that LDPE required much higher inflation pressure than the other melts. In a recent article, Kurtz [24] speculates that as the take-off rate goes to zero the pressure difference across the bubble must also go to zero. Our results shows that this is not true, in particular for LDPE. Wagner [3] and Tas [8] have also observed that the P_i value increases with decreasing TUR for LDPE.

In the case of the LLDPE, the measurements at the extrusion temperature of 220 °C were restricted to TUR values up to about 12 because of bubble instabilities. The bubble stability, however, increased when decreasing the extrusion temperature to 150 °C so that we were able to reach higher TUR values, as shown in Figure 9. In the case of the LDPE, bubble break up was observed at high TUR values. This was also reported by Kwack and Han [25] and attributed to the strain hardening behavior of LDPE in elongational flow. In the case of the HDPE, We did not observed either bubble instability or bubble break up within the limit of our take-up device.

5.5.4.2. Effect of BUR

The effect of BUR on the P_i value is shown in Figure 10. The P_i value is a decreasing function of the BUR for all the resins, at both extrusion temperatures. These results are in agreement with the results of Kanai and White [6] and Tas [8] but not with those of Wagner [3] who observed that the P_i value remained almost constant with increasing BUR for a

LDPE. This disagreement may be due to different experimental procedures. In our experiments, the cooling air flow rate was adjusted to maintain a constant FLH, while in the Wagner's experiments the cooling air flow rate was likely kept constant and consequently the FLH was altered with increasing BUR. In other words, Wagner probably considered the FLH as a dependent variable. An increase in the BUR with decreasing the pressure inside the bubble has been predicted using various viscous and viscoelastic models [26-30]. Han and Park [27] have explained this behavior as follows. In order to balance the surface tension forces between the inflated bubble and the air, a greater excess pressure is required for a small bubble radius. Here, we examine the observed behavior from a rheological point of view. In the neck zone, where the second derivative of the radius can be assumed to be zero, Equation 4 is reduced to:

$$\frac{\Delta P}{h} = \frac{\sigma_{33}}{r} \qquad (6)$$

We can also assume that the film thickness, the bubble radius, and the strain rates are almost the same for different BUR values in the neck zone, below the bubble inflation point. However, as we already observed [13], the melt temperature increases as the BUR increases in this zone since the cooling air flow rate has to be decreased in order to maintain a constant FLH. Therefore, a lower value of σ_{33} is expected with increasing film temperature at higher BUR explaining why ΔP decreases with increasing BUR. We also observed that the rate of decrease in the P_i value with the BUR depended on the FLH as it was higher at lower FLH.

5.5.4.3. Effect of FLH

As shown in Figure 11, there is a very steep increase in the P_i values for all the resins as the FLH is decreased to very small values for which the bubble is very close to the air ring. Under these circumstances, the cooling air jet produces a significant axial force on the bubble [31] and causes the rapid increase in the P_i value. We observed that at lower BUR values, the P_i was not increased as much as at higher BUR values. This can be simply explained by noticing that at lower BUR the axial force acting on the bubble is lower. Such aerodynamics forces are generally assumed to be negligible in film blowing modeling (see Equations 3 and 4). Obviously, such an assumption is not valid at very low FLH. At axial distances far from the air ring, we observed that the three PE resins had quite different behaviors. For the LLDPE, the P_i value noticeably increases with decreasing FLH. For the HDPE, it increases very slightly at high extrusion temperature and is almost constant at low extrusion temperature. Finally, in the case of the LDPE, the P_i value very slightly increases at high extrusion temperature but decreases at low extrusion temperature with increasing FLH. In addition to this interaction between the FLH and the extrusion temperature influencing the P_i, the interaction between the FLH and the TUR was also observed. For the HDPE and at the extrusion temperature of 150°C, with decreasing FLH, the P_i increased at lower TUR but decreased at higher TUR (in the region far from the air ring). Kanai and White [6] have observed for different PE resins that the pressure inside the bubble considerably increases with decreasing FLH.

5.5.4.4. Effect of Extrusion Temperature

The effect of the extrusion temperature on the P_i value is depicted in Figures 9-11. For the three resins, the P_i value increases as the extrusion temperature decreases. This can simply be explained in terms of the melt strength of resins, which increases with decreasing extrusion temperature [32]. Hence, it is expected that more pressure is required to inflate the molten tube leaving the die at lower temperature. Figure 10 shows that the effect of extrusion temperature is most pronounced for the LLDPE and least for the HDPE.

5.5.4.5. Effect of Polymer Flow Rate

Figure 12 shows that the P_i values increase as the polymer flow rate increases at almost constant TUR. This can be explained from a rheological point of view. As the polymer flow rate increases the strain rates and, therefore, stresses increase. From Equation 4 one can then expect an increase in the pressure inside the bubble. The effect of the polymer flow rate may also be partly due to the aerodynamic forces which increase with the polymer flow rate. As the polymer flow rate increases the cooling air flow rate has to be increased in order to keep the FLH at the same value, causing an increase in the aerodynamic forces acting on the bubble. Note that these forces are neglected in force balance Equations 3 and 4. In the range of the polymer flow rate studied, the P_i values are the highest for the LLDPE except at very low polymer flow rate. The rate of increase in the P_i value is the highest for the LLDPE and

the lowest for the HDPE indicating that the LLDPE has the highest sensitivity to the variations of the polymer flow rate.

5.5.5. FLH vs. TUR and FLH vs. BUR Curves

The effects of the TUR and the BUR on the FLH at constant cooling air flow rate are presented in Figure 13. The FLH is treated as a dependent variable in these experiments. The FLH drastically decreases with increasing BUR for all the polymers studied. Wagner [3] observed the same trend for LDPE. This can be explained by the more efficient heat transfer due to more surface created as the BUR increases. Therefore, the bubble temperature decreases faster which makes the FLH decrease. The three polyethylene resins show different dependences of the FLH on the TUR, as illustrated in Figure 13. For the HDPE and the LLDPE, increasing TUR makes the FLH increase monotonously. The HDPE shows somewhat stronger dependence of the FLH. For the LDPE, the FLH first increases slightly with increasing TUR and then it becomes almost constant. A similar result was also observed for the LDPE at a higher level of the FLH. Our results are not in agreement with those of McNally et al. [33] who obtained an almost linear increase in the FLH with increasing take-off speed for a LDPE. One can relate the different behaviors of these PE resins to the bubble shapes. As the TUR increases, the bubble contour is changed to fulfil the new force equilibria. The bubble diameter in the melt zone decreases with increasing TUR for the HDPE and the LLDPE, causing a decrease in the surface area available for heat transfer and resulting in a

FLH increase. For the LDPE, the bubble diameter does not vary significantly with the TUR explaining why the FLH remains almost constant with increasing TUR.

5.5.6. Birefringence

The in-plane birefringence measurements were carried out along the length of the bubble in the melt zone, i.e., up to the beginning of the temperature plateau, for the three polymers and at two different TUR values. The maximum value of the bubble inflation angle was observed for the HDPE at high TUR which amounted to 19°. The contribution of the out-of-plane birefringence was then calculated, as explained elsewhere [13], and found to be less than 5%. For the LDPE, it was less than 2%. Therefore, on-center light beam was assumed to give the in-plane birefringence ($n_{11} - n_{33}$). Figure 14 presents the results of the birefringence measurements. In general, the LDPE shows the highest birefringence except in the region close to the FLH in which the HDPE has the highest birefringence possibly due to some crystallization. The LLDPE displays the lowest birefringence along the entire length of the bubble. The birefringence values increase with increasing TUR for all PE resins. The increase in the birefringence in the region close to the die exit is much more pronounced for the LDPE than for the HDPE and the LLDPE.

5.5.7. Machine and Transverse Stresses

The MD and TD stresses were calculated from the stress-optical law and the force

balance perpendicular to the film (Equation 4), using the birefringence and pressure data. For the stress-optical coefficient of PE, an average value from literature [34] equal to 2.1×10^{-9} m^2/N was used. Figure 15 compares the stress field of the three polymers at similar film blowing conditions. In general, for all the polymers, the MD stress was always greater than the TD stress which obviously resulted from observed positive birefringences. At low axial distance, the LDPE shows considerably higher MD stress than the other two polymers. For the HDPE, the MD stress is somewhat lower than that for the LLDPE. However, at high axial distance, i.e., vicinity of the FLH, this order is reversed: the HDPE shows the highest MD stress and the LDPE, the lowest. In the region close to the die the LDPE shows the highest TD stress and the HDPE, the lowest. At higher axial distance, the highest TD stress is observed for the LLDPE and the lowest for the LDPE.

We now compare the strain rate data (Figure 5) and stress data (Figure 15). For the LDPE, the MD strain rate is lower than the TD strain rate in the region of bubble expansion while the MD stress is always higher than the TD stress. Moreover, we note that the differences between the MD and TD strain rates in the neck zone for the LLDPE are higher than those for the HDPE whereas the differences between the MD and TD stresses in this zone for the LLDPE are lower than those for the HDPE. From these observations, one can conclude that there is no simple equation relating stresses and strain rates in film blowing. One expects that most constitutive equations would fail handling these situations. The strain rate data do not appear to be sufficient to portray the effects of melt rheology in film blowing.

Farber and Dealy [1] attempted to correlate melt rheology of a LDPE to molecular orientation in solidified film by means of strain rate and film shrinkage data. They found that the MD shrinkage was always greater than the TD shrinkage but the TD strain rate was not consistently lower than the MD strain rate. They then concluded that melt rheology does not play an important role on orientation. However, our stress data for the LDPE show similar trends as the shrinkage data of Farber and Dealy. One cannot rule out the influence of melt rheology in film blowing, which is obviously quite complex.

The stress data of Figure 15 disclose another important point. It is commonly believed in the literature (see for example Dealy and Wissbrun [35]) that LLDPE exhibits lower extensional stresses in the molten blown bubble, because of its strain softening behavior, and this renders the LLDPE bubble more prone to instabilities. Our data show that this is not necessarily true. Indeed, the extensional stresses of the LLDPE are comparable with those of the HDPE. What makes the LLDPE different from the others is in fact its lower stress ratio, the ratio of the MD stress to the TD stress. We feel that the bubble instabilities of LLDPE may be related to its lower stress ratio.

The effect of the TUR on the stresses is shown in Figure 16. In general, both the MD and the TD stresses increase as the TUR increases. However, different behaviors among the three PE resins can be discriminated. For the HDPE and the LDPE, the MD stress increases more significantly than the TD stress does. For the LLDPE, the increase in the MD and the

TD stresses is quite comparable. In other words, the LLDPE retains a more balanced MD and TD stresses even at higher TUR values. For the LDPE and the LLDPE, the MD stress noticeably increases along the entire length of the bubble. For the HDPE, however, it increases slightly at low axial distance but significantly at high axial distance.

5.5.8. Biaxial Elongational Viscosity

The stress and strain rate data can be used to calculate an apparent non-uniform biaxial viscosity. Han and Park [2] suggested that the elongational viscosity in non-uniform biaxial stretching, η_{be}, may be represented as:

$$\eta_{be} = \frac{\sigma_{11}}{2\,\dot{\gamma}_{11} + \dot{\gamma}_{33}} \qquad (7)$$

or

$$\eta_{be} = \frac{\sigma_{33}}{2\,\dot{\gamma}_{33} + \dot{\gamma}_{11}} \qquad (8)$$

Not surprisingly, the two elongational viscosities calculated from these equations for our data were not identical; the disagreement being worse for the LDPE. Kanai and White [6] used only Equation 7 to examine the apparent elongational viscosity in film blowing. Agassant et al. [36] have suggested that a non-uniform biaxial elongational viscosity can be obtained by

adding the two components of the stress tensor:

$$\sigma_{11} + \sigma_{33} = \eta_{be} (\dot{\gamma}_{11} + \dot{\gamma}_{33}) \qquad (9)$$

This idea is used here and Figure 17 reports η_{be} for the three PE resins and at typical film blowing conditions as a function of the effective rate of deformation defined as:

$$\dot{\bar{\gamma}} = \sqrt{\frac{1}{2} II_{\dot{\gamma}}} = \sqrt{\frac{1}{2} (\dot{\gamma}_{11}^2 + \dot{\gamma}_{22}^2 + \dot{\gamma}_{33}^2)} \qquad (10)$$

For the HDPE, η_{be} appears to be almost constant at low axial distances. As the rate of deformation increases, it decreases rapidly, showing a sharp peak. Then, as the rate of deformation decreases, η_{be} increases. For the LDPE, η_{be} increases monotonously along the length of the bubble and the rate of deformation exhibits a smoother profile. The LLDPE shows a tendency intermediate between the HDPE and the LDPE. At the end of the melt zone, the LDPE exhibits the highest η_{be} . Note that as we are dealing with a non-isothermal process, the apparent elongational viscosity is also influenced by the melt temperature (see Figure 3). These biaxial elongational viscosities are much higher, roughly by the order of two decades, than the isothermal uniaxial elongational viscosities (Figure 2). The large differences may be explained by differences in flow kinematics, cooling effects and much lower strain rates experienced by the melts in film blowing.

5.6. CONCLUDING REMARKS

Our extensive experimental results reveal the effects of the material characteristics and processing variables on the kinematics and dynamics of the film blowing process. The three PE resins used in this study display different bubble diameter and axial film velocity profiles which lead to quite different strain rate profiles. The peak MD strain rate of the HDPE is higher than that of the LLDPE. For the LDPE, it occurs at very low axial position, close to the die exit. It is observed that both MD and TD strain rates significantly increase with increasing TUR and/or polymer flow rate. Increasing BUR increases the TD strain rate considerably but not the MD strain rate. Increasing FLH mostly affects the MD strain rate for the HDPE. For the LDPE, no clear effect of the FLH on the MD strain rate is observed in the range of axial distance studied. The extrusion temperature shows no noticeable effect on the strain rates for the HDPE but it has some effects on the MD strain rate for the LDPE.

The LLDPE was found to require the highest pressure inside the bubble, whereas the LDPE, the lowest, that is: the relative order of the pressure inside the bubble is as follows:

$$\text{LLDPE} > \text{HDPE} > \text{LDPE}.$$

We observed that the P_i value increased with decreasing BUR, decreasing extrusion temperature, and increasing polymer flow rate. The effects of TUR and FLH depend on the polymer and processing conditions. Strong interactions between the various process parameters are observed. It appears that the LLDPE is the most sensitive polymer to the

variations of processing variables and the HDPE, the least one. In summary, the pressure inside the bubble is clearly a dependent variable. It is a rather complex response of several variables such as polymer melt rheology, film thickness, bubble temperature, axial velocity, bubble radius, and polymer flow rate.

The LDPE had the highest birefringence and the LLDPE, the lowest. This order is consistent with the above-mentioned order for P_i. The higher the P_i value, the higher the TD orientation is expected which means a lower birefringence, as observed.

Comparing the results of pressure and birefringence measurements with the apparent uniaxial elongational viscosities obtained from the convergent flow analysis for the three polymers, we note that the higher the elongational viscosity, the lower the P_i value and the higher the birefringence. This correlation is expected as a higher uniaxial elongational viscosity indicates a higher molecular orientation in the machine direction. It must be, however, noted that since the range of elongational strain rate in the film blowing experiments is quite different from that in the converging flow experiments, the comparison should be viewed with caution. Moreover, it should be mentioned that the deformation occurring in the bubble lies somewhere between biaxial extension and planar extension. Thus, the biaxial and planar elongational viscosities should be more appropriate tools in order to establish correlations between rheology and processing in film blowing. We also notice that P_i and birefringence data can be correlated with bubble instabilities reported in our previous study

[11]. The most unstable polymer (LLDPE) requires the highest P_i and has the lowest birefringence.

The stress data were calculated with the help of the birefringence and P_i data. At the same processing conditions, the LLDPE exhibits the lowest stress ratio indicating that a more isotropic film is achievable with LLDPE. This may be attributable to the absence of the long chain branching in LLDPE [25]. From a comparison between strain rate and stress data, we find that there is no simple correlation between stresses and strain rates in film blowing; known rheological constitutive equations would probably fail describing the experimental data. Therefore, the findings in our recent article [13] should not mislead one to conclude that the Newtonian model might be a suitable model to qualitatively predict the stresses occurring in film blowing. We feel that the strain rate data are not sufficient to represent the effects of melt rheology and to discern between behaviors of different resins in film blowing. Any attempt to correlate final film properties to processing conditions and material characteristics should utilize the stress as well as the strain rate data. The pressure inside the bubble and the stress data are, to our point of view, very sensitive parameters, that could be used for model assessment. Apparent non-uniform biaxial elongational viscosities were calculated along the length of the bubble using the stress and strain rate data. At the end of the melt zone, the LDPE exhibits the highest elongational viscosity and the lowest rate of deformation.

5.7. ACKNOWLEDGMENT

The authors wish to acknowledge financial support received from the FCAR programme of the Province of Quebec and from NSERC. We are also thankful to Union Carbide, Petromont, and Novacor for supplying the polymers used in this study.

5.8. REFERENCES

1. Farber, R., and J.M. Dealy, (1974) "Strain History of the Melt in Film Blowing," *Polym. Eng. Sci.*, **14**, 435.
2. Han, C.D., and J.Y. Park, (1975) "Studies on Blown Film Extrusion. I. Experimental Determination of Elongational Viscosity," *J. Appl. Polym. Sci.*, **19**, 3257.
3. Wagner, M.H., (1978) "Experimental Investigations into the Analysis of the Film Blowing Process," *Kunststoffe*, **68**, 15.
4. Gupta, R.K., A.B. Metzner, and K.F. Wissbrun, (1982) "Modelling of Polymeric Film-Blowing Processes," *Polym. Eng. Sci.*, **22**, 172.
5. Winter, H.H., (1983) "A Collaborative Study on the Relation Between Film Blowing Performance and Rheological Properties of Two Low-Density and Two High-Density Polyethylene Samples," *Pure & Appl. Chem.*, **55**, 943.
6. Kanai, T., and J. L. White, (1984) "Kinematics, Dynamics and Stability of the Tubular Film Extrusion of Various Polyethylenes," *Polym. Eng. Sci.*, **24**, 1185.
7. Huang, T.A., and G.A. Campbell, (1985) "Deformational History of LLDPE/LDPE Blends on Blown Film Equipment," *Advances in Polymer Technology*, **5**, 181.
8. Tas, P.P., (1994) *Film Blowing: from Polymer to Product*, Ph.D. Dissertation, Dept. Mech. Eng., Eindhoven University of Technology, The Netherlands.
9. Michaeli, W., and G. Schmitz, (1995) "Investigation of Blown Film Extrusion Using the Laser Doppler Velocimetry," *ANTEC '95*, 181.

10. Cogswell, F.N., (1972) "Converging Flow of Polymer Melts in Extrusion Dies," *Polym. Eng. Sci.*, **12**, 64.

11. Ghaneh-Fard, A., P.J. Carreau, and P.G. Lafleur, (1996) "Study of Instabilities in Film Blowing," *AIChE J.*, **42**, 1388.

12. Ghaneh-Fard, A., P.J. Carreau, and P.G. Lafleur, (1996) "Application of Birefringence to Film Blowing," *J. Plastic Film & Sheeting*, **12**, 68.

13. Ghaneh-Fard, A., P.J. Carreau, and P.G. Lafleur, (1996) "On-Line Birefringence Measurement in Film Blowing of a Linear Low Density Polyethylene," Submitted for publication in *Int. Polym. Process.*

14. Shroff, R.N., L.V. Cancio, and M. Shida, (1977) "Extensional Flow of Polymer Melts," *Trans. Soc. Rheol.*, **21**, 429.

15. Laun, H.M., and H. Schuch, (1989) "Transient Elongational Viscosities and Drawability of Polymer Melts," *J. Rheol.*, **33**, 119.

16. Covas, J.A., and O.S. Carneiro, (1990) "Assessing the Convergent Flow Analysis as a Technique for Characterizing the Extensional Flow of Polymer Melts," *Polymer Testing*, **9**, 181.

17. Chohan, R.K., (1994) "Shear and Elongational Flow of Some Branched Polyethylenes," *J. Appl. polym. Sci.*, **54**, 487.

18. Bird, R.B., R.C. Armstrong, and O. Hassager, (1987) *Dynamics of Polymeric Liquids*, 2nd ed., Wiley-Interscience, New York.

19. Cox, W.P., and E.H. Merz, (1958) "Correlation of Dynamic and Steady Flow

Viscosities," *J. Polym. Sci.*, **28**, 619.

20. Cogswell, F.N., (1972) "Measuring the Extensional Rheology of Polymer Melts," *Trans. Soc. Rheol* , **16**, 383.

21. Shroff, R.N., and M. Shida, (1970) "Effect of Long-Chain Branching on the Relation between Steady-Flow and Dynamic Viscosity of Polyethylene Melts," *J. Polym. Sci.*, Part A-2, **8**, 1917.

22. Utracki, L.A., and R. Gendron, (1984) "Pressure Oscillation During Extrusion of Polyethylenes. II," *J. Rheol.*, **28**, 601.

23. Venkatraman, S., M. Okano, and A. Nixon, (1990) "A Comparison of Torsional and Capillary Rheometry for Polymer Melts: the Cox-Merz Rule Revisited," *Polym. Eng. Sci.*, **30,** 308.

24. Kurtz, S.J., (1995) "Relationship of Stresses in Blown-film Processes," *Int. Polym. Process.*, **10**, 148.

25. Kwack, T.H., and C.D. Han, (1983) "Rheology-Processing-Property Relationships in Tubular Blown Film Extrusion. II. Low-Pressure Low-Density Polyethylene," *J. Appl. Polym. Sci.*, **28**, 3419.

26. Pearson, J.R.A., and C.J.S. Petrie, (1970) "A Fluid-Mechanical Analysis of the Film-Blowing Process," *Plast. Polym.*, **38**, 85.

27. Han, C.D., and J.Y. Park, (1975) "Studies on Blown Film Extrusion. II. Analysis of the Deformation and Heat Transfer Processes," *J. Appl. polym. Sci.*, **19**, 3277.

28. Luo, X-L., and R.I. Tanner, (1985) "A Computer Study of Film Blowing," *Polym.*

Eng. Sci., **25**, 620.

29. Cain, J.J., and M.M. Denn, (1988) "Multiplicities and Instabilities in Film Blowing," *Polym. Eng. Sci.*, **28**, 1527.

30. Alaie, S.M., and T.C. Papanastasiou, (1993) "Modeling of Non-isothermal Film Blowing with Integral Constitutive Equations," *Int. Polym. Process.*, **8**, 51.

31. Campbell, G.A., N.T. Obot, and B. Cao, (1992) "Aerodynamics in the Blown Film Process," *Polym. Eng. Sci.*, **32**, 751.

32. Goyal, S.K., (1994) "Influence of Polymer Structure on the Melt Strength Behavior of Polyethylene Resins," *SPE ANTEC'94*, 1232.

33. McNally, G.M., C. Bermingham, and W.R. Murphy, (1993) "Optimization of Performance Characteristics of LDPE/LLDPE Blends in Blown Film Extrusion," *Trans. IChemE*, 71, Part A, 223.

34. Janeschitz-Kriegl, H., (1983) *Polymer Melt Rheology and Flow Birefringence*, Berlin, Springer-Verlag.

35. Dealy, J.M., and K.F. Wissbrun, (1990) *Melt Rheology and Its Role in Plastics Processing: Theory and Applications*, New York, Van Nostrand Reinhold.

36. Agassant, J.-F., J. Avenas, J.-Ph. Sergent, and P.J. Carreau, (1991) *Polymer processing: Principles and Modeling*, New York, Hanser Publisher.

Table 1. Materials used in this study

Polymer	Supplier	MI (dg/min)	Density (kg/m^3)	η_0† (Pa.s)
HDPE	Petromont DMDC-6400	0.7	960	136400
LDPE	Novacor LF0219-A	2.0	919	21800
LLDPE	Union Carbide TUFLIN HS-7028	1.0	918	11200

† Melt viscosity at 180 °C.

FIGURE HEADINGS

Figure 1. Complex and steady shear viscosity data for HDPE, LDPE, and LLDPE at 180°C. Solid lines represent the Carreau-Yasuda model.

Figure 2. Apparent uniaxial elongational viscosity (a) and Trouton ratio (b) data for HDPE, LDPE, and LLDPE at 180°C.

Figure 3. Bubble temperature profiles along the length of the bubble for the three polymers. Polymer flow rate = 4.05 kg/h, extrusion temperature = 220 °C, TUR = 9.5, BUR = 2.0, FLH ≈ 250 mm.

Figure 4. Axial film velocity and bubble diameter profiles. Solid lines are the results of curve fitting using polynomial functions. The film blowing conditions are the same as in Figure 3.

Figure 5. Strain rates in MD and TD. The film blowing conditions are the same as in Figure 3.

Figure 6. Effect of BUR on MD and TD strain rates for HDPE (a) and LDPE (b). The other film blowing conditions are the same as in Figure 3.

Figure 7. Effect of FLH on MD and TD strain rates for HDPE (a) and LDPE (b). The other film blowing conditions are the same as in Figure 3.

Figure 8. Effect of extrusion temperature on MD and TD strain rates for HDPE (a) and LDPE (b). The other film blowing conditions are the same as in Figure 3.

Figure 9. Effect of TUR on P_i values at extrusion temperatures of 220°C (a) and 150°C

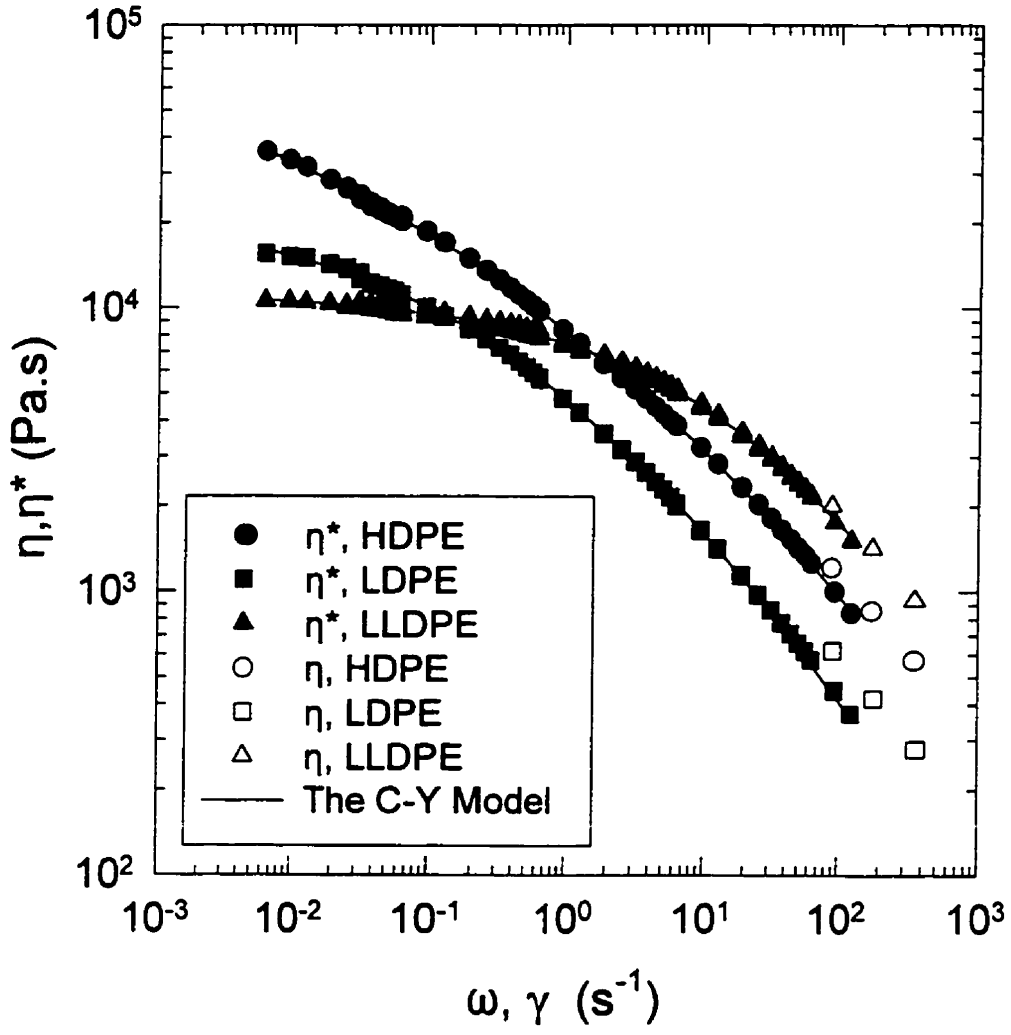

Figure 1. Complex and steady shear viscosity data for HDPE, LDPE, and LLDPE at 180°C. Solid lines represent the Carreau-Yasuda model.

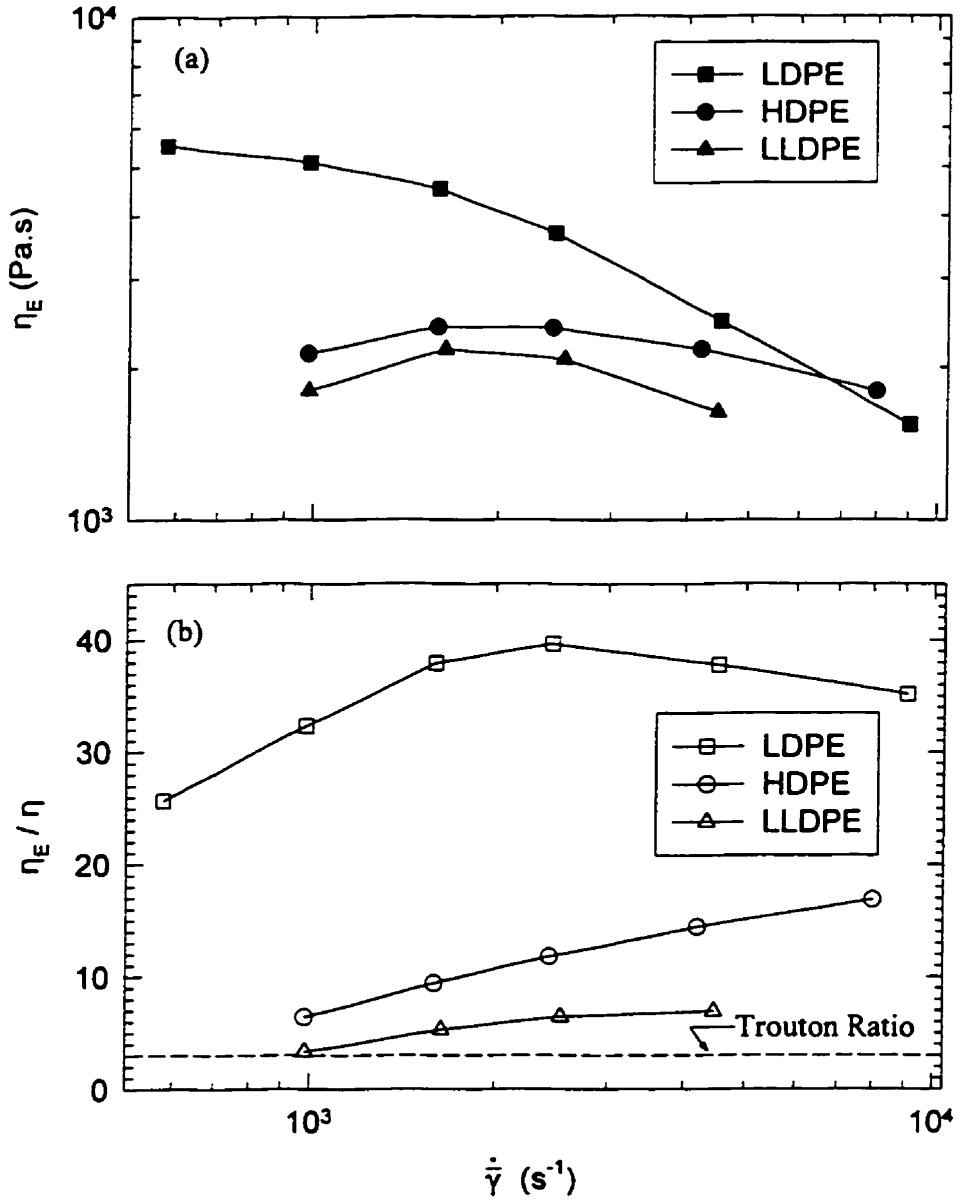

Figure 2. Apparent uniaxial elongational viscosity (a) and Trouton ratio (b) data for HDPE, LDPE, and LLDPE at 180°C.

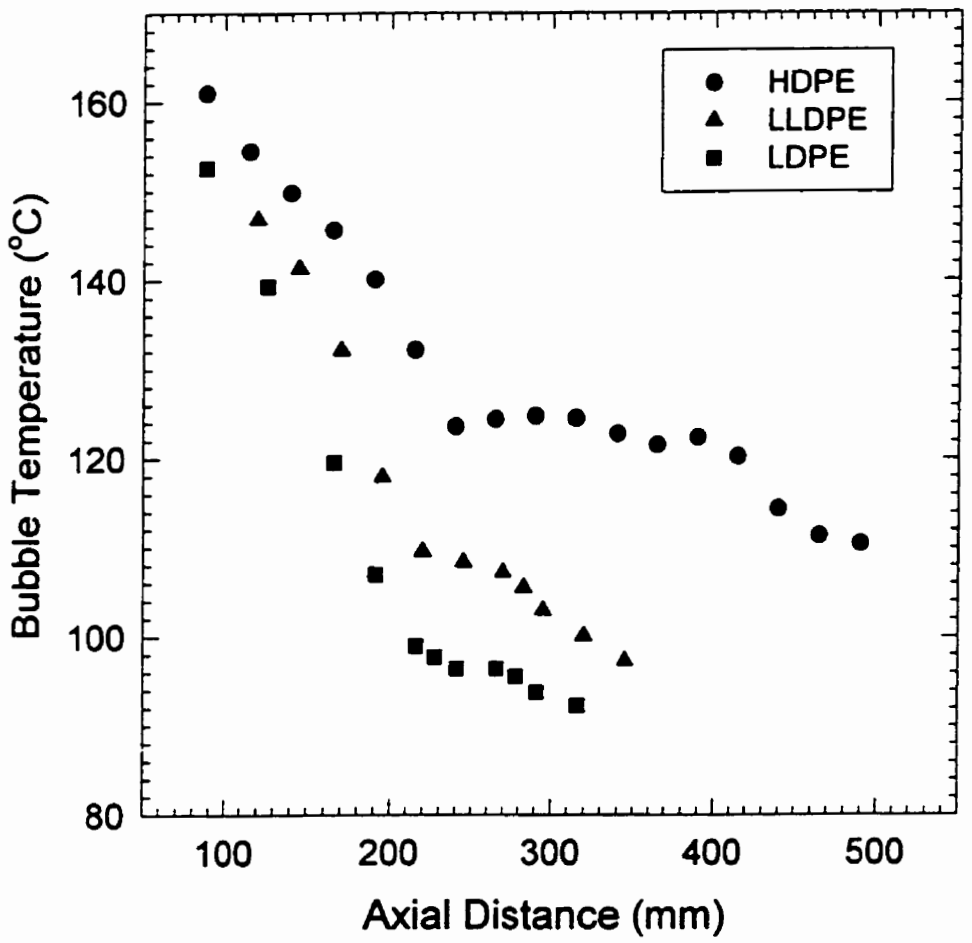

Figure 3. Bubble temperature profiles along the length of the bubble for the three polymers. Polymer flow rate = 4.05 kg/h, extrusion temperature = 220 °C, TUR = 9.5, BUR=2.0, FLH ≈ 250 mm.

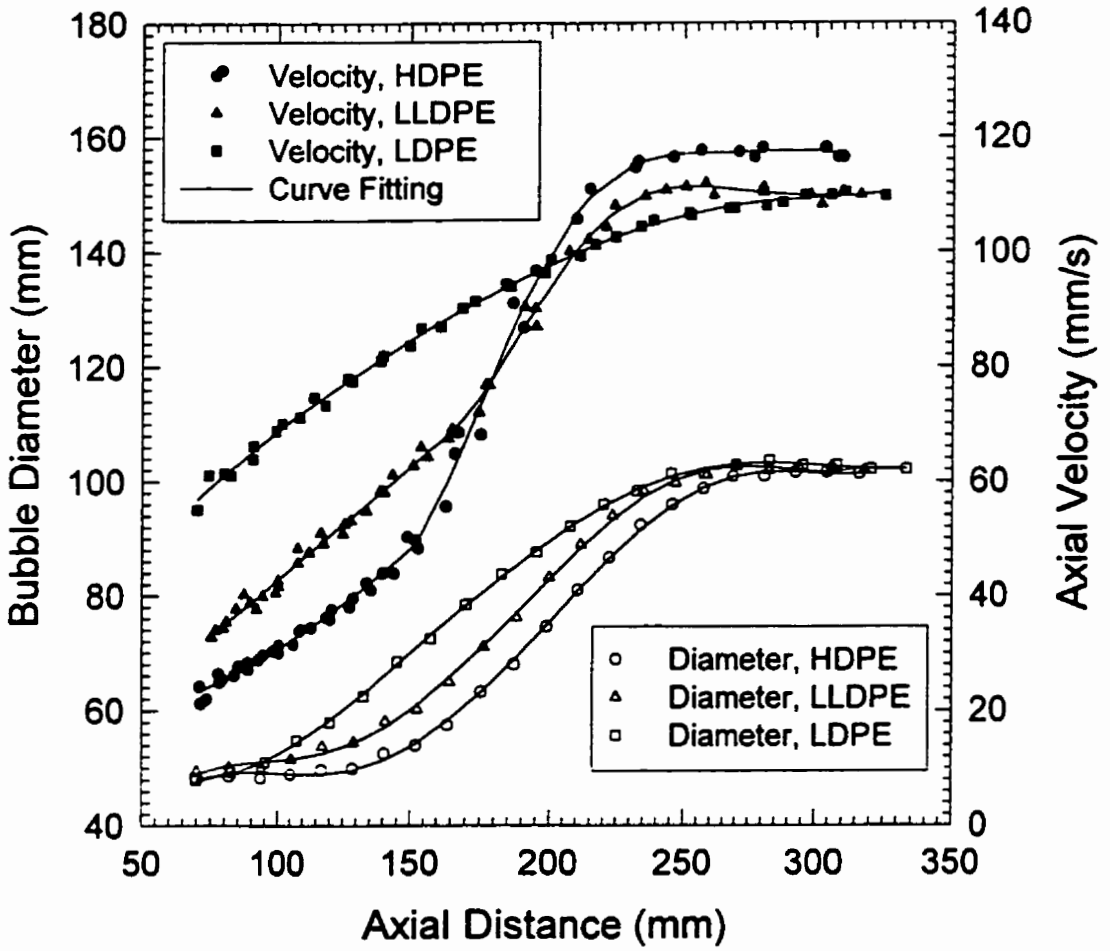

Figure 4. Axial film velocity and bubble diameter profiles. Solid lines are the results of curve fitting using polynomial functions. The film blowing conditions are the same as in Figure 3.

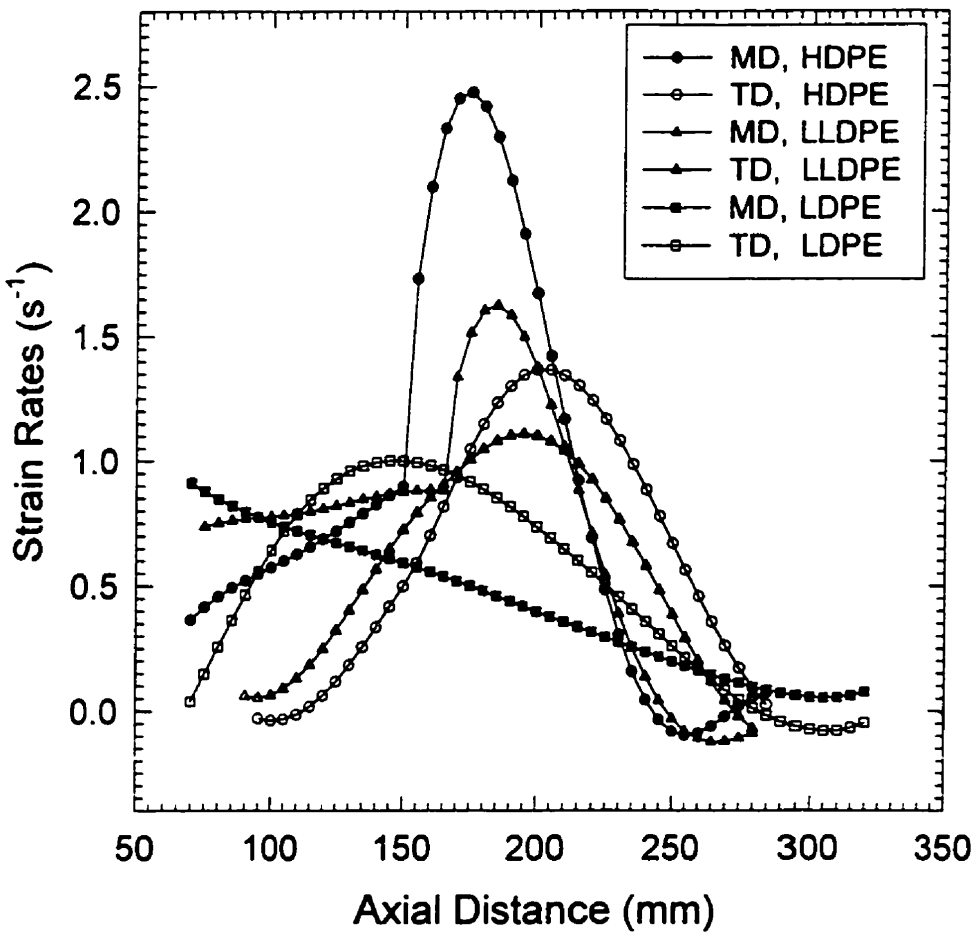

Figure 5. Strain rates in MD and TD. The film blowing conditions are the same as in Figure 3.

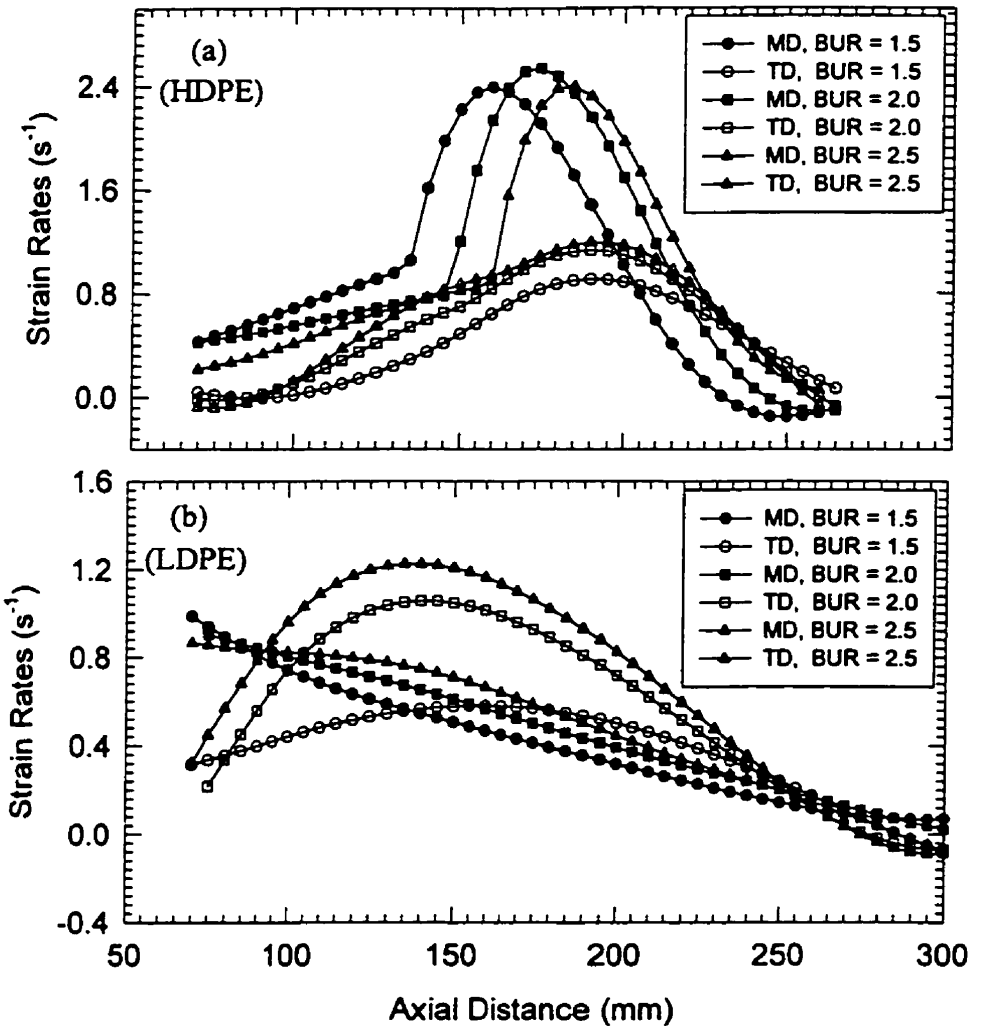

Figure 6. Effect of BUR on MD and TD strain rates for HDPE (a) and LDPE (b). The other film blowing conditions are the same as in Figure 3.

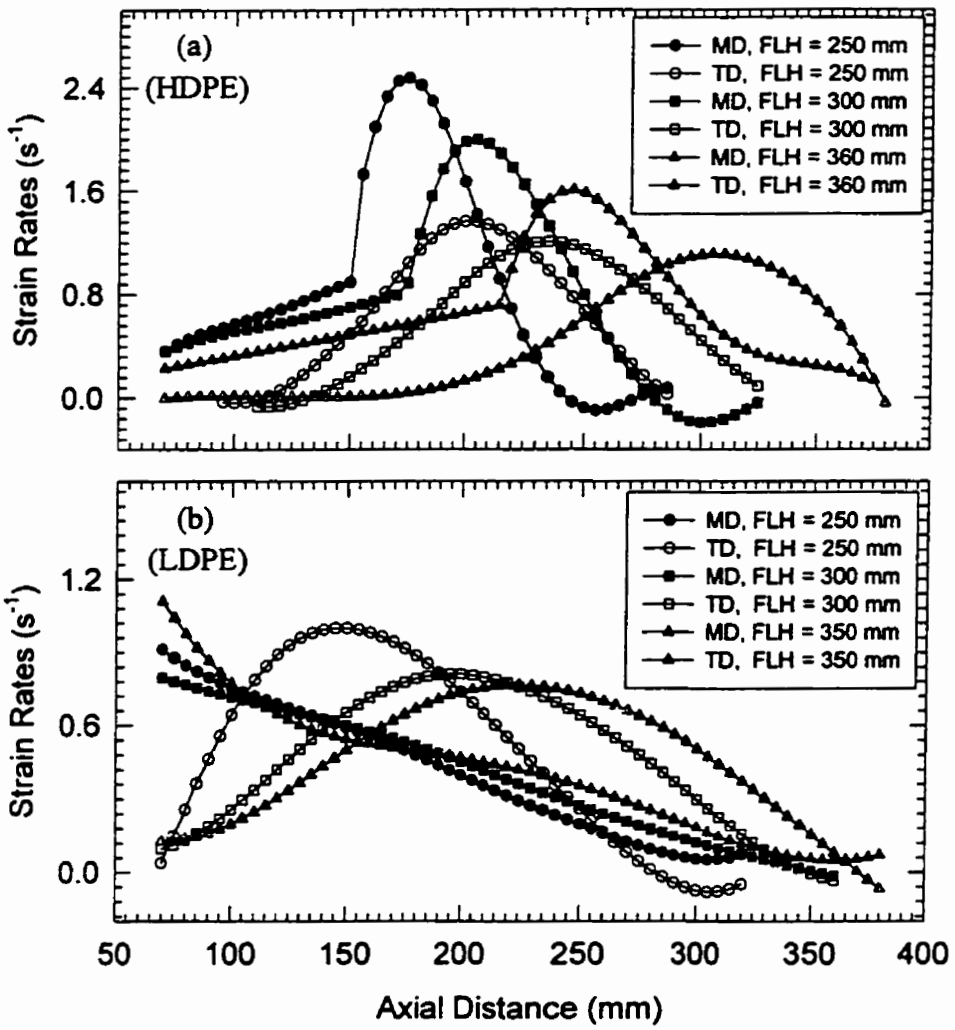

Figure 7. Effect of FLH on MD and TD strain rates for HDPE (a) and LDPE (b). The other film blowing conditions are the same as in Figure 3.

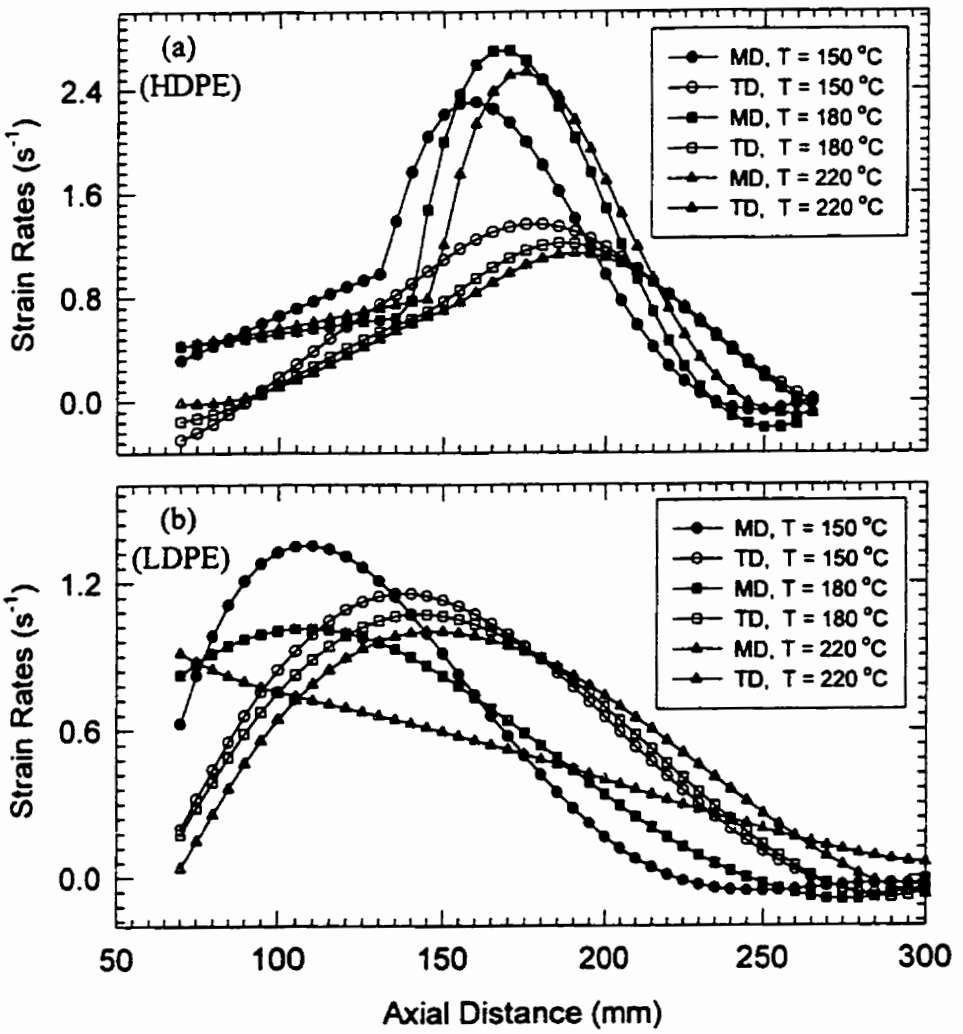

Figure 8. Effect of extrusion temperature on MD and TD strain rates for HDPE (a) and LDPE (b). The other film blowing conditions are the same as in Figure 3.

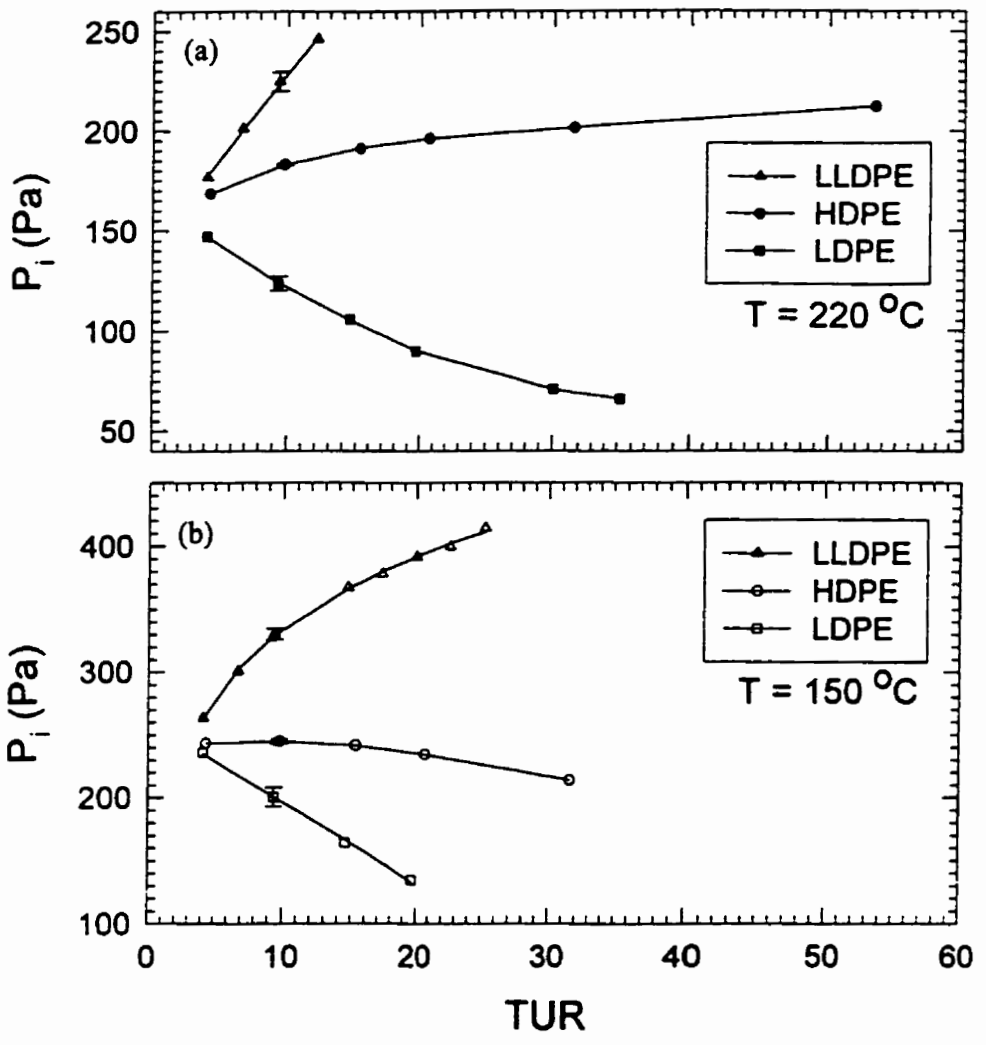

Figure 9. Effect of TUR on P_i values at extrusion temperatures of 220°C (a) and 150°C (b). The other film blowing conditions are the same as in Figure 3.

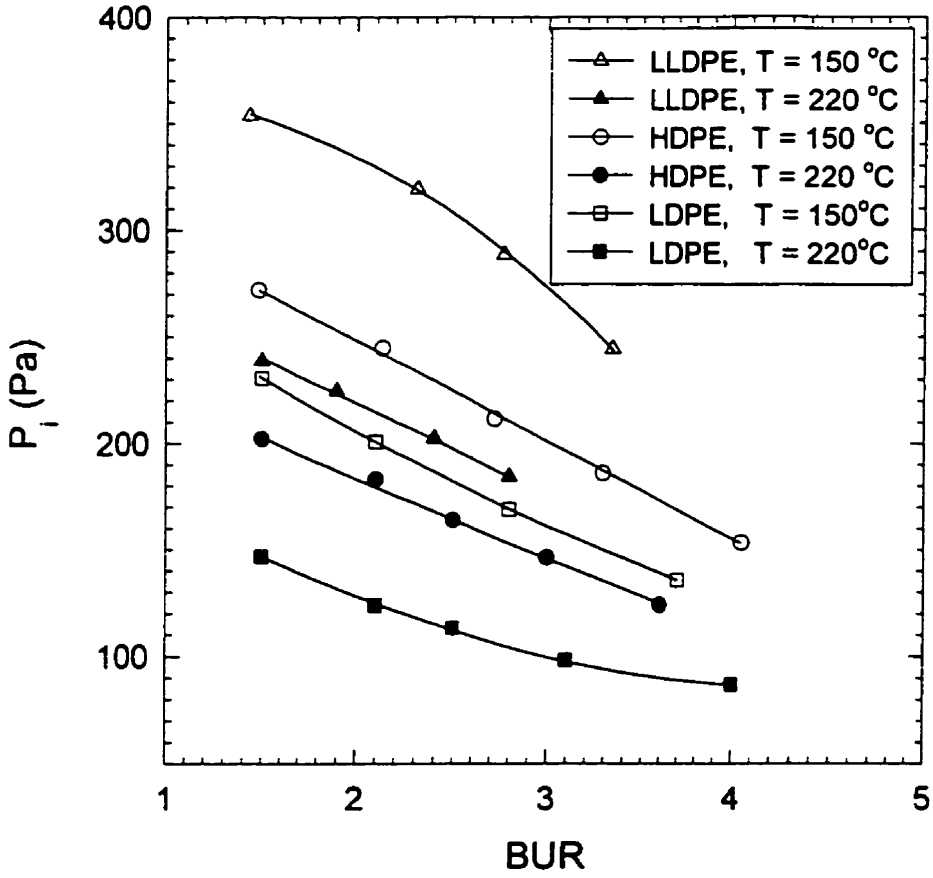

Figure 10. Effect of BUR on P_i values at extrusion temperatures of 220 °C and 150 °C. The other film blowing conditions are the same as in Figure 3.

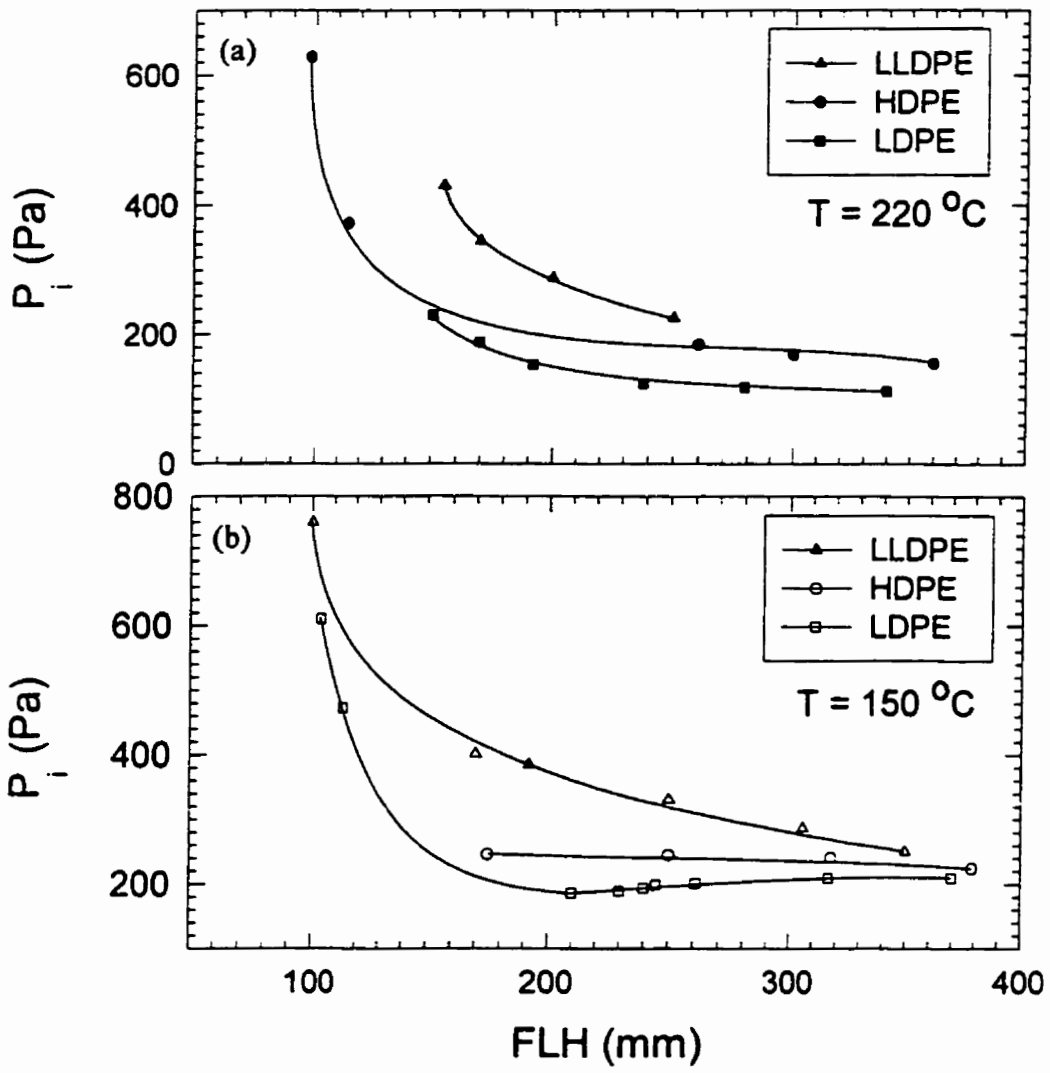

Figure 11. Effect of FLH on P_i values at extrusion temperatures of 220°C (a) and 150 °C (b). The other film blowing conditions are the same as in Figure 3.

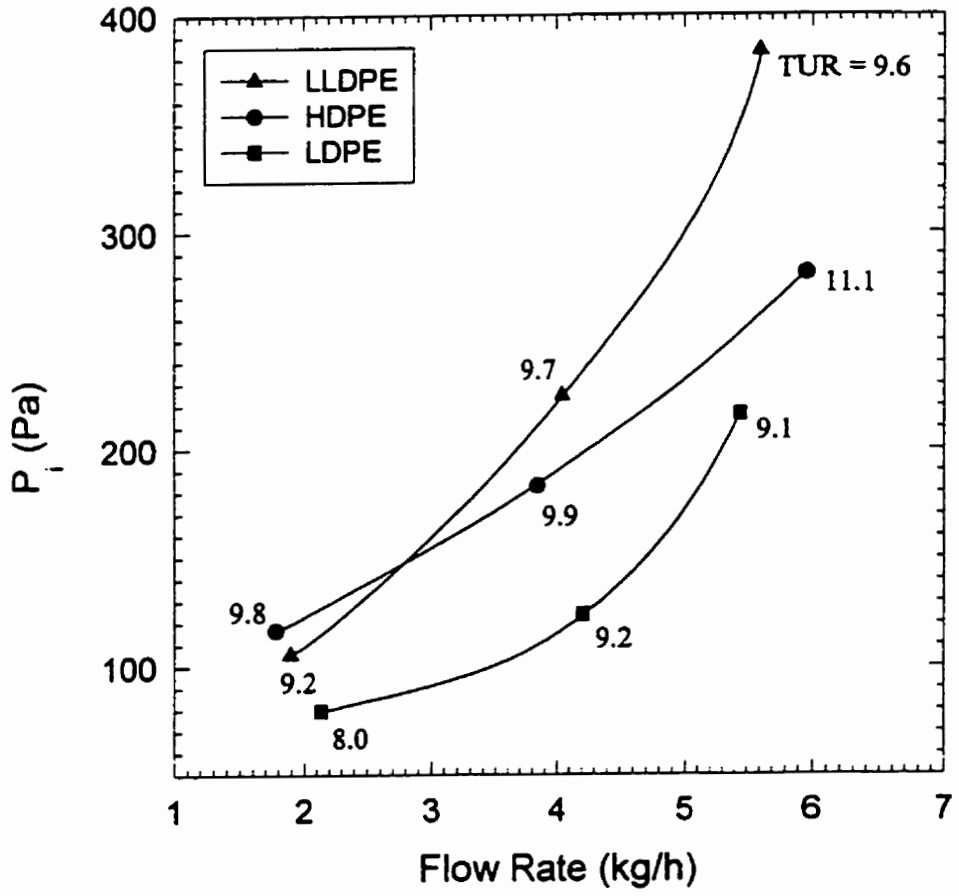

Figure 12. Effect of polymer flow rate on P_i values. The numbers represent TUR values. The other film blowing conditions are the same as in Figure 3.

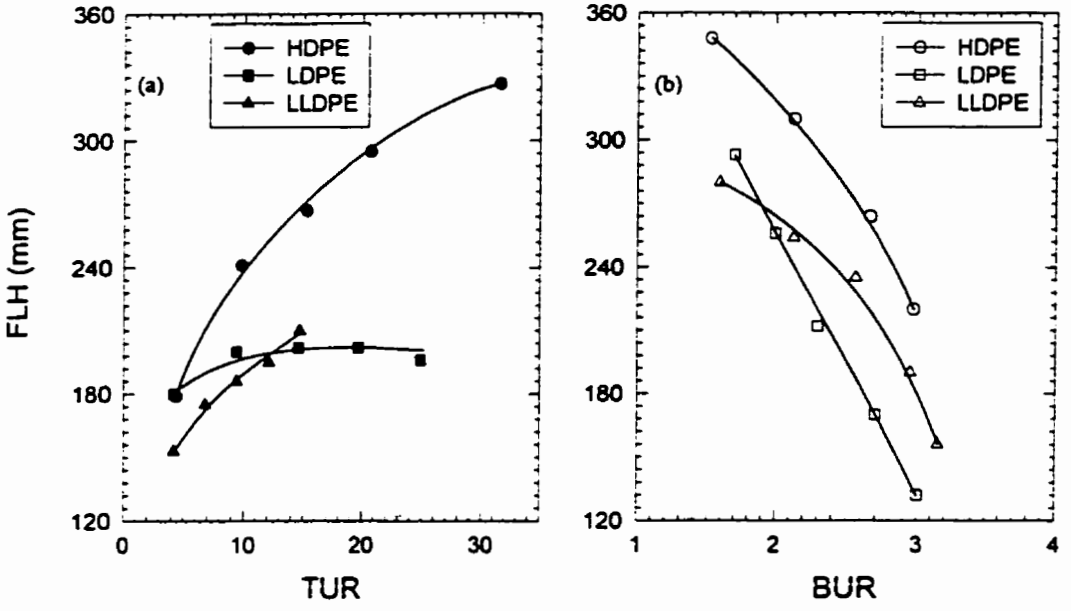

Figure 13. Effect of TUR (a) and BUR (b) at constant cooling air flow rate on FLH. The other film blowing conditions are the same as in Figure 3.

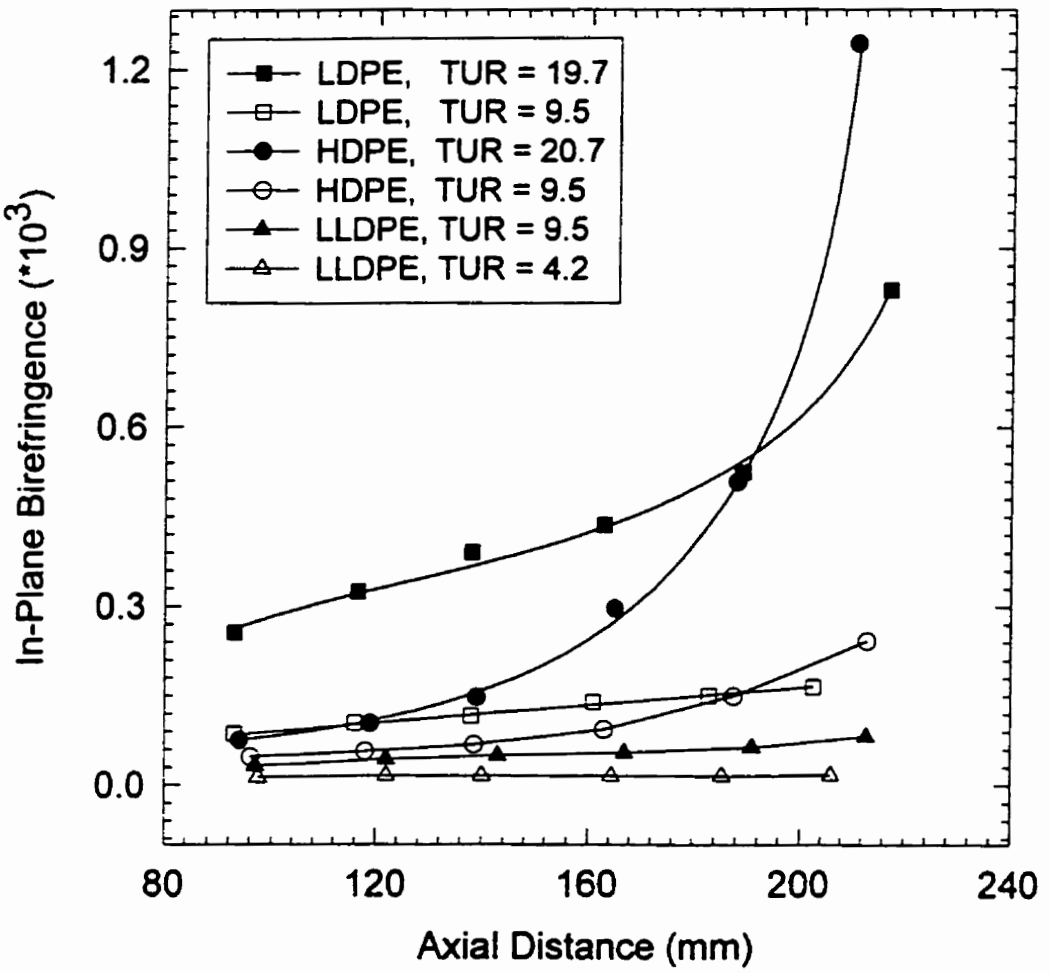

Figure 14. In-plane birefringence along the length of the bubble at two different TUR values. The other film blowing conditions are the same as in Figure 3.

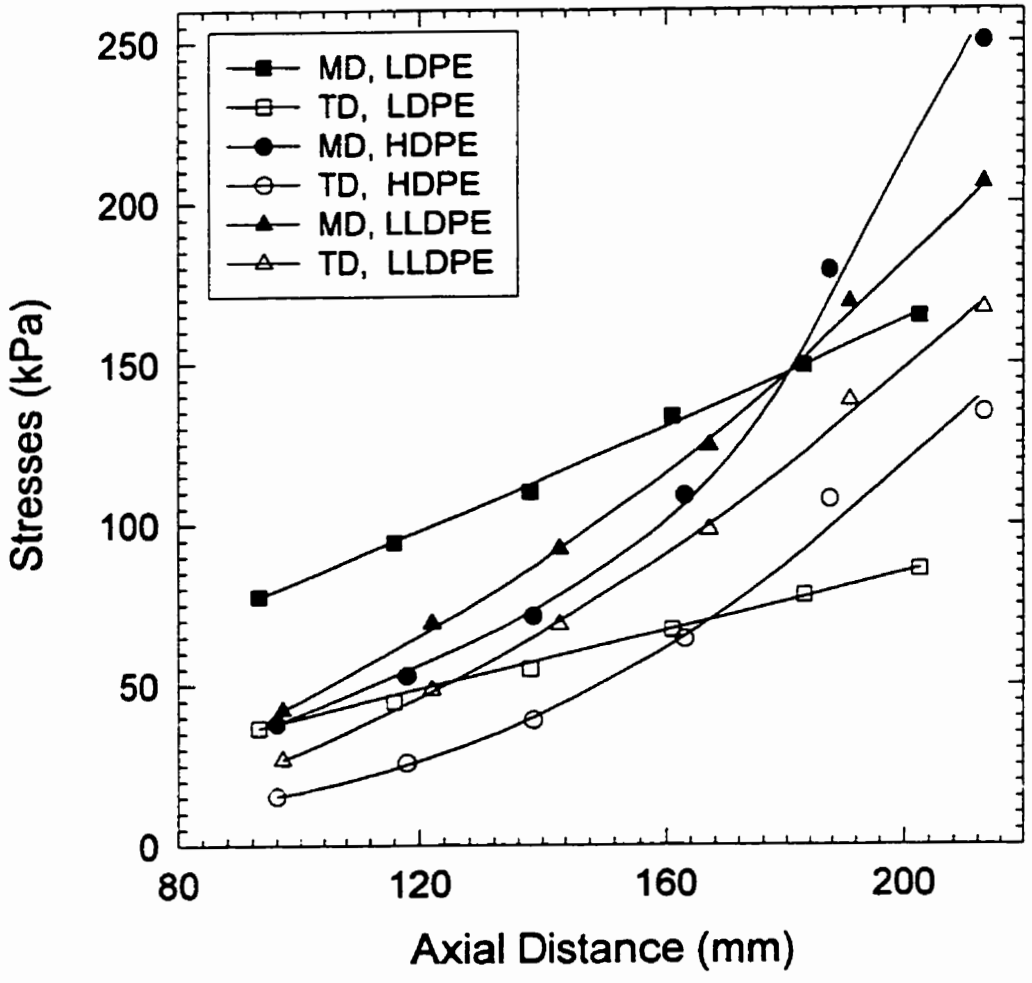

Figure 15. Stress profiles in MD and TD. The film blowing conditions are the same as in Figure 3.

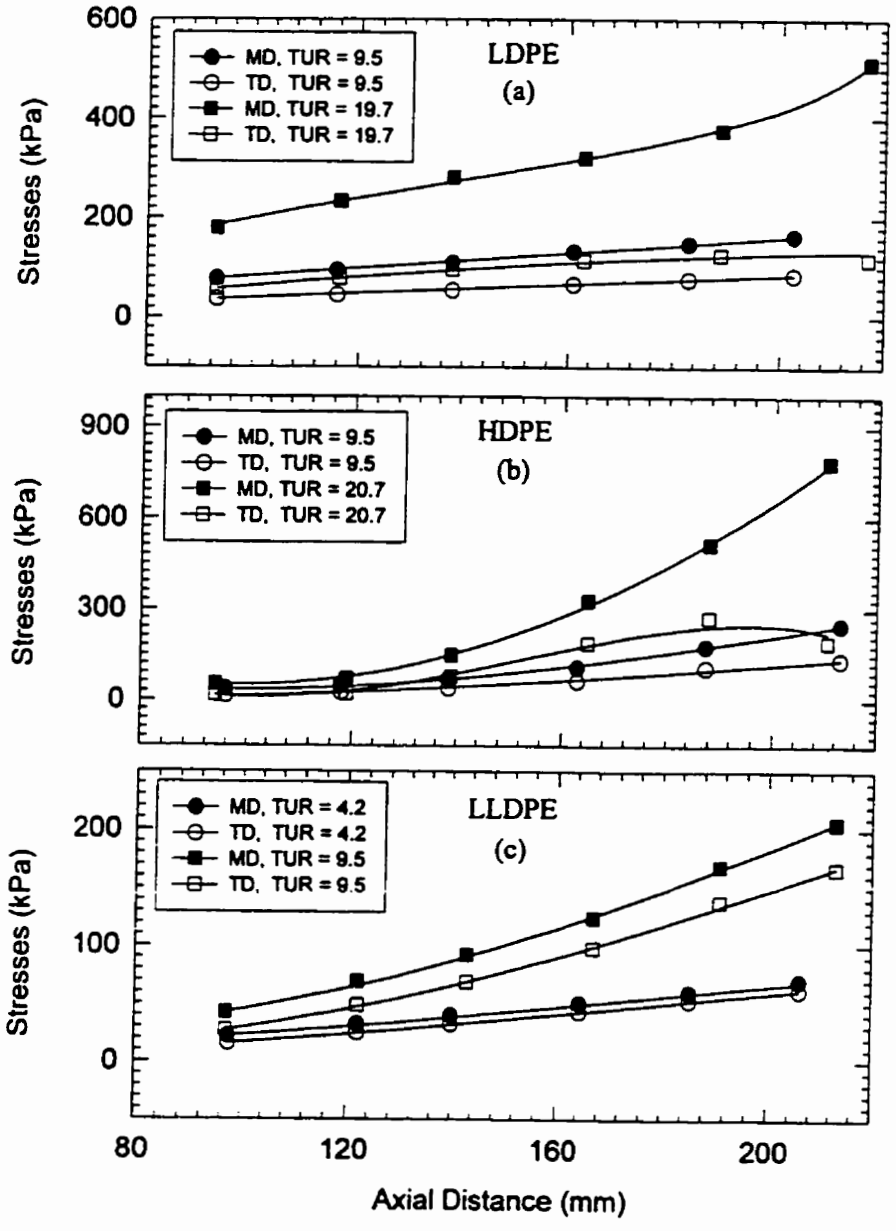

Figure 16. Effect of TUR on MD and TD Stresses for LDPE (a), HDPE (b), and LLDPE (c). The other film blowing conditions are the same as in Figure 3.

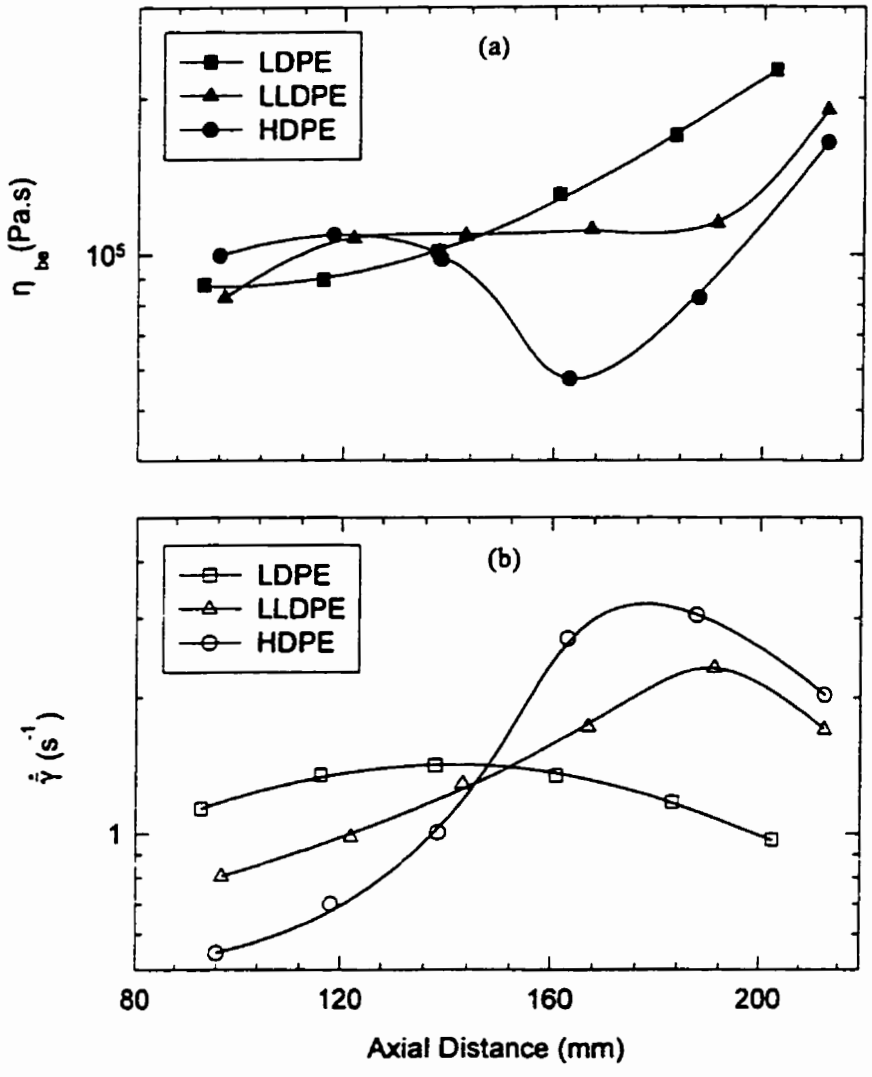

Figure 17. Apparent biaxial elongational viscosity (a) and the rate of deformation (b) profiles along the length of the bubble. The film blowing conditions are the same as in Figure 3.

CHAPTER 6

CONCLUSIONS AND RECOMMENDATIONS

6.1. Conclusions

The main objective of the present study was to gain a better understanding of the effects of the rheology of molten polymers on the processing performance in film blowing. To achieve this goal, the flow birefringence technique was implemented to measure stresses in the molten blown film. Furthermore, bubble instabilities, kinematics, and dynamics of the process were extensively investigated. The conclusions of the work presented in this dissertation are highlighted below.

For the four polymers studied the relative order of stability is as follows:

LDPE > HDPE > LLDPE > PP.

It is shown that bubble instabilities can not be correlated with the simple shear rheological data. We recall that it is virtually impossible to predict the extensional properties from simple shear data: film blowing is controlled by the extensional flow behavior of the material and coupling effects between heat transfer and rheological properties. Regions of multiple and non-existing solutions were detected for the LDPE as the TUR value was increased. Bubble instability at low BUR was observed with the LLDPE and the PP. Die exit effects such as extrudate swelling as well as extensional properties may play an important role on bubble

stability. Helical instability was observed with all the polymers. Air drag forces play an important role on the helical instability. Finally, our experimental results are in little or no agreement with the predictions of existing models in the literature.

The flow birefringence is a non-contacting technique which can be effectively used for on-line rheological investigation of a polymeric process. Analyzing the transmission of light through the blown film at oblique angle, we demonstrated that both MD and TD normal stresses can be determined by on-line birefringence measurements. The birefringence value is shown to be small in the molten zone and increase rapidly as crystallization proceeds. This is attributed to oriented nucleation and growth processes. The increase in the birefringence is observed even after the completion of the apparent crystallization. This behavior may be an indication of continued stretching and/or further crystallization in the solid zone. The in-plane birefringence measurements in the melt zone also indicate that the LDPE has the highest birefringence and the LLDPE, the lowest.

The three PE resins investigated display different bubble diameter and axial film velocity profiles which lead to quite different strain rate profiles. The peak MD strain rate of the HDPE is higher than that of the LLDPE. For the LDPE, it occurs at very low axial positions. It is observed that both the MD and TD strain rates considerably increase with increasing TUR and polymer flow rate. The magnitude of the TD strain rate is increased with increasing BUR. Increasing FLH mostly affects the MD strain rate for the HDPE and the

LLDPE. The extrusion temperature shows no noticeable effect on the strain rates for the HDPE and LLDPE but it has some effects on the MD strain rate for the LDPE. The results demonstrate that the TUR is not sufficient to define the film blowing process; one also needs to specify the polymer flow rate.

It was observed that processing conditions had no noticeable effect on the temperature at the plateau in the crystallization zone. However, the length of the plateau changed with varying the FLH, indicating that the crystallization kinetics depend on the cooling rate of the bubble. Moreover, the length of the plateau is not noticeably different for the LLDPE and the LDPE. The HDPE shows a broader plateau. The bubble temperature in the melt zone decreased with decreasing FLH, BUR, and extrusion temperature.

The LLDPE was found to require the highest pressure inside the bubble, whereas the LDPE, the lowest, that is: the relative order of the pressure inside the bubble is as follows:

$$\text{LLDPE} > \text{HDPE} > \text{LDPE}.$$

This order is consistent with the in-plane birefringence results. The higher the pressure inside the bubble, the higher the TD orientation is expected which means a lower birefringence, as observed. The pressure value inside the bubble increased with decreasing BUR, decreasing extrusion temperature, and increasing polymer flow rate. The effects of the TUR and the FLH depend on the polymer and processing conditions. There are interactions between various process parameters affecting the pressure value. The LLDPE was the most sensitive

polymer to the variations of processing variables and the HDPE, the least one. Our data demonstrate that the pressure inside the bubble is clearly a dependent variable. It is a rather complex response of several variables such as polymer melt rheology, film thickness, bubble temperature, axial velocity, bubble radius, and polymer flow rate.

Comparing the results of pressure and birefringence measurements with the apparent uniaxial elongational viscosities obtained from the convergent flow analysis for the three polymers, we note that the higher the elongational viscosity, the lower the pressure inside the bubble and the higher the birefringence. We also notice that the pressure and birefringence data can be correlated to bubble instabilities. The most unstable polymer (LLDPE) requires the highest pressure inside the bubble and has the lowest birefringence.

The stress data in the molten film were calculated using the birefringence, pressure, bubble diameter, and film velocity data. Both the MD and TD normal stresses increased considerably with decreasing FLH, increasing TUR, and increasing polymer flow rate and slightly with decreasing extrusion temperature. With increasing BUR, a higher TD stress was obtained. At the same processing conditions, the LLDPE exhibited the lowest stress ratio indicating that a more isotropic film is achievable with LLDPE. This may be attributable to the absence of the long chain branching in LLDPE. No simple correlation could be obtained between stresses and strain rates in film blowing; known rheological constitutive equations would probably fail describing the experimental data. Therefore, the strain rate data are not

sufficient to represent the effects of melt rheology and to discern between behaviors of different resins in film blowing. Any attempt to correlate final film properties to processing conditions and material characteristics should utilize the stress as well as the strain rate data.

Apparent non-uniform biaxial elongational viscosities were calculated along the length of the bubble using the stress and strain rate data. At the end of the melt zone, the LDPE exhibited the highest elongational viscosity and the lowest rate of deformation.

6.2. Recommendations for Future Work

As a result of our extensive experimental study on film blowing, a broad spectrum of questions have emerged and will have to be examined in future. Some recommendations are listed below.

1. At the present time, the rheological source of various behaviors of different polyolefin resins are far from being understood. In order to get a clearer picture of the process, it is indispensable to collect reliable elongational viscosity data, in particular planar and biaxial elongational data. One may then be able to relate different stability, kinematic, and dynamic behaviors to relevant rheological parameters.

2. The ultimate goal of study of film blowing is to predict final film properties from

material characteristics and processing parameters. We feel that the birefringence of the film in the melt and/or solid zone should be a very appropriate variable to correlate film properties to polymer rheology and processing conditions. It would be highly interesting to examine this possibility. On-line birefringence measurements could then serve as invaluable tools for quality control purposes.

3. Various rheological equations have been so far used to simulate film blowing with limited success. As the Carreau and K-BKZ models have been shown to be able to predict most of viscoelastic behaviors of polymeric liquids (Attané et al., 1988), it is recommended to examine and compare the predictions of these models in film blowing. It would also be highly interesting to incorporate a simple second-order fluid equation in film blowing modeling in order to get qualitative ideas about the effects of the elasticity of different melts. Moreover, As some of our experimental observations cannot be described by any known rheological equation, it is required to develop new models in order to handle the observed situations. In order to test film blowing models, it is urged to use the pressure inside the bubble and birefringence data as they appear to be the most critical parameters.

4. It would be desirable to perform a comprehensive study of the effects of aerodynamic forces on bubble instabilities. This will enable us to understand the effects of cooling air flow patterns and formation of vortices. It will also serve to clarify how aerodynamic forces interact with polymer melt rheology and cooling effects.

5. The out-of-plane birefringences can be measured by the transmission of light at oblique angle. Although such measurements are very difficult as it is necessary that the bubble be completely stable and uniform along the bubble circumference, they will enable us to reexamine the dynamic equations, in particular the magnitude of the aerodynamic forces.

6. It is recommended to measure the biaxial elongational viscosity of different melts by means of film blowing under isothermal conditions at least for a part of bubble forming zone over a wide range of operating conditions and compare these results with steady-state planar and biaxial elongational viscosities. Such a study will elucidate applicability of film blowing as a rheometric method.

REFERENCES

1. AGASSANT, J.-F., J. AVENAS, J.-Ph. SERGENT, and P.J. CARREAU, (1991) *Polymer processing: Principles and Modeling*, New York, Hanser Publisher.
2. ALAIE, S.M., and T.C. PAPANASTASIOU, (1993) "Modeling of Non-isothermal Film Blowing with Integral Constitutive Equations," *Int. Polym. Process.*, **8**, 51-65.
3. ASHIZAWA, H., J.E. SPRUIELL, and J.L. WHITE, (1984) "An Investigation of Optical Clarity and Crystalline Orientation in Polyethylene Tubular Film," *Polym. Eng. Sci.*, **24**, 1035-1042.
4. ASHOK, B.K., and G.A. CAMPBELL, (1992) "Two-phase Simulation of Tubular Film Blowing of Crystalline Polymers," *Int. Polym. Process.*, 7, 240-247.
5. AST, W., (1974) "Air Cooling on Blown Film Lines," *Kunstoffe*, **64**, 146-152.
6. ATTANÉ, P., G. TURREL, J.M. PIERRARD, and P.J. CARREAU, (1988) "On the Use of Transient Data for the Evaluation of Integral Constitutive Equations," *J. Rheol.*, **32**, 23-46.
7. AZZAM, R.M.A., and N.M. BASHARA, (1979) *Elipsometry and Polarized Light*, Amsterdam, North-Holland Publishing Company.
8. BABEL, A.K., and CAMPBELL, G.A. (1993) "Correlating the Plastic Strain with the Properties of the Low Density Polyethylene Blown Film," *J. Plastic Film & Sheeting*, **9**, 246-258.
9. BABEL, A.K., and CAMPBELL, G.A. (1995) "A Model Linking Process Variables to

the Strength of Blown Films Produced from LDPE and LLDPE," *Tappi J.*, **78**, 199-204.

10. BIRD, R.B., R.C. ARMSTRONG, and O. HASSAGER (1987), *Dynamics of Polymeric Liquids*, 2nd Ed., Wiley-Interscience , New York.

11. BORN, M., and WOLF, E., (1965) *Principles of Optics*, 3rd. Edn., Oxford, Pergamon Press.

12. BRANDRUP, J., and E.H. IMMERGUT (Eds), (1975) *Polymer Handbook*, 2nd. Edn., Toronto, John Wiley.

13. BUTLER, T.I., and R. PATEL, (1993) "Blown Film Bubble Forming and Quenching Effects on Film Properties," *J. Plastic Film & Sheeting*, **9**, 181-200.

14. CAIN, J.J., and M.M. DENN, (1988) "Multiplicities and Instabilities in Film Blowing," *Polym. Eng. Sci.*, **28**, 1527-1541.

15. CAMPBELL, G.A., N.T. OBOT, and B. CAO, (1992) "Aerodynamics in the Blown Film Process," *Polym. Eng. Sci.*, **32**, 751-759.

16. CAO, B., and G.A. CAMPBELL, (1990) "Viscoplastic-Elastic Modeling of Tubular Blown Film Processing," *AIChE J.*, **36**, 420-430.

17. CAO, B., P. SWEENEY, and G.A. CAMPBELL, (1990) "Simultaneous Surface and Bulk Temperature Measurement of Polyethylene During Film Blowing," *J. Plastic Film & Sheeting*, **6**, 117-130.

18. CHOHAN, R.K., (1994) "Shear and Elongational Flow of Some Branched Polyethylenes," *J. Appl. polym. Sci.*, **54**, 487-495.

19. CHOI, K., J.L. WHITE, and J.E. SPRUIELL (1980) "Orientation Development in Tubular Film Extrusion of Polystyrene," *J. Appl. Polym. Sci.*, **25**, 2777-2788.

20. CHOI, K., J.E. SPRUIELL, and J.L. WHITE, (1982) "Orientation and Morphology of High-Density Polyethylene Film Produced by the Tubular Blowing Method and its Relationship to Process Conditions," *J. Polym. Sci.: Polym. Phys. Ed.*, **20**, 27-47.

21. COGSWELL, F.N., (1972a) "Converging Flow of Polymer Melts in Extrusion Dies," *Polym. Eng. Sci.*, **12**, 64-73.

22. COGSWELL, F.N., (1972b) "Measuring the Extensional Rheology of Polymer Melts," *Trans. Soc. Rheol* , **16**, 383-403.

23. COVAS, J.A., and O.S. CARNEIRO, (1990) "Assessing the Convergent Flow Analysis as a Technique for Characterizing the Extensional Flow of Polymer Melts," *Polymer Testing*, **9**, 181-194.

24. COX, W.P., and E.H. MERZ, (1958) "Correlation of Dynamic and Steady Flow Viscosities," *J. Polym. Sci.*, **28**, 619-622.

25. DEALY, J.M., and K.F. WISSBRUN, (1990) *Melt Rheology and Its Role in Plastics Processing: Theory and Applications*, New York, Van Nostrand Reinhold.

26. FARBER, R., and J.M. DEALY, (1974) "Strain History of the Melt in Film Blowing," *Polym. Eng. Sci.*, **14**, 435-440.

27. FLEISSNER, M., (1988) "Elongational Flow of HDPE Samples and Bubble Instability in Film Blowing," *Int. Polym. Process.*, **2**, 229-233.

28. FULLER, G.G., (1990) "Optical Rheometry," *Annu. Rev. Fluid. Mech.*, **22**, 387-417.

29. FULLER, G.G., (1994) "Optical Rheometry: Optical Methods for Structure and Dynamics," Short course presented for the Society of Rheology at the 66th Annual Meeting, Philadelphia, PA.

30. FULLER, G.G., and K.J. MIKKELSEN, (1989) "Optical Rheometry Using Rotary Polarization Modulator," *J. Rheol.*, **33**, 761-769.

31. GHANEH-FARD, A., P.J. CARREAU, and P.G. LAFLEUR, (1996) "Study of Instabilities in Film Blowing," *AIChE J.*, **42**, 1388-1396.

32. GHANEH-FARD, A., P.J. CARREAU, and P.G. LAFLEUR, (1996) "Application of Birefringence to Film Blowing," *J. Plastic Film & Sheeting*, **12**, 68-86.

33. GHANEH-FARD, A., P.J. CARREAU, and P.G. LAFLEUR, (1996) "On-Line Birefringence Measurement in Film Blowing of a Linear Low Density Polyethylene," Submitted for publication in *Int. Polym. Process.*

34. GHANEH-FARD, A., P.J. CARREAU, and P.G. LAFLEUR, (1996) "Study of Kinematics and Dynamics of Film Blowing of Different Polyethylenes," Submitted for publication in *Polym. Eng. Sci.*

35. GHIJSELS, A., J.J.S.M. ENTE, and J. RAADSEN, (1990) "Melt Strength Behavior of PE and its Relation to Bubble Stability in Film Blowing," *Int.. Polym. Process.*, **5**, 284-286.

36. GOYAL, S.K., (1994) "Influence of Polymer Structure on the Melt Strength Behavior of Polyethylene Resins," *SPE ANTEC'94*, 1232-1238.

37. GRIFFITHS, D.V., and I.M. SMITH (1991) *Numerical Methods for Engineers*, CRC

Press, Boston.

38. GUPTA, R.K., (1980) *A New Non-isothermal Rheological Constitutive Equation and its Application to Industrial Film Blowing Processes*, Ph.D. Dissertation, Dept. Chem. Eng., University of Delaware, USA.

39. GUPTA, R.K., A.B. METZNER, and K.F. WISSBRUN, (1982) "Modeling of Polymeric Film-Blowing Processes," *Polym. Eng. Sci.*, **22**, 172-181.

40. HABER, A., and M.R. KAMAL, (1987) "Morphology and Orientation in Polyethylene Tubular Blown Films," *SPE ANTEC '87*, 446-449.

41. HAN, C.D., and T.H. KWACK, (1983) "Rheology-Processing-Property Relationships in Tubular Blown Film Extrusion. I. High-Pressure Low-Density Polyethylene," J. Appl. Polym. Sci., **28**, 3399-3418.

42. HAN, C.D., and J.Y. PARK, (1975a) "Studies on Blown Film Extrusion. I. Experimental Determination of Elongational Viscosity," *J. Appl. Polym. Sci.*, **19**, 3257-3276.

43. HAN, C.D., and J.Y. PARK, (1975b) "Studies on Blown Film Extrusion. II. Analysis of the Deformation and Heat Transfer Processes," *J. Appl. Polym. Sci.*, **19**, 3277-3290.

44. HAN, C.D., and J.Y. PARK, (1975c) "Studies on Blown Film Extrusion. III. Bubble Instability," *J. Appl. Polym. Sci.*, **19**, 3291-3297.

45. HAN, C.D., and R. SHETTY, (1977) "Flow Instability in Tubular Film Blowing. 1. Experimental Study," *IEC Fundam.*, **16**, 49-56.

46. HINGMANN, R., and B.L. MARCZINKE, (1994) "Shear and Elongational Flow Properties of Polypropylene Melts", *J. Rheol.*, **38**, 573-587.

47. HONGLADAROM, K., and W.R. BURGHARDT, (1994) "Measurement of the Full Refractive Index in Sheared Liquid Crystalline Polymer Solutions," *Macromolecules*, **27**, 483-489.

48. HUANG, T.A., and G.A. CAMPBELL, (1985) "Deformational History of LLDPE/LDPE Blends on Blown Film Equipment," *Advances in Polymer Technology*, **5**, 181-192.

49. HUANG, T.A., and G.A. CAMPBELL, (1986) "Deformational and Temperature History Comparison for LLDPE and LDPE Elements in the Bubble Expansion Region of Blown Films," *J. Plastic Film & Sheeting*, **2**, 30-39.

50. JANESCHITZ-KRIEGL, H., (1983) *Polymer Melt Rheology and Flow Birefringence*, Berlin, Springer-Verlag.

51. KALYON, D.M., and F.H. MOY, (1988) "Ultimate Properties of Blown Films of Linear Low Density Polyethylene Resins as Affected by Alpha-Olefin Comonomers," *Polym. Eng. Sci.*, **28**, 1551-1558.

52. KANAI, T., (1987) "Theoretical Analysis of Tubular Film Extrusion and its Applications for HMW-HDPE," *Int. Polym. Process.*, **1**, 137-143.

53. KANAI, T., and J.L. WHITE, (1984) "Kinematics, Dynamics and Stability of the Tubular Film Extrusion of Various Polyethylenes," *Polym. Eng. Sci.*, **24**, 1185-1201.

54. KANAI, T., and J.L. WHITE, (1985) "Dynamics, Heat Transfer and Structure Development in Tubular Film Extrusion of Polymer Melts: A Mathematical Model

and Predictions," *J. Polym. Eng.*, **5**, 135-156.

55. KANG, H.J., J.L. WHITE, and M. Cakmak (1990) "Single and Double Bubble Tubular Film Extrusion of Polyethylene Terephthalate," *Int. Polym. Process.*, **5**, 62-73.

56. KELLER, A., and M.J. MACHIN, (1967) "Oriented Crystallization in Polymers," *J. Macromol. Sci.*, **Part B, 1**, 41-91.

57. KIMURA, S., K. OSAKI, and M. KURATA, (1981) "Stress Relaxation of Polybutadiene at Large Deformation. Measurements of Stress and Birefringence in Shear and Elongation," *J. Polym. Sci.: Polym. Physics Edition*, **19**, 151-163.

58. KOYOMA, K., and O. ISHIZUKA, (1989) "Birefringence of Polyethylene Melt in Transient Elongational Flow at Constant Strain Rate," *J. Polym. Sci.: Part B, Polym. Physics*, **27**, 297-306.

59. KURTZ, S.J., (1995) "Relationship of Stresses in Blown-film Processes," *Int. Polym. Process.*, **10**, 148-154.

60. KWACK, T.H., (1984) *Processing-Structure-Property Relationship in Blown Film Extrusion*, Ph.D. Dissertation, Polytechnic Institute of New-York, USA.

61. KWACK, T.H., and C.D. HAN, (1983) "Rheology-Processing-Property Relationships in Tubular Blown Film Extrusion. II. Low-Pressure Low-Density Polyethylene," *J. Appl. Polym. Sci.*, **28**, 3419-3433.

62. KWACK, T.H., and C.D. HAN, (1988) "Development of Crystalline Structure during Tubular Film Blowing of Low-Density Polyethylene," *J. Appl. Polym. Sci.*, **35**, 363-389.

63. LAUN, H.M., and H. SCHUCH, (1989) "Transient Elongational Viscosities and Drawability of Polymer Melts," *J. Rheol.*, **33**, 119-175.

64. LUO, X-L., and R.I. TANNER, (1985) "A Computer Study of Film Blowing," *Polym. Eng. Sci.*, **25**, 620-629.

65. MADDAMS, W.F., and J.E. PREEDY, (1978a) "X-Ray Diffraction Orientation Studies on Blown Polyethylene Films. I. Preliminary Measurements," *J. Appl. Polym. Sci.*, **22**, 2721-2737.

66. MADDAMS, W.F., and J.E. PREEDY, (1978b) "X-Ray Diffraction Orientation Studies on Blown Polyethylene Films. II. Measurements on Films from a Commercial Blowing Unit," *J. Appl. Polym. Sci.*, **22**, 2739-2749.

67. MADDAMS, W.F., and J.E. PREEDY, (1978c) "X-Ray Diffraction Orientation Studies on Blown Polyethylene Films. III. High-Stress Crystallization Orientation," *J. Appl. Polym. Sci.*, **22**, 2751-2759.

68. MCNALLY, G.M., C. BERMINGHAM, and W.R. MURPHY, (1993) "Optimization of Performance Characteristics of LDPE/LLDPE Blends in Blown Film Extrusion," *Trans. IChemE*, **71**, Part A, 223-231.

69. MICHAELI, W., and G. SCHMITZ, (1995) "Investigation of Blown Film Extrusion Using the Laser Doppler Velocimetry," *ANTEC '95*, 181-185.

70. MINOSHIMA, W., and J.L. WHITE, (1986) "Instability Phenomena in Tubular Film, and Melt Spinning of Rheologically Characterized High Density, Low Density and Linear Low Density Polyethylene," *J. Non-Newt. Fluid Much.*, **19**, 275-302.

71. NAGASAWA, T., T. MATSUMURA, S. HOSHINO, and K. KOBAYASHI, (1973a) "Film Forming Process of Crystalline Polymer. I. Factors Inducing a Molecular Orientation in Tubular Blown Film," *Applied Polymer Symposium*, **20**, 275-293.

72. NAGASAWA, T., T. MATSUMURA, and S. HOSHINO, (1973b) "Film Forming Process of Crystalline Polymer. II. Microstructure," *Applied Polymer Symposium*, **20**, 295-313.

73. OBIJESKI, T.J., and K.R. PRUITT, (1992) "Improving the Output and Bubble Stability of Thick Gauge Blown Film," *ANTEC '92*, 150-153.

74. OSAKI, K., N. BESSHO , T. KOJIMOTO, and M. KURATA, (1979) "Flow Birefringence of Polymer Solutions in Time-Dependent Field," *J. Rheol.*, **23**, 457-475.

75. PATEL, R.M., T.I. BUTLER, K.L. WALTON, and G.W. KNIGHT, (1994) "Investigation of Processing-Structure-Properties Relationships in Polyethylene Blown Films," *Polym. Eng. Sci.*, **34**, 1506-1514.

76. PEARSON, J.R.A., (1985) *Mechanics of Polymer Processing.* London, Elsevier Applied Science Publishers.

77. PEARSON, J.R.A., and C.J.S. PETRIE, (1970a) "The Flow of a Tubular Film. Part 1. Formal Mathematical Representation," *J. Fluid Mech.*, **40**, 1.

78. PEARSON, J.R.A., and C.J.S. PETRIE, (1970b) "A Fluid-Mechanical Analysis of the Film-Blowing Process," *Plast. Polym.*, **38**, 85-94.

79. PETRIE, C.J.S., (1973) "Memory Effects in a Non-uniform Flow: A Study of the Behavior of a Tubular Film of Viscoelastic Fluid," *Rheol. Acta*, **12**, 92-99.

80. PETRIE, C.J.S., (1975) "A Comparison of Theoretical Predictions with Published Experimental Measurements on the Blown Film Process," *AIChE J.*, **21**, 275-282.

81. PICOT, J.J.C., (1984) "Molecular Orientation in Film Extrusion of High-Density Polyethylene," *Polym. Eng. Sci.*, **24**, 415-420.

82. SAMUELS, R.J., (1974) *Structured Polymer Properties*, Toronto, John Wiley.

83. SEO, Y., and E.H. WISSLER, (1989) "The Effect of Extrudate Swell on Modeling the Film Blowing Process," *Polym. Eng. Sci.*, **29**, 722-730.

84. SHIMOMURA, Y., J.E. SPRUIELL, and J.L. WHITE, (1982) "Orientation Development in the Tubular Film Extrusion of Polypropylene," *J. Appl. Polym. Sci.*, **27**, 2663-2674.

85. SHROFF, R.N., L.V. CANCIO, and M. SHIDA, (1977) "Extensional Flow of Polymer Melts," *Trans. Soc. Rheol.*, **21**, 429-446.

86. SHROFF, R.N., and M. SHIDA, (1970) "Effect of Long-Chain Branching on the Relation between Steady-Flow and Dynamic Viscosity of Polyethylene Melts," *J. Polym. Sci.*, Part A-2, **8**, 1917-1925.

87. SIMPSON, D.M., and I.R. HARRISON, (1994) "A Study of the Effects of Processing Parameters on the Morphologies and Tensile Modulus of HDPE Blown Films: Application of Composite Theories on a Molecular Level to Characterize Tensile Modulus," *J. Plastic Film & Sheeting*, **10**, 302-325.

88. STEIN, R.S., (1957) "Measurement of Birefringence of Biaxially Oriented Films," *J. Polym. Sci.*, **24**, 383-396.

89. SUBRAMANIAN, R., D.R. WILSON, and J.J.C. PICOT (1992) "Flow Birefringence in

Polymer Rheology," *Polym. Eng. Sci.*, **32**, 573-578.

90. SWEENEY, P.A., G.A. CAMPBELL, and F.A., FEENEY, (1992) "Real Time Video Techniques in the Analysis of Blown Film Instability," *Int. Polym. Process.*, 7, 229-239.

91. SWEENEY, P.A., and G.A. CAMPBELL, (1993)"Blown Film Stability," *SPE ANTEC'93*, 461-464.

92. TAS, P.P., (1994) *Film Blowing: from Polymer to Product*, Ph.D. Dissertation, Dept. Mech. Eng., Eindhoven University of Technology, The Netherlands.

93. TERRY, B.W., and K. YANG, (1964) "A New Method for Determining Melt Density as a Function of Pressure and Temperature," *SPE Journal*, **20**, 540-543.

94. UTRACKI, L.A., and R. GENDRON, (1984) "Pressure Oscillation During Extrusion of Polyethylenes. II," *J. Rheol.*, **28**, 601-623.

95. VAN AKEN, J.A., and H. JANESCHITZ-KRIEGL, (1980) "New Apparatus for the Simultaneous Measurement of Stresses and Flow Birefringence in Biaxial Extension of Polymer Melts," *Rheol. Acta*, **19**, 744-752.

96. VAN GURP, M., B.J. KIP, J.P.C. VAN HEEL, and S. DE BOER, (1994) "On the Development of Orientation in LDPE Blown Films," *J. Plastic Film & Sheeting*, **10**, 156-176.

97. VENKATRAMAN, S., M. OKANO, and A. NIXON, (1990) "A Comparison of Torsional and Capillary Rheometry for Polymer Melts: the Cox-Merz Rule Revisited," *Polym. Eng. Sci.*, **30**, 308-313.

98 WAGNER, M.H., (1978) "Experimental Investigations into the Analysis of the Film Blowing Process," *Kunststoffe*, **68**, 15-17.

99. WALES, J.L.S., (1976) *The Application of Flow Birefringence to Rheological Studies of Polymer Melts*, The Netherlands, Delft University Press.

100. WHITE, J.L., and H. YAMANE, (1987) "A Collaborative Study of the Stability of Extrusion, Melt Spinning and Tubular Film Extrusion of Some High-, Low- and Linear-Low Density Polyethylene Samples," *Pure and Applied Chem.*, **59**, 193-216.

101. WINTER, H.H., (1983) "A Collaborative Study on the Relation Between Film Blowing Performance and Rheological Properties of Two Low-Density and Two High-Density Polyethylene Samples," *Pure & Appl. Chem.*, **55**, 943-976.

102. YAMANE, H., and J.L. WHITE, (1987) "Simulation of Tubular Film Extrusion of Polymer Melts," *Int. Polym. Process.*, **2**, 107-112.

103. YEOW, Y.L., (1976) "Stability of Tubular Film Flow: A Model of the Film-Blowing Process," *J. Fluid Mech.*, **75**, 577-591.

104. YOON, K.-S., and C.-W. PARK, (1992) "Analysis of Isothermal Two-Layer Blown Film Coextrusion," *Polym. Eng. Sci.*, **32** , 1771-1777.

APPENDIX I

FLOPPYDISKS OF RESULTS

The floppydisks containing all the drawings presented in this dissertation are available upon request at the following address:

Professor Pierre J. Carreau

Department of Chemical Engineering

Ecole Polytechnique of Montreal

P.O. Box 6079, Stn. "Centre Ville"

Montreal, QC, H3C 3A7 CANADA

IMAGE EVALUATION
TEST TARGET (QA-3)

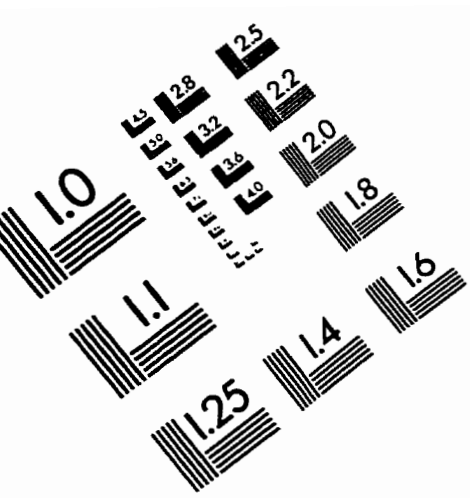

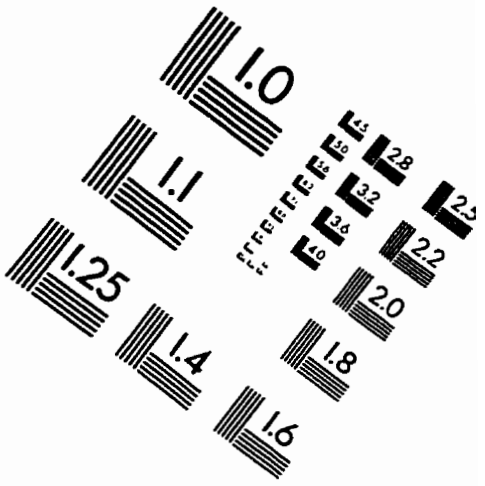

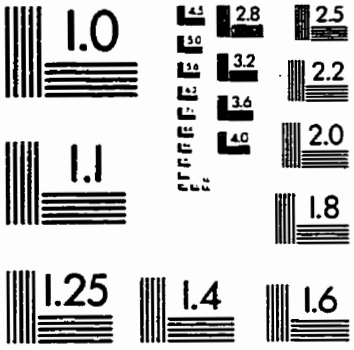

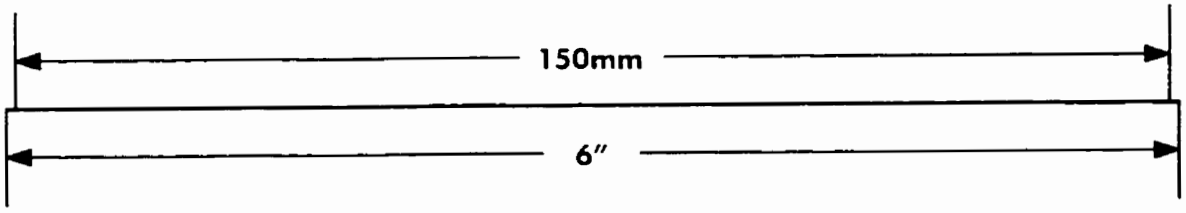

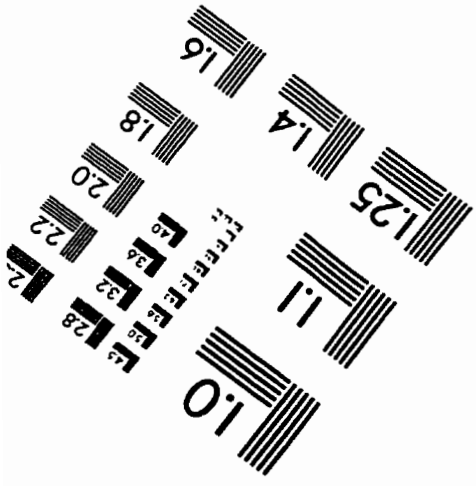

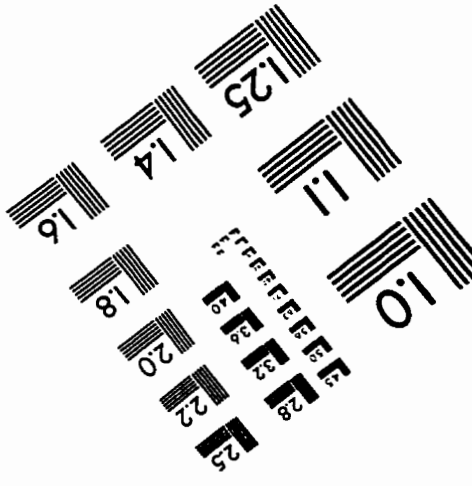

APPLIED IMAGE, Inc
1653 East Main Street
Rochester, NY 14609 USA
Phone: 716/482-0300
Fax: 716/288-5989